Theses and Dissertations   Graduate School

2010

Identification and Characterization of a Second Wolfram Syndrome Gene

Sami Amr
Virginia Commonwealth University

IDENTIFICATION AND CHARACTERIZATION OF A SECOND WOLFRAM SYNDROME GENE

A dissertation submitted in partial fulfillment of the requirements for the degree of Doctor of Philosophy at Virginia Commonwealth University

By Sami Samir Amr
B.A. Biological Psychology
The College of William and Mary, 2002
B.Sc. Genetic Engineering and Biotechnology
Jordan University of Science and Technology, 2005

Director: Rita Shiang, Associate Professor
Department of Human and Molecular Genetics

Virginia Commonwealth University
Richmond, Virginia
April 2010

TABLE OF CONTENTS

LIST OF TABLES

LIST OF FIGURES

LIST OF ABBREVIATIONS

7-AAD	7-amino-actinomycin D
AD	Alzheimer's disease
AGE	Advanced glycosylation end-products
ALS	Amyotrophic lateral sclerosis
ANOVA	Analysis of variance
APP	β-amyloid precursor protein
ATF4	Activating transcription factor 4
ATF6	Activating transcription factor 6
Aβ	amyloid-β
BafA1	Bafilomycin A1
BAX	BCL-2 associated protein X
BCL-2	B cell lymphoma 2 protein
Bec1	Beclin 1 protein
BrdU	5-bromo-2-deoxyuridine
BSA	Bovine serum albumin
Ca^{2+}	Calcium
CHOP	C/EBP-homolgous protein, also known as growth arrest- and DNA damage-inducible gene 153 (GADD153)

CISD2	Conserved iron sulfur domain 2 (synonyms: ZCD2, Miner1, ERIS, NAF-1, NOXP70)
CLN3	Ceroid-palmitoyl-palmitoyl-protien thioesterase 3 protein
DI	Diabetes insipidus
DM	Diabetes mellitus
eIF2α	eukaryotic initiation factor 2 alpha
ER	Endoplasmic reticulum
ESE	Exon splicing enhancer
FAD	Familial Alzheimer's disease
FBS	Fetal bovine serum
FFA	Free fatty acids
GADD34	growth arrest- and DNA damage inducible gene 34
GPX	Glutathione peroxidase
GRIN1	Glutamate receptor zeta subunit protein
GRP78/BiP	Binding immunoglobulin protein
GRP94	Glucose regulated protein 94
GSIS	glucose-stimulated insulin secretion
H_2O_2	Hydrogen peroxide
HD	Huntington's disease
HEK293	Human embryonic kidney cells
HNE	4-hydroxy-2-nonenal
IDV	Integrated density value
INS1	Rat pancreatic insulinoma cells

IP	Immunoprecipitation
IP$_3$R	Inositol-1,4,5-triphosphate receptor
IRE1	Inositol-required enzyme 1
LC3-II	Light chain 3 protein (cleaved)
MDA	Malondialdehyde
MTT	3-[4,5-dimethylthiazol-2-yl]-2,5-diphenyltetrazolium bromide
N1E115	Mouse neuroblastoma cells
NeuroD1	Neurogenic differentiation 1 protein
NF-κB	Nuclear factor-κB
NO	Nitric oxide
O$_2^-$	Superoxide anion
OA	Optic atrophy
OH$^-$	Hydroxyl radical
ONOO$^-$	Peroxynitrite
P19	Mouse embryonic stem cell like tetracarcinoma cells
p38 MAPK	p38 mitogen activated pathway kinase
PD	Parkinson's disease
PERK	PKR-like endoplasmic reticulum kinase, also known as eukaryotic translation initiation factor kinase 2α kinase (EIF2AK3)
PKC	Protein kinase C
PPT1	Palmitoyl-protein hydrolase 1 protein
PS1	Presenilin-1 protein
PS2	Presenilin-2 protein

PTP	Permeability transition pore
RAGE	Receptor for AGE
RCS	Reactive chlorine species
RNS	Reactive nitrogen species
ROS	Reactive oxygen species
RyR	Ryanodine receptor
SERCA	sarco(endo)plasmic Ca^{2+}-ATPases
SOD	Superoxide dismutase
SOD1	Copper zinc superoxide dismutase
SOD2	Manganese superoxide dismutase
SSCP	Single stranded conformational polymorphism
TCA	Tricarboxylic acid cycle
TG	thapsisgargin
UCP1	Uncoupler protein 1
UPR	Unfolded protein response
WFS	Wolfram syndrome
WFS1	Wolfram syndrome type I or Wolfram syndrome type I gene
WFS2	Wolfram syndrome type II or Wolfram syndrome type II gene
WRS	Wolcott-Rallison syndrome
XBP-1	X-box binding protein

ABSTRACT

**IDENTIFICATION AND CHARACTERIZATION OF A SECOND WOLFRAM
SYNDROME GENE**

A dissertation submitted in partial fulfillment of the requirements for the degree of
Doctor of Philosophy at Virginia Commonwealth University

By Sami Samir Amr
B.A. Biological Psychology
The College of William and Mary, 2002
B.Sc. Genetic Engineering and Biotechnology
Jordan University of Science and Technology, 2005

Director: Rita Shiang, Associate Professor
Department of Human and Molecular Genetics

Virginia Commonwealth University
Richmond, Virginia
April 2010

Wolfram Syndrome (WFS) is a debilitating autosomal recessive neurodegenerative
disorder characterized by juvenile onset insulin dependent diabetes mellitus (DM) and optic
atrophy (OA) as well as a number of neurological and endocrine complications that result in
early death due to respiratory complications. Previous research has mapped Wolfram syndrome
to chromosome 4p16.1 and the disease has been attributed to mutations in the *WFS1* gene
affecting the WFS1 protein (wolframin), an ER membrane glycoprotein that plays an important
role in the unfolded protein response (UPR) and in intracellular Ca^{2+} homeostasis. An additional
locus for WFS on chromosome 4q22-24 was identified by linkage studies of four Jordanian
Bedouin families with 16 affected individuals (El-Shanti *et al*., 2000).

In this study, we attempted to identify the causative gene for the second WFS locus and identified a single missense mutation in a novel highly conserved iron-sulfur binding domain gene, *CISD2*, in the three consanguineous families of Jordanian descent from the El-Shanti *et al.* (2000) study (Amr *et al*., 2007). A G→C transversion at nucleotide 109 predicts an amino acid change from glutamic acid to glutamine (E37Q). Although the amino acid is conserved and the mutation is nonsynonymous, the missense mutation was found to disrupt messenger RNA splicing by eliminating exon 2 which results in the introduction of a premature stop codon. CISD2 is expressed in a wide variety of tissues, including those affected in WFS, the brain and pancreas. The *CISD2*-encoded protein, ERIS (endoplasmic reticulum intermembrane small protein) localizes to the endoplasmic reticulum but does not appear to interact directly with wolframin. Furthermore, lymphoblastoid cells from affected individuals show a significantly greater rise in intracellular calcium when stimulated with thapsigargin, compared with controls, although no difference was observed in resting concentrations of intracellular calcium.

To understand the underlying pathogenesis in WFS2 patients, we examined cell death as well as known stress pathways. *Cisd2* was knocked down in three cell lines derived from tissues most affected by the disease, namely rat pancreatic insulinoma cells (INS1), mouse neuroblastoma cells (N1E115), and mouse embryonic stem cell like cells (P19) which could be differentiated into neuronal cells. *Cisd2* knockdown in INS1 cells shows an increase in apoptotic cell death and in the expression of the apoptotic markers *CHOP* and BAX, but no increase in the autophagic marker LC3-II. Assessment of the UPR in CISD2 deficient cells shows no activation of the UPR response, while *Cisd2* expression in wild-type INS1 and N1E115 cells did not increase under conditions of ER stress. These findings indicate that there is an increase in apoptosis in WFS2 similar to WFS1 but the pathogenesis involves a molecular mechanism that is

different than that in WFS1. Investigation of markers of oxidative stress, another major contributor to diabetes and neurodegeneration, show an increase in expression of the antioxidant enzymes *Sod1* and *Sod2* as well as an increase in global tyrosine nitration in INS1 *Cisd2* knockdown cells compared with controls. Cell death in those cells was exacerbated with addition of known oxidative stressors, thapsigargin and paraquat compared with controls. These findings indicate that oxidative stress is a contributor to WFS2 pathogenesis, but it is not clear whether it is the primary causative factor.

A recent article implicated ERIS in the BCL-2 associated inhibition of autophagy (Chang *et al*., 2009) and showed an increase in levels of autophagy in response to starvation in *Cisd2* knockdown in a human epithelial carcinoma cell line (H1299). Starvation of INS1 *Cisd2* knockdown cells did not elicit a greater autophagic response compared with controls, but did show an increase in expression of *Cisd2*. P19 *Cisd2* knockdown cells that were differentiated into neurons by retinoic acid treatment did not show an inhibition in differentiation markers, but *Cisd2* levels returned to levels similar to pre-differentiation wildtype P19 cells, which indicates that *Cisd2* is upregulated during neuronal differentiation. In conclusion, the pathogensis of WFS2 can be attributed to apoptotic death of cells in affected tissues, with oxidative stress and not endoplasmic reticulum stress contributing to the development of disease, while ERIS' relationship with BCL-2-mediated autophagy and neuronal differentiation suggest its important role in cell differentiation and survival.

CHAPTER 1

INTRODUCTION AND REVIEW OF THE LITERATURE

1.1 Wolfram Syndrome: Clinical description and background

Wolfram syndrome (WFS) or DIDMOAD (<u>d</u>iabetes <u>i</u>nsipidus, <u>d</u>iabetes <u>m</u>ellitus, <u>o</u>ptic <u>a</u>trophy, and <u>d</u>eafness), is a debilitating autosomal recessive neurodegenerative disorder characterized by juvenile-onset diabetes mellitus (DM) and optic atrophy (OA) (Wolfram & Wagner, 1938; Blasi *et al.,*1986). Other common symptoms that may manifest during disease progression include diabetes insipidus, deafness, renal tract and gastrointestinal complications, neurological complications, and psychiatric illnesses (Barret *et al.,*2003; Barret *et al.,*1995). Affected individuals have a mean age of death of about 30 years, usually from central respiratory failure (Domenech *et al.,*2006). WFS is a rare disorder, with a reported prevalence of 1/770,000 and a carrier frequency of 1/375 in one UK study (Barret *et al.,*1995), and an estimated prevalence of less than 1/100,000 in the US (Fraser & Gunn, 1977) with roughly 1% of the US population being heterozygous carriers (reviewed by Polymeropoulos *et al.,*1994). As is common in autosomal recessive disorders, the prevalence is greater in countries with higher rates of consanguinity; the prevalence is estimated at 1/68,000 in the Lebanese population (Baz *et al.,*1999).

Clinical features associated with WFS affect the nervous system, urinary tract and endocrine glands. Neurological complications include diabetes insipidis, mental retardation, sensorineural hearing loss, cerebellar ataxia, myoclonus, epilepsy, anosmia, axial rigidity, Parinaud's syndrome, bulbar dysfunction, hyporeflexia, extensor plantar reflexes, and psychiatric illnesses (Barret *et al.,*1995, Shanon *et al.,*1999). Urinary tract infections, bladder instability, and

bladder atony also manifest in patients (Barret *et al.,* 1995). Endocrine complications include hypothyroidism, testicular atrophy, delayed sexual maturity, and growth retardation (Cremers *et al.*; 1977, Barret *et al.,*1995). Post mortem and MRI studies of WFS patients reveal morphological aberrations that affect neuronal circuitry and endocrine function, including loss of neurons and atrophy of various brain regions and selective damage of pancreatic β-cells. In the brain, atrophy of optic nerves and cochlear nuclei, loss of neurons of the hypothalamic nuclei and thalamic nuclei, and other diffuse neurodegeneration is seen in patients (Genis *et al.,*1997; Rando *et al.,*1992). Psychiatric manifestations, which present in 60% of WFS patients, include episodes of severe depression, psychosis, impulsive verbal and physical aggression, and suicidal tendencies (Swift *et al.,* 1990).

Heterozygous carriers, estimated at 1% in the US population (Fraser & Gunn, 1977), have been reported to be eight times more likely to be hospitalized for psychiatric illnesses. This finding implicates that heterozygosity of Wolfram syndrome may be a major contributor of psychiatric illnesses in the general population (Swift *et al.,* 1998). Another related observation is the increased prevalence of diabetes mellitus in first-degree relatives of WFS patients (Fraser & Gunn, 1977).

1.2 Genetics of Wolfram Syndrome

1.2.1 Discovery of WFS1

Polymeropoulos *et al.* (1994) carried out a linkage analysis study of 11 families in the United States, where they identified a critical region of 5 cM on the short arm of chromosome 4 that was linked to WFS. A few years later, two research groups simultaneously discovered the gene for WFS in the identified critical region and named it *WFS1* (Inoue *et al.,* 1998), and the

encoded protein wolframin and WFS1 (Inoue *et al*., 1998; Strom *et al.,* 1998). Both groups reported that *WFS1* is a putative transmembrane protein that is expressed ubiquitously in all tissues, with high expression in adult heart, pancreas, brain, placenta, and lung (Strom *et al.,* 1998; Inoue *et al.,* 1998).

WFS1 consists of 8 exons spanning 33.4 kb of genomic DNA, encoding a protein with 890 amino acids with 9 predicted membrane spanning domains and a predicted molecular weight of 100 kDa (Strom *et al.,* 1998; Inoue *et al.,* 1998), which homo-oligomerizes to form a high molecular weight structure of ~400 kDa (Hoffman *et al.,* 2003). Further *WFS1* characterization studies by Takeda *et al*. (2001) revealed the WFS1 protein to be an integral, endoglycosidase H-sensitive membrane glycoprotein that is localized in the endoplasmic reticulum (ER).

Mutation screening of *WFS1* by several groups showed allelic heterogeneity with patients being either homozygous or compound heterozygous for various mutations (Inoue *et al.,* 1998; Strom *et al.,* 1998; Hardy *et al.,* 1999; Gomez-Zaera *et al.,* 2001; Khanim *et al.,* 2001). More than 50 different types of mutations in *WFS1* have been identified including nonsense mutations, missense mutations, and insertion/deletion aberrations. The variety of mutations supports the notion that *WFS1* loss-of-function was responsible for the disease phenotype.

1.2.2 Locus heterogeneity in Wolfram syndrome

Locus heterogeneity of WFS was first shown in a study by Collier *et al.* (1996). In their study, linkage analysis of 12 UK families with WFS showed that, although most of the families showed linkage of the disease phenotype to the *WFS1* locus, one family, family K, was not linked across the entire locus. While the affected members in the other 11 families developed progressive OA after the onset of DM, affected members of family K exhibited non-progressive

OA more than a decade before the onset of DM (Collier *et al.*, 1996). Since diagnosis of WFS depends on presentation of juvenile OA and DM in patients, the unlinked family indicated locus heterogeneity of WFS.

Another study by El-Shanti *et al.* (2000) further supported the notion of locus heterogeneity of WFS. In their study of 4 Jordanian Bedouin families with 16 affected individuals, only one family, WS1, showed significant allelic homozygosity for markers on the 4p16 locus - the WFS1 locus. They carried out homozygosity mapping via a 20-cM genomewide scan for additional loci by means of a DNA-pooling strategy for families WS-3 and WS-4, two of the three families unlinked to the WFS1 locus, thereby identifying homozygosity at marker D4S1647. Subsequent linkage analysis of additional markers in the three families and recombination analysis identified a 7.1-cM region between markers D4S1591 and D4S3240 on chromosome 4q22-24 as another locus for WFS. Although the families are not related, haplotype analysis showed a common affected haplotype among the families. The WFS critical region, named WFS2 locus, contains 22 mapped genes and a number of expressed sequence tags (El-Shanti *et al.*, 2000).

1.2.3 Genotype-Phenotype correlations in Wolfram syndrome

Despite the presence of DM and OA, the two diagnostic features of WFS, several characteristic features were only associated with either the *WFS1* locus or with the *WFS2* locus. Diabetes insipidus, for example, is only observed in patients with mutations or those showing linkage to the *WFS1* locus, but is completely absent from any patients who show linkage to the *WFS2* locus (Ajlouni K. *et al.*,2002). In addition, the Jordanian WFS2 patients manifested clinical features that were not reported in any other WFS patients including defective platelet

4

aggregation with collagen leading to a bleeding tendency, and peptic ulcer disease that was compounded by the bleeding tendency, causing gastrointestinal-tract bleeding (Ajlouni *et al.,*2002; Al-Sheyyab *et al.,*2001) (Table 1). These genotype-phenotype correlations provide support to the idea that, although many diagnostic features are present in all WFS patients, these two variants of WFS are clinically distinct and, quite possibly, arise from different molecular pathways of disease.

Table 1: Comparison of clinical manifestations in WFS1 and WFS2 patients

Clinical Symptom	WFS1	WFS2
Diabetes mellitus	++	++
Optic atrophy	++	++
Diabetes insipidus	+	-
Sensorineural deafness	+	+
Renal tract involvement	+	+
Peptic ulcer disease	-	++
Bleeding tendency	-	++

(++) manifests in all; (+) manifests in some; (-) does not manifest. Adapted from Ajlouni *et al.,* 2002.

1.3 Pathogenesis in Diabetes and Neurodegeneration

Type I DM is characterized by β-cell destruction, usually caused by an autoimmune process, leading to insulin deficiency. The great majority of type I patients develop the disease before 25 years of age. No islet cell antibodies are detected in some patients with similar clinical presentation so the etiology of the disease in those patients is unknown. Type II DM is characterized by insulin resistance in peripheral tissues and an insulin secretory defect from the β-cells. This more common type of diabetes is associated with family history, old age, obesity and lack of exercise (Reviewed in Report of the Expert Committee on the Diagnosis and Classification of Diabetes Mellitus, 1997; Barnett *et al.,* 1981; Newman *et al.,* 1987). DM in WFS results from selective β-cell lost with no evidence of autoimmunity.

The pancreatic β-cells are the insulin secreting cells that play a vital role in controlling blood glucose levels. Partial loss of β-cell function may be an etiological factor in the development of both type I and type II diabetes (Donath & Halban, 2004). Decreased β-cell mass may occur due to the disruption of the balance between the rate of proliferation and the rate of death of β-cells due to increased apoptosis (Rhodes, 2005). For example, in a study of human pancreatic tissue taken from autopsies, the frequency of β-cell apoptosis increased 10-fold in lean and 3-fold in obese type 2 diabetes cases compared with lean and obese controls respectively, while replication and neogenesis of β-cells was comparable across the experimental groups and their relevant control groups (Butler *et al.,* 2003).

Neurodegenerative disorders are characterized by a progressive loss or dysfunction of specific cellular populations in the central and peripheral nervous system. The most common of these are Alzheimer's disease (AD), Parkinson's disease (PD), and motor neuron disease which affect some 20 million people worldwide (Mayeux, 2003). These diseases usually have an onset

during middle or old age, occur sporadically or are inherited, and commonly involve aggregation and deposition of aberrant proteins as part their pathogenesis. The type and specific location of protein aggregates accounts for the variability in the clinical manifestations of these disorders (Skovronsky *et al.,* 2006).

In both diabetes and neurodegeneration, cell death, whether apoptotic, necrotic, or autophagic, is a key driver of the progression of disease, with several recognized triggers stimulating the activation of converging downstream pathways. These triggers include accumulation of misfolded proteins or protein aggregates, oxidative stress, and mitochondrial dysfunction. In turn, cellular responses are activated that attempt to restore cellular viability and homeostasis, but under persistent insult, eventually give in to cell death pathways. The following is an overview of some major triggers associated with cell death seen in the pathogenesis of diabetes and neurodegeneration.

1.3.1 ER dysfunction in pathogenesis of disease

The ER is the site of many crucial cellular activities such as the synthesis, folding, and trafficking of secretory, membrane, and ER resident proteins. ER stress, such as oxidative damage, disruption of ER calcium concentrations $[Ca^{2+}]_{ER}$ homeostasis, or aggregation of mutant proteins, causes an accumulation of misfolded proteins in the ER activating the unfolded protein response (UPR) (Paschen & Douthel, 1999). The UPR acts to restore ER homeostasis by activation of chaperone proteins, attenuation of global protein expression, and degradation of misfolded proteins. This occurs through a series of signaling pathways initiated by the dissociation of binding immunoglobulin protein (GRP78/BiP) from three master regulators of the UPR: PKR-like endoplasmic reticulum kinase (PERK, also known as eukaryotic translation

initiation factor kinase 2α kinase [EIF2AK3]), inositol-required enzyme 1 (IRE1), and activating transcription factor 6 (ATF6). As GRP78/BiP is sequestered by the accumulation of unfolded proteins in the ER lumin, these three regulators are free to become activated and send signals to initiate the UPR (Figure 1). Activation of PERK, which involves its homodimerization and autophosphorylation, leads to the phosphorylation of eukaryotic initiation factor 2 alpha (eIF2α), attenuating its normal function of initiating mRNA translation. IRE1, which also homodimerizes and autophosphorylates, excises a small intron in the pre-mRNA of the transcription factor X-box binding protein (*XBP-1*). The resultant protein then translocates to the nucleus where it is involved in the transcription of different protein folding chaperones that can alleviate ER stress (Lee *et al.,* 2003). The third UPR master regulator, ATF6, translocates to the Golgi apparatus where it is cleaved by proteases and is activated to also act as an important transcription factor for ER resident chaperones (Boyce & Yuan, 2006, Schroder & Kaufman, 2005; Lee *et al.,* 2003). The major regulatory factors involved in UPR are illustrated in Figure 1 (adapted from Boyce & Yaun, 2006; Schroder & Kaufman, 2005).

However, persistent assault on the ER results in the initiation of cellular death pathways (Boyce & Yuan, 2006; Lindholm *et al.,* 2006). In addition to promoting survival by global translational attenuation and transcriptional upregulation of ER chaperones, the major regulators of the UPR upregulate a proapoptotic response due to chronic ER stress. Phosphorylation of eIF2α inhibits the translation of most mRNAs but activates the translation of a small number of transcripts including ATF4, a transcription factor that activates the expression of the proapoptotic signaling molecule C/EBP-homologous protein (CHOP/GADD153), and GADD34, a component protein of an enzyme that facilitates the dephosphorylation of eIF2α thereby

promoting apoptotic pathways (Boyce & Yuan, 2006). The other two major regulatory components of the UPR, IRE1 and ATF6, have also been shown to upregulate proapoptotic pathways (Boyce & Yuan, 2006; Ron & Walter, 2007). The decision by the cell to undergo apoptosis or to continue the UPR to promote cell survival is poorly understood; however, it can be deduced that the balance between the two different cell fates depends on the severity and persistence of the assault on the ER by extracellular stressors or intracellular factors and the ability of the UPR to restore protein folding capacity.

Dysfunction of the UPR, or any of its components, has been associated with diseases such as neurodegeneration and diabetes. Wolcott-Rallison syndrome (WRS), a rare autosomal recessive disorder characterized by neonatal or early-infancy insulin-dependent nonimmune-related diabetes mellitus and epiphyseal dysplasia, is caused by disruption of *PERK* (Senee *et al.,* 2004, Delephine *et al.,* 2000). One study of WRS patients from 11 families identified a wide variety of mutations in *PERK*, including frameshift mutations, nonsense mutations, missense mutations, and splice-site mutations, all of which resulted in a truncated protein that is expected to lead to a complete loss of its kinase activity (Senee *et al.,* 2004). An *in vitro* assay to study the phophorylation activity of five of the resultant mutant proteins showed a complete absence of autophosphorylation and eIF2α phosphorylation except in one mutant (N665K) which showed residual levels of phosphorylation activity. Interestingly, the patient that carried the N665K mutation had a much later age of onset than the other patients (30 months vs. 6 months) (Senee *et al.,* 2004).
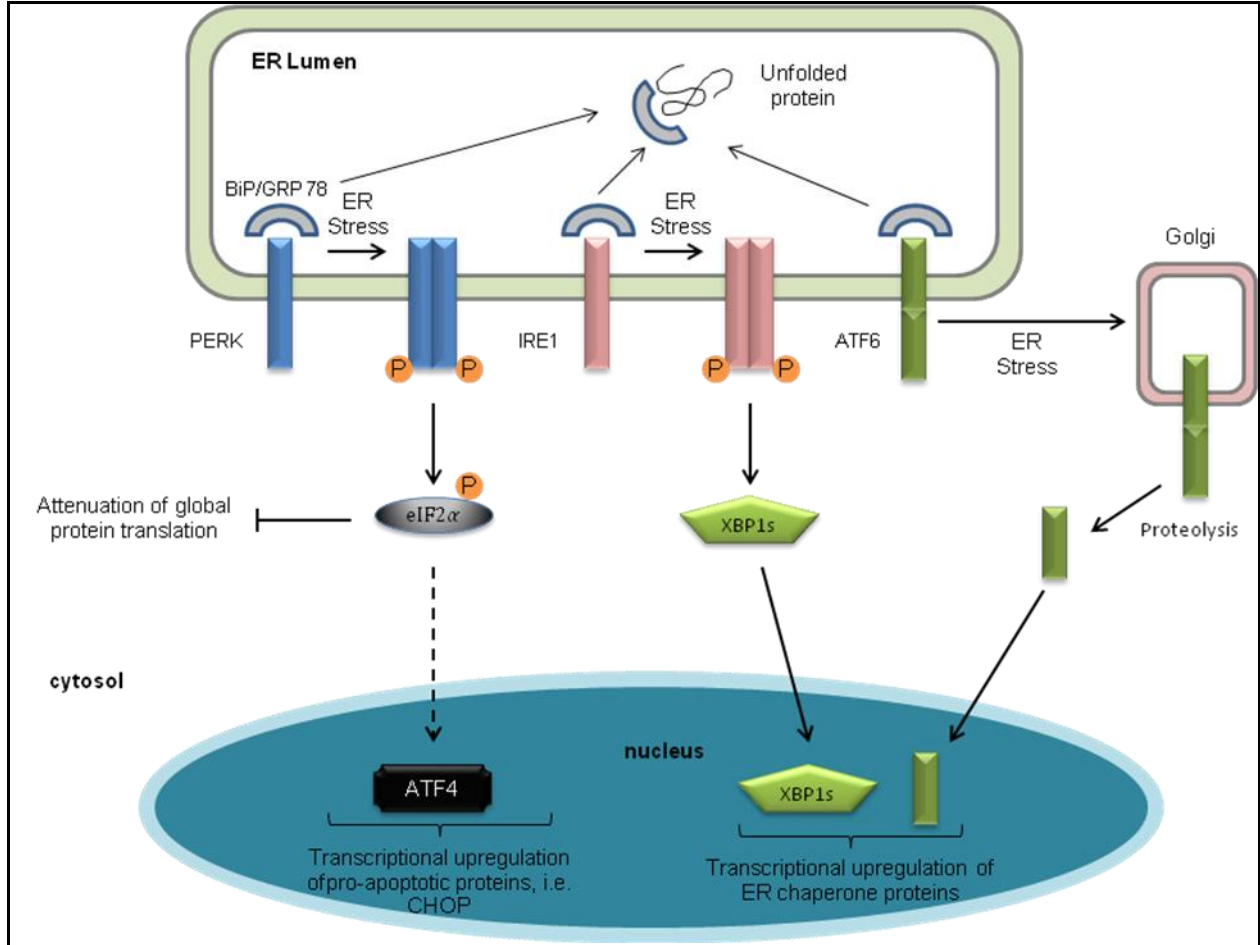
Figure 1. The unfolded protein response (UPR). Upon accumulation of misfolded proteins in the ER, BiP/GRP 78 dissociates from three master regulators of the UPR response, PERK, IRE1, and ATF6, which activate downstream molecular players involved in the response. Initially, the UPR acts to restore ER homeostasis by attenuating global protein translation to alleviate the ER from excessive protein processing, while promoting the expression of chaperone proteins that can assist with the removal or folding of misfolded proteins. However, after persistent ER stress, this response begins activating proapoptotic pathways, such as the upregulation of the transcription factor ATF4 responsible for expression of the major apoptotic molecule CHOP. Adapted from Boyce & Yaun, 2006; Schroder & Kaufman, 2005.

A transgenic mouse study in which the researchers altered the PERK phosphorylation site on eIF2α, impairing its ability to be phosphorylated and thus rendering it unable to respond to any ER stress, found that homozygous transgenic mice are born with severe β-cell deficiency by late embryonic development (Scheuner *et al.,* 2001). Heterozygote transgenic mice normally do not develop diabetes and have normal β-cells, but exhibit features of the "metabolic syndrome" associated with type 2 diabetes when they are exposed to a high fat diet (Scheuner *et al.,* 2005). In another study of *Perk* knockout mice, researchers also observed the development of diabetes due to progressive β-cell loss (Harding *et al.,* 2001). Mouse knockout studies of *Ire1* and *Xbp-1* showed that homozygous knockout of either gene in mice was embryonic lethal (Zhao & Ackerman, 2006).

Several neurodegenerative diseases, including AD, PD, and Huntington's disease (HD), are characterized by the accumulation and aggregation of misfolded proteins, which result in the activation of the UPR (Zhao & Ackerman, 2006). A study of postmortem brain tissue from AD patients showed upregulated levels of the UPR molecular chaperone BiP and increased phosphorylation of PERK. It was also observed that these two markers are also upregulated in cytologically normal-appearing neurons suggesting a role for the UPR early in AD neurodegeneration, initially playing a neuroprotective role but, after sustained activation, leading to neuronal death (Hoozemans *et al.,* 2005). Additionally, expanded polyglutamine (polyQ) repeats are implicated in several neurodegenerative diseases, such as HD and spinocerebellar ataxias, due to the accumulation of intracellular protein aggregates. Again, the upregulation of different components of the ER stress response is observed as part of the molecular signature of these polyQ neurodegenerative diseases (Lindholm *et al.,* 2006).

1.3.2 Calcium homeostasis and ER dysfunction

Ca^{2+} is an important signaling molecule in the cell, whose temporal and spatial regulation throughout the cell is vital for cell survival. The ER is the main cellular Ca^{2+} store having $[Ca^{2+}]$ concentrations that are 10^4 times greater than cytoplasmic $[Ca^{2+}]_C$. The maintenance of high $[Ca^{2+}]_{ER}$ is necessary for the function of ER resident chaperones in the folding of proteins, and for cellular Ca^{2+} signaling (Schroder & Kaufman, 2005; Verhratsky & Toescu, 2003). In neurons, $[Ca^{2+}]_{ER}$ regulation controls several facets of neuronal physiology including activity, growth and differentiation, synaptic plasticity, learning and memory, and activation of cellular degeneration pathways (Verhatsky, 2005, Berridge *et al.,* 2000). A disruption in Ca^{2+} homeostasis is known to contribute to cellular stress and trigger various forms of neurodegeneration (Missiaen *et al.,*2000; Verhratsky & Toescu, 2003). Highly active cells that depend on Ca^{2+} signaling and regulation for their function and viability, such as excitatory neuronal cells, skeletal muscle cells, and secretory pancreatic β-cells, are more vulnerable to a dysfunction of cellular Ca^{2+} regulation (Berridge *et al.,*2000).

Modulation of Ca^{2+} into and out of the ER is dependent on various ER membrane bound proteins including the family of uptake channels called the SR/ER Ca^{2+}-ATPases (SERCA pumps), and the two release channel families: the inositol-1,4,5-triphosphate receptor (IP$_3$R) family and ryanodine receptor (RyR) family (Clapham, 1995; Berridge *et al.,*2000). A mutation or abnormalities in any of these proteins, or any proteins that associate with these channel proteins, often lead to disease, such as diabetes mellitus and neurodegenerative disorders (Missiaen *et al.,*2000). In Alzheimer's disease, for example, dysregulation of ER Ca^{2+} can occur due to mutations in two integral ER membrane proteins, known as presenilin-1 (PS1) and presenilin-2 (PS2), which are expressed in neurons. PS1 and PS2 affect the stimulation and

normal function of both IP$_3$Rs and RyRs. A study of PS1 in the *Xenopus oocyte* expression system showed that PS1 plays a role in modulating IP$_3$-mediated Ca^{2+} ER release and that mutant PS1 causes a greater stimulation of IP$_3$R Ca^{2+} release compared with wild-type PS1 (Leissring *et al.,*1999).

More recently, a study by Cheung *et al.* (Cheung *et al.,*2008) of two Familial Alzheimer's Disease (FAD) associated mutant PS1 and PS2 proteins showed a stimulatory effect of these two mutants on IP$_3$R channel activity resulting in a dysregulation of Ca^{2+} homeostasis and signaling, highlighting a possible etiological element in the pathogenesis of AD. Another study of fibroblasts derived from AD patients identifies enhanced IP$_3$R mediated activity as a highly predictive diagnostic feature of AD (Hirashima *et al.,* 1996). These studies, along with many others, have invoked a mitochondrial "Ca^{2+} overload" hypothesis to explain the high levels of Ca^{2+} seen in mutant presenilin expressing cells in the development of AD (Stutzman, 2005, Cheung *et al.,* 2008).

AD is a well studied example of a long list of diseases that exhibit abnormal Ca^{2+} homeostasis as part of their pathophysiology (Missiaen *et al.,* 2000). The list includes diseases of muscle, skin, eyes, the nervous system, the cardiovascular system and pancreatic β-cells (Missiaen *et al.,*2000; Berridge *et al.,*2000). All of these diseases have a disruption of some aspect of cellular Ca^{2+} homeostasis, whether it is Ca^{2+} sensors on the cell membrane or Ca^{2+} release channels on the ER membrane. This highlights the importance of Ca^{2+} signaling and regulation for the normal function of several different types of cells, as well as the large number of molecular players involved in Ca^{2+} homeostasis.

1.3.3 Oxidative stress in disease pathogenesis

Oxidative stress occurs when the cellular levels of free radicals exceed the capacity of the antioxidant defenses to counteract the molecular effects of these molecules. Free radicals are a broad group of highly reactive molecules that include reactive oxygen species (ROS), reactive nitrogen species (RNS), and reactive chlorine species (RCS) (Rosen *et al.,*2001). The most common member of ROS is the one-electron product of oxygen reduction, the superoxide anion radical (O_2^-), which acts as a precursor to many other ROS molecules including hydrogen peroxide (H_2O_2), the highly reactive hydroxyl radical (OH^-), as well as members of the RNS family (Rosen *et al.,*2001; Evans *et al.,*2002; Bayir & Kagen*,* 2008). A prominent member of the RNS family of free radicals is nitric oxide (NO), which can interact with O_2^- to form peroxynitrite ($ONOO^-$), another powerful oxidant (Rosen *et al.,* 2001; Newsholme *et al.,* 2007; Figueroa-Romero *et al.,*2008). These molecules, under normal physiological conditions, act as cellular signaling molecules in growth and differentiation pathways (Valko *et al.,* 2007; Newsholme *et al.,* 2007) as well as mediators of immune responses (Rosen *et al.,* 2001; Valko *et al.,* 2007).

Free radicals are normally produced in cells as a byproduct of mitochondrial respiration during the process of oxidative phosphorylation. During oxidative phosphorylation, energy carried by electrons from reducing substrates, such as NADH and $FADH_2$, are used by three of the four respiratory chain complexes, complexes I, III, and IV, to pump protons out of the mitochondrial matrix, creating an electrochemical gradient across the mitochondrial inner membrane. Electrons are transferred from each complex via the electron transporters, ubiquionone and cytochrome c, to complex IV where their final destination is the reduction of

molecular oxygen (O_2) to H_2O. The resulting electrochemical gradient drives the synthesis of ATP, the energy currency of cells, from ADP via ATP synthase (complex V).

One to four percent of O_2 in mitochondrial respiration, however, is incompletely reduced to O_2^-, due to electron "leakage" from the respiratory chain complexes, primarily from complex I and complex III (Bayir & Kagan, 2008; Figueroa-Romero *et al.,* 2008; Orrenius *et al.,* 2007). Superoxide anion produced in complex I are predominantly released in the matrix, while complex III releases O_2^- to both sides of the mitochondrial inner membrane (Figueroa-Romero *et al.,*2008; Orrenius *et al.,* 2007). Due to its charged nature, O_2^- does not readily diffuse across mitochondrial membranes, but its uncharged molecular descendants, such as H_2O_2, can easily cross these membranes (Figueroa-Romero *et al.,* 2008). Outside the mitochondria, NADPH oxidases, xanthine oxidases, and cytochrome P450-dependent oxygenases are additional sources of superoxide anion production in the cell (Newsholme *et al.,* 2007; Bayir & Kagan, 2008).

To offset the accumulation of ROS/RNS production in the cell, the mitochondria possess multiple antioxidant defenses systems, including superoxide dismutase (SOD), glutathione peroxidase (GPX), thioredoxin and soluble antioxidants, such as vitamins C and E (Orrenius *et al.,*2007). SODs are specialized enzymes that are responsible for converting superoxide anion to hydrogen peroxide. Copper zinc SOD (Cu, Zn-SOD), also known as SOD1, acts to eliminate O_2^- in the cytosol and the intermembrane space of mitochondria. O_2^- in the mitochondrial matrix is eliminated by manganese SOD (Mn-SOD), also called SOD2. After O_2^- is converted to H_2O_2, GPX reduces the H_2O_2 molecule to water and molecular oxygen by using glutathione, or, if not degraded, H_2O_2 can interact with transition metals to produce the volatile OH^- (Maritim *et al.,* 2003). The physiological importance of SOD2 has been illustrated in *Sod2* homozygous knockout mice which die shortly after birth (Li *et al.,* 1995), compared with the phenotypically

healthy *Sod1* knockout mice (Reaume *et al.,* 1996). SOD2's vital role as an antioxidant that promotes organism survival is also seen in a *Sod2* knockdown *Drosophila* model, in which *Sod2* knockdown in the musculature alone is sufficient to cause shortened lifespan and accelerated locomoter decline (Martin *et al.,* 2009). The protective effects of SOD2 have been demonstrated in several models including transgenic *Sod2* overexpressing mice, in which myocardial necrosis after myocardial injury/reperfusion was significantly attenuated (Valko *et al.,* 2007), and by the resistance of cultured cells transfected with *Sod2* cDNA to the effects of the potent oxidative stressor, paraquat (Mates, 2000).

At the cellular level, ROS generation can cause damage to macromolecules, including nucleic acids, phospholipids, and proteins, altering or completely disabling their normal role and function. The highly potent OH- can react with all components of the DNA molecule, incurring damage on both the purine and pyrimidine bases as well as the deoxyribose backbone (Halliwell & Gutteridge, 1999). Additionally, oxidative damage to DNA may induce single and double strand breaks, as well as crosslinks to other molecules. Permanent DNA modification due to reactivity with ROS are mutagenic and contribute to carcinogenesis, age related illnesses, and neurodegenerative diseases (Bohr, 2002).

Another effect of ROS is the peroxidation of polyunsaturated fatty acid residues in phospholipids, also induced by the potent OH- (Orrenius *et al.,* 2007). This may cause damage to the lipid bi-layer of the cell membrane and cause lysosomal fragility (Orreneus *et al.,* 2007). Byproducts of lipid peroxidation include malondialdehyde (MDA) and 4-hydroxy-2-nonenal (HNE), both of which are toxic and exhibit mutagenic and carcinogenic potential (Valko *et al.,*2007).

Proteins are also vulnerable to the deleterious effects of exposure to free radicals. Studies in which amino acids and peptides were exposed to different sources of ROS and RNS show that all amino acid residues, particularly cysteine and methionine residues, are susceptible to oxidative damage (Stadtman, 2004). Direct oxidation of particular amino acids, such as lysine, arginine, proline, and threonine, in a polypeptide chain promotes the formation of protein carbonyls, altering the structure of a protein, resulting in its partial or complete unfolding . This, in turn, causes the protein to be unable to function and promote its proteolytic degradation (Orrenius *et al.,* 2007). ONOO$^-$ which is derived from the interaction between O_2^- and NO, is highly toxic to proteins by having the ability to nitrosate cysteine sulfhydryl groups, nitrate tyrosine and tryptophan residues of proteins, and oxidize methionine residues to methionine sulfoxide. Nitration of tyrosines, is an irreversible process that interferes with the phosphorylation or adenylation of tyrosine residues of protein, thus compromising their normal function (Stadtman, 2004). These effects have even been reported to occur on the respiratory chain complexes and cytochrome c, leading to their inactivation (Bayir and Kagan, 2008).

The above discussion of the elements involved in the generation of cellular oxidative stress, its effects on the macromolecules of the cell, and examples of antioxidant defense enzymes is by no means a comprehensive examination of this highly complicated and intricate feature in living cells (Figure 2). It is meant to illustrate some of the main components involved in the cell's balancing act between the rate of production of ROS and their derivatives, and the rate of neutralization or removal of these harmful molecules by antioxidant defenses. The disruption of this balance, due to increased ROS production or an aberration in the normal function of antioxidant defenses, damages macromolecules and interferes with cellular processes,
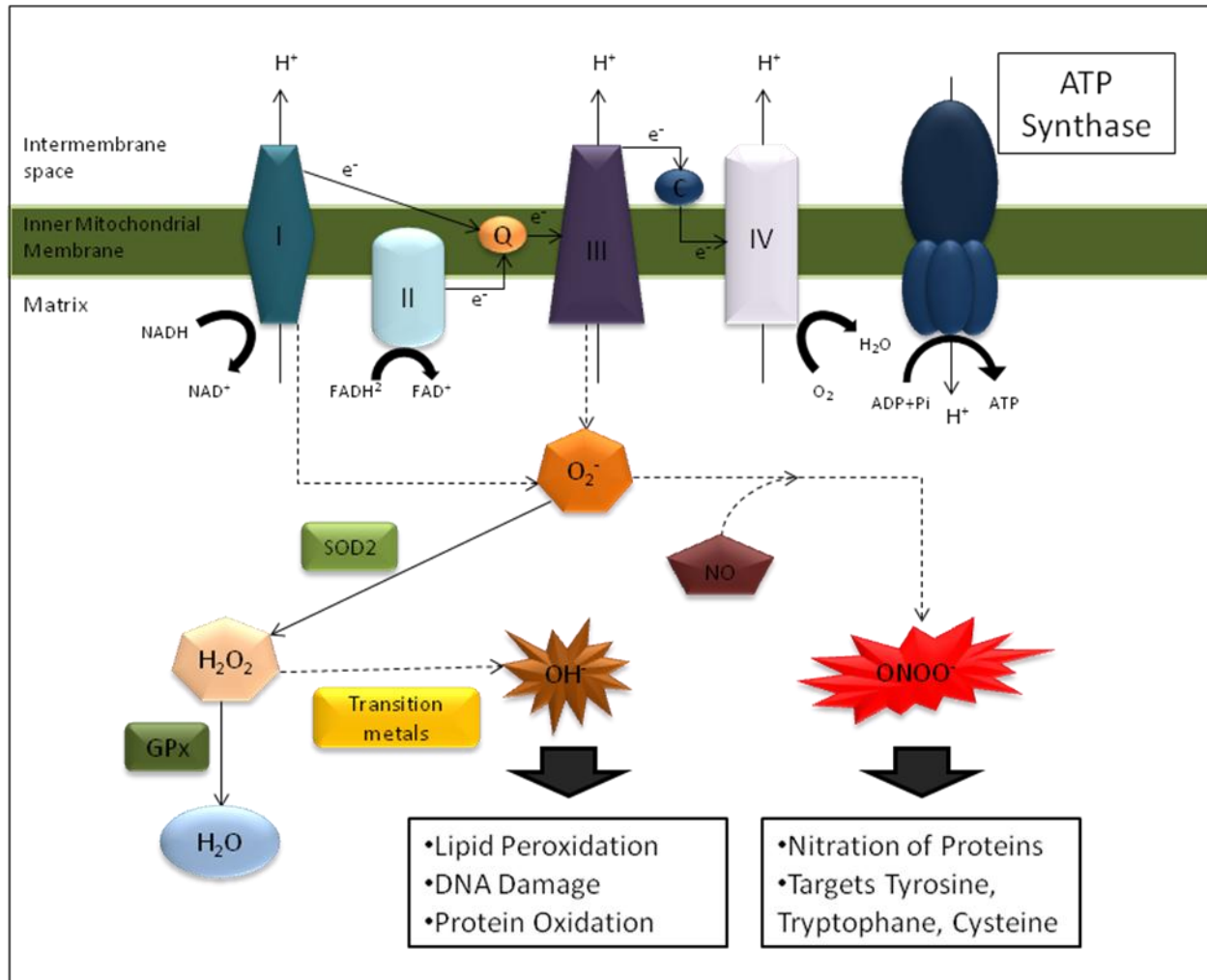
Figure 2: Mitochondrial oxidative stress. In the mitochondria, superoxide anion (O^-) is produced by mitochondrial respiratory complexes I and III during oxidative phosphorylation. Superoxide is detoxified by superoxide dismutase (SOD) to hydrogen peroxide (H_2O_2). Glutathione peroxidases (GPx) convert hydrogen peroxide to water, but transition metals can also react with hydrogen peroxide to produce the highly reactive hydroxyl radical (OH^-). Nitric oxide (NO) generated from nitric oxide synthase (not shown) can compete with SOD to react with superoxide to form peroxynitrite ($ONOO^-$). The hydroxyl radical causes damage to cellular macromolecules including lipids, nucleic acids, and proteins. Peroxynitrite causes oxidation or nitration or specific residues of amino acids in proteins often affecting their stability and function. C, cytochrome c; Q, ubiquinone. (Adapted from Bayir & Kagan, 2008; Green *et al*., 2004).

which will ultimately lead to cell death. Chronic oxidative stress is thought to be a major contributor to aging and pathogenesis of disease, including diabetes and neurodegeneration.

There is an increasing amount of experimental and clinical evidence that oxidative stress plays a role in the onset and progression of DM and its complications. Clinical evidence shows the increase in the levels of oxidative stress markers in plasma (Nourooz-Zadeh *et al.,*1997) and urine (Davi *et al.,*1999) of type II DM patients. While type I DM is attributed to the autoimmune destruction of pancreatic β-cells, the more common type II DM is characterized by excessive hepatic glucose production (hyperglycemia), decreased insulin secretion, and insulin resistance (Evans, 2002). In many instances, hyperglycemia has been shown to precede the onset of DM, and actually lead to its development (Rolo *et al.,*2006). This is mediated through the oxidative stress-related damage that hyperglycemia exerts on cells and tissues, including increased production of mitochondrial ROS, nonenzymatic glycation of proteins, and glucose autoxidation (Evans *et al.,*2002). Evidence of hyperglycemia induced ROS was presented by Nishikawa *et al.* (2000) where bovine endothelial cells exposed to hyperglycemia exhibited increased ROS formation and activated the stress inducible nuclear factor-κB (NF-κB) pathway. Furthermore, overexpression of *SOD2*, the mitochondrial inner membrane uncoupler protein UCP1, or treatment with an uncoupler molecule, all alleviated the hyperglycemia-induced ROS production and suppressed the stress inducible pathways (Nishikawa *et al.,*2000). In another study using nondiabetic rats, high glucose exposure led to a significant increase in muscle protein carbonyl content, an oxidative stress marker, as well as elevated levels of MDA and HNE, both of which are markers of lipid peroxidation (Haber *et al.,*2003). This increase in ROS was also seen in adipocytes of a high-fat diabetes mouse model compared with control mice, along with an increase of basal glucose uptake in the high-fat mice (Talior *et al.,*2003).

An elevated level of free fatty acids (FFA), another characteristic component in DM development, also contributes to oxidative stress via increased mitochondrial uncoupling and β-oxidation (Evans *et al.,*2002). Piro *et al.,*(2002) showed increased apoptosis, possibly due to ROS induced signaling, in rat pancreatic islets treated with high levels of FFA, an effect that was exacerbated with co-treatment with high levels of glucose. Oxidative stress was thought to induce the apoptosis since nicotinamide, a known antioxidant, is able to suppress apoptosis in FFA treated cells (Piro *et al.,*2002). This hypothesis is reinforced by the observation of mitochondrial uncoupling and increased ROS production following treatment of rat pancreatic islets with the long chain fatty acid sodium palmitate (Carlsson *et al.,*1999) These studies lead to the proposal that elevated levels of blood glucose and/or FFA play a key role in insulin resistance and β-cell dysfunction, mediated in part by oxidative stress activated stress-sensitive pathways, including nuclear factor-κB (NF-κB), p38 MAPK, NH2-terminal Jun kinases/stress-activated protein kinases, advanced glycosylation end-products (AGE)/receptor for AGE (RAGE), and protein kinase C (PKC) (Evans *et al.,*2002; Evans *et al.,*2003; Newsholme *et al.,*2007).

It is important to note that pancreatic β-cells are highly susceptible to the effects of ROS due to their high mitochondrial ROS production and relatively low levels of antioxidant capacity when compared to other cell types (Robertson *et al.,*2004, Newsholme, 2007). Their high mitochondrial ROS production is a result of their activity in glucose-stimulated insulin secretion (GSIS), which enhances ROS production as a byproduct of increased ATP production and Ca^{2+} influx into the cell (Newsholme *et al.,*2007). As for antioxidant defenses, β-cells have been reported to have lower levels of SOD1, SOD2, and GPX (Grankvist *et al.,*1981) compared with other cell types. In turn, these two components, under hyperglycemia, increased FFA conditions, or genetic predisposing factor, render the pancreatic β-cells more susceptible to the deleterious

effects of ROS, enhancing their dysfunction and destruction. This will lead to disruption in insulin secretion and a rapid progression of DM and its complications.

Cells of the brain, notably neurons, are also vulnerable to the effects of oxidative stress due to their high metabolic rate, diminished capacity for cellular regeneration, rich composition of fatty acids prone to peroxidation, high intracellular concentrations of transition metals capable of catalyzing OH^- formation, and relatively low levels of antioxidants (Andersen, 2004; Reynolds *et al.,*2007). In samples of human frontal cortex, age related cognitive decline is accompanied by a reduction of genes involved in synaptic plasticity, vesicular transport, and mitochondrial function, followed by an induction of stress response, antioxidant, and DNA repair genes (Lu *et al.,*2004). Interestingly, promoters of age-downregulated genes were more sensitive to oxidative damage, induced by H_2O_2 treatment of a human neuroblastoma cell line, compared with age-upregulated genes (Lu *et al.,*2004). Evidence of oxidative damage has been well documented in patients with age related neurodegenerative disease in a region specific manner, including the hippocampus of AD patients (Hensley *et al.,*1998; Butterfield *et al.,*2002), the substantia nigra of PD patients (Dexter *et al*., 1989), and the spinal fluids of amyotrophic lateral sclerosis (ALS) patients (Pedersen *et al.,*1998). Familial forms of such neurodegenerative disorders may include aberration in genes involved in protection against oxidative stress, such as *PARK7* which encodes for DJ-1 in PD, or gene products that lead to an increase in oxidative stress, such as SOD1 in ALS and β-amyloid precursor protein (APP*)* in AD (Lin & Beal, 2007). These findings led researchers to investigate the role of oxidative damage in the onset and progression of neurodegenerative diseases.

In AD patients, oxidative damage occurs early during the progression of disease and precedes the accumulation of amyloid-β (Aβ) deposits, a characteristic feature of AD brains

22

(Nunomura *et al.,*2001). Patrico *et al*. (2001) found similar findings in a transgenic *App* mouse model, with increasing age-dependent lipid peroxidation preceding Aβ accumulation in the hippocampus, but not the cerebellum, of transgenic animals compared with wild-type animals. Evidence for oxidative stress directly contributing to the pathogenesis of AD was provided in an *in vitro* study using fetal guinea pig neurons, in which treatment with increasing concentrations of H_2O_2 resulted in increased levels of Aβ deposits and induction of apoptosis (Ohyagi *et al.,*2000). This direct casual relationship between oxidative stress and Aβ plaque formation was reinforced in a cross between an *App* transgenic mouse line with a *Sod2* knockout mouse line. *App* transgenic mice which were also heterozygous *Sod2* knockouts developed increased Aβ deposits than *App* transgenic only mice at different time points (Li *et al.,*2004).

Parkinson's disease, characterized pathologically by loss of pigmented neurons in the substantia nigra and the presence of Lewy bodies, appears to develop from mitochondrial dysfunction with a possible oxidative stress component. This is based on findings that revealed the inhibition of mitochondrial complex I, which was suggested to stimulate ROS production and lead to the depletion of the antioxidant glutathione in the substantia nigra of PD patients (Schapira *et al.,*1989). Several genes implicated in the development of PD are involved in the mitochondria, including *DJ-1*, *PINK*, and parkin (Lin & Beal, 2007). *DJ-1*, which protects against oxidative stress induced cell death, is associated with an autosomal recessive juvenile form of PD (Lin & Beal, 2007). Primary cortical neurons from *Dj-1* knockout mice are hypersensitive to the effects of a complex I inhibitor but not that of a nonoxidant stimulus (Kim *et al.,*2005). In *Drosophila*, *DJ-1* (*Dj-1b* in flies) deletion mutants were also more sensitive to the effects of another oxidative stressor, paraquat (Meulener *et al.,*2005). Mutational analysis of *Dj-*

1b in *Drosophila* revealed that its protective function against oxidative stress is hampered by oxidation of a conserved cysteine residue (C104) seen in aged flies (Meulener *et al.,*2006).

These studies implicate oxidative damage in the onset and progression of neurodegenerative diseases, providing evidence for direct links between oxidative stress and pathogenesis of AD and PD. Other neurodegenerative diseases with similar links are ALS, in which mutant SOD1 expression results in an increase in ROS expression (Mattiazzi *et al.,*2002), and Friedreich's ataxia, which exhibits a hampered antioxidant response to oxidative stress (Chantrel-Groussard *et al.,*2001). Although the mode of accumulation of oxidative stress may differ in the various types of neurodegenerative diseases, or even in different forms of the same disease, the stress inducible pathways that are activated are similar, and after persistent insult, they lead to the same fate: cell death (Valko *et al.,*2007; Lin & Beal, 2006).

1.3.4 Ca^{2+} and oxidative stress

In addition to its role in cellular respiration, the mitochondrion acts as a Ca^{2+} buffering organelle. The proximity to the ER, where Ca^{2+} is in high concentrations and its use in cellular signaling, makes the mitochondria an important site of intracellular Ca^{2+} handling. Ca^{2+} is transported into mitochondria via a low-affinity uniporter driven by the force of the electrical gradient across the mitochondrial membrane, and is released by Na^+ dependent and Na^+-independent efflux mechanisms (Missiaen *et al.,*2000; Duchen *et al.,*2008). Although mitochondria have a lowered affinity for Ca^{2+} compared with the ER, mitochondrial function is also dependent on Ca^{2+} for signaling and activation of some of its resident proteins. Mitochondrial Ca^{2+} uptake activates three major rate limiting enzymes of the TCA cycle, namely pyruvate dehydrogenase, isocitrate dehydrogenase, and oxoglutarate dehydrogenase, which in

turn leads to an increase in ATP production fueled by the increase in NADH (Giacomello *et al.,*2007; Szabadkai & Duchen, 2008).

Due to proximity of the mitochondria to the ER Ca^{2+} release channels, mitochondria are sensitive to ER Ca^{2+} fluctuations. Abnormally high levels of ER Ca^{2+} release increase Ca^{2+} loading into the mitochondria which will lead to opening of the permeability transition pore (PTP) causing a release of Ca^{2+} into the cytoplasm and activating cell death pathways (Pinton *et al*., 2008; Giacomello *et al.,*2007; Ott *et al.,*2007). The threshold for mitochondrial PTP opening due to increases in mitochondrial Ca^{2+} concentration decreases in the presence of oxidative stress (Ott *et al.,*2007). Jacobson and Duchen (2001) showed that ROS and induction of ER Ca^{2+} release were both necessary events for mitochondrial PTP opening in rat primary astrocytes. The formation of PTPs has detrimental effects on mitochondria, causing a collapse of the mitochondrial membrane potential, rapid depletion of ATP levels, increased ROS production, eventually leading to necrosis (Giacomello *et al.,*2007, Duchen *et al.,*2008). Apoptotic pathways can be also be triggered by the same type of insults if PTP openings are limited to a subpopulation of mitochondria in the cell, and the remaining organelles are still able to produce enough ATP to support the more subtle and controlled form of cell death (Ott *et al.,*2007; Giacomello *et al.,*2007).

Ca^{2+} influx into pancreatic β cells is the primary driver of the GSIS mechanism, but can also enhance mitochondrial and NADPH oxidase-dependent ROS production (Newsholme *et al.,*2008). This represents an additional component of ROS exposure to the already increased vulnerability of β cells to oxidative stress. An increase in intracellular $[Ca^{2+}]$ in neurons, whether as part of neuronal signaling or due to aberrant protein aggregation, can also trigger NO and ROS production (Halliwell, 2006). On the other hand, oxidative stress can also disrupt Ca^{2+}

homeostasis by lipid peroxidation and protein oxidation, rendering membranes 'leaky' to Ca^{2+}, affecting mitochondrial Ca^{2+} buffering capacity, and increasing intracellular [Ca2+] to toxic levels (Halliwell, 2006; Ott *et al.,*2007). Oxidative stress and a disruption of Ca^{2+} homeostasis appear to act synergistically in causing different forms of cell death, with both having the capability of causing the other.

1.4 Pathogenesis in WFS1

As mentioned above, the ER stress-mediated apoptotic pathway results when the ER stress coping mechanisms, namely the unfolded protein response (UPR) fail to sustain cells under increasing levels of ER stress. In addition, several animal models with deficiencies that disrupt the functionality or expression of UPR proteins exhibit loss in β-cell mass and develop diabetes. Based on this information and the fact that wolframin, the *WFS1* gene product, is localized in the ER membrane, several studies using *in vitro* and *in vivo* models investigated a possible link between WFS1 and ER-stress mediated apoptosis to explain the underlying molecular pathogenesis of WFS.

Ishihara *et al.* (2004) inactivated the *Wfs1* gene by disrupting exon 2 in mice by direct gene targeting via homologous recombination. They did not observe WFS1 protein expression in pancreatic islets and brains of homozygous mutant mice ($Wfs1^{-/-}$). $Wfs1^{-/-}$ mice exhibit impaired glucose homeostasis and progressive β-cell loss that is also observed in WFS patients. The authors attributed the pathophysiological basis of diabetes in WFS to insufficient insulin secretion due to progressive β-cell loss via apoptosis and impaired stimulus-secretion coupling in β-cells (Ishihara *et al.,*2004).

WFS1 has increased levels of expression in isolated pancreatic islets (Yamaguchi *et al.,*2004), human fibroblasts (Ueda *et al.,*2005), pancreatic β-cell derived MIN6 cells (Ueda *et al.,*2005), and Ins2 $^{96Y/Y}$ cells derived from a juvenile diabetes mouse model (Ueda *et al.,*2005), in response to ER stress inducing chemicals, such as thapsigargin and dithiothreitol, in the former three cell types and increased insulin expression in the Ins2 $^{96Y/Y}$ cells. Ueda *et al.* (2005) also carried out *WFS1* promoter luciferase reporter assays that revealed an increase in *WFS1* promoter activity in response to the aforementioned ER stressors. Furthermore, Fonseca *et al.* (2005) showed that mouse fibroblasts with homozygous mutations in either one of two major regulatory UPR proteins, *Ire1α* or *Perk*, results in attenuation of *Wfs1* induction by ER stressors. In addition, *Wfs1* knockdown in a β-cell line, INS-1 832/13, results in increase expression of several UPR markers including BiP, spliced *Xbp-1*, and total *Xbp-1* mRNA (Fonseca *et al.,*2005). Similar results were observed in pancreatic islets derived from *Wfs1*-deficient mice and *Wfs1*-deficient MIN6 clonal β-cells along with an increase of apoptosis, reduction of BrdU incorporation, and increase expression of the cell cycle inhibitor p21^{CIP1} (Yamada *et al.,*2006). Taken together, this data demonstrates that *WFS1* plays a role in ER homeostasis (Yamaguchi *et al.,*2004, Ueda *et al.,*2005, Fonseca *et al.,*2005, Yamada *et al.,*2006), particularly in pancreatic β-cells, and is an important regulator of the UPR (Fonseca *et al.*, 2005, Yamada *et al.,*2006). Thus, homozygous mutations in *WFS1* lead to an inability to cope with chronic ER stress resulting in impaired function and proliferation, and increased apoptosis in β-cells which, in turn, contribute to disease pathogenesis (Yamada *et al.,*2006).

Wolframin is shown to play a role in Ca^{2+} homeostasis in cells (Osmani *et al.,*2003 and Takei *et al.,*2006), which is consistent with it being a transmembrane protein localized in the ER, the main intracellular calcium store. Using Fura-2 staining to detect [Ca^{2+}]$_i$, it was shown that

Xenopus tropicalis oocytes injected with an expression vector carrying human *WFS1* cDNA showed significantly higher $[Ca^{2+}]_i$ than sham injected oocytes and oocytes injected with a vector carrying a R456H WFS1 mutant (Osmani *et al.,*2003). In addition, wolframin is observed to increase the outward current in microsomal membrane preparations from *WFS1* overexpressing oocytes, which were repressed by the addition of divalent ions such as Ca^{2+} and Mg^{2+}. It also increased IP_3 sensitivity in the ER calcium-releasing IP_3 channels in those membranes (Osmani *et al.,*2003).

A second study showed that *WFS1* knockdown HEK293 cells exhibited lower $[Ca^{2+}]$ release with thapsigargin treatment, an inhibitor of SERCA pumps, as detected by Fura-2 staining, and decreased calcium concentration levels in the ER ($[Ca^{2+}]_{ER}$) as detected by using an ER-targeted Ca^{2+}-sensitive photoprotein aequorin (Takei *et al.,*2006). Another experiment that measured the amount of $[Ca^{2+}]_{ER}$ uptake showed a lower rate and concentration of uptake in *WFS1* knockdowns (Takei *et al.,*2006). These studies implicate a role for wolframin in Ca^{2+} homeostasis in cells, possibly by modulating either ER Ca^{2+} - releasing channels, such as IP3 channels (Osmani *et al.,*2003), or ER Ca^{2+} uptake channels, such as the SERCA pump channels (Takei *et al.,*2006). Since protein folding chaperones require Ca^{2+} for the function, a dysfunction in Ca^{2+} homeostasis can result in an increased level of stress in the ER due to the accumuluation of unfolded proteins, activating the UPR and, after persistent Ca^{2+} mishandling, can trigger apoptotic pathways.

1.5 Aims and Rationale of Study

Wolfram Syndrome is a debilitating genetic disorder in which affected individuals suffer from the early and rapid onset of diabetes mellitus and optic atrophy followed by a slew of

complications and death at a mean age of 30 years. In addition, first degree relatives of affected individuals have an increased risk for diabetes, hearing loss, and psychiatric illnesses. At the beginning of this study, only one gene, *WFS1*, had been cloned for Wolfram syndrome, however several studies reported that not all affected individuals had mutations in that gene. Locus heterogeneity was confirmed by El-Shanti's group (2000) who identified the WFS2 locus by showing linkage between WFS and the 4q22-24 locus in three consanguineous Bedouin families. Kanki & Klionsky (2009) categorize Wolfram syndrome patients into two groups, WFS1 group for those carrying mutations in the *WFS1* gene, and WFS2 group for those carrying the mutation in the WFS2 critical region identified in El-Shanti *et al*., (2000), which we discovered to be *CISD2*.

The goal of the present study was to identify and characterize the *CISD2* gene in the locus identified by El-Shanti *et al*. (2000). Identification of the gene was carried out using mutational screening. Once the gene was found and the disease causing mutation was identified, our focus turned to understanding more about this gene, its protein product and how its dysfunction leads to the disease phenotype. The characterization of the *CISD2* gene entailed identification of its tissue expression pattern, subcellular localization, and whether it interacts with *WFS1*. To understand the pathogenesis associated with *CISD2*, knockdowns of the *CISD2* gene in transformed cell lines derived from tissues or cells affected by the disease, namely pancreatic β-cells and neuronal cells, were created. The effect of the knockdown of the *Wfs2* gene in these cells was studied. Our hypothesis was that *CISD2* deficiency in the cells would increase cell death due to increased apoptosis, similar to what is seen in *WFS1* mutants. Other modes of cell death, such as autophagy, were also investigated. In addition, we hypothesized that cell death occurred due to the increase in ER stress due to Ca^{2+} dysregulation and a possible role

of the *CISD2* gene in the UPR, similar to what is seen in *WFS1* deficiency. If our hypothesis was found to be incorrect we planned to investigate other modes of disease pathogenesis that may be involved in the etiology and progression of WFS2, such as oxidative stress. Understanding the underlying molecular mechanisms involved in the progression of WFS2, will not only help explain the pathogenesis of this disorder, but will also shed light on the mechanisms of related common complex disorders such as diabetes and neurodegeneration.

CHAPTER 2

MATERIALS AND METHODS

Cell Culture

Human lymphoblastoid cells and INS1 rat pancreatic insulinoma cells (a gift from Dr. Les Satin) were maintained in RPMI 1640 with L-glutamate (Invitrogen) supplemented with 10% fetal bovine serum (FBS). P19 mouse embryonic carcinoma cells were grown in α-minimum essential medium (α-MEM) (Invitrogen) supplemented with 7.5% bovine calf serum, 2.5% FBS, and 50 μg/ml gentamycin. HEK293 human embryonic kidney cells and N1E115 mouse neuroblastoma cells were maintained in Dulbecco's Modified Eagle's Medium (DMEM) (Invitrogen) supplemented with 10% FBS and 100 unit/ml penicillin and 100 μg/ml streptomycin. All cell lines were maintained in 5% CO_2 at 37°C. P19, HEK293, INS1 and N1E115 cells were maintained in the described media without antibiotic supplementation just prior to transfection.

SSCP Analysis

Primer sets were individually optimized for single-band amplification. PCR was performed in 25.0 μl reactions with 100 ng of DNA, 1 X PCR buffer (GeneChoice), 0.2 mM dNTPs, 0.5 pmol/μl of each primer, and 1 U of Taq polymerase (GeneChoice).For SSCP samples were prepared by mixing 7 μl of PCR products with 3 μl SSCP loading dye (23.75 M formamide, 20 mM EDTA, 0.25 μg/ml xylene cyanol, and 0.25 μg/ml bromophenol blue), were denatured at 95°C for 5 minutes, and were quickly cooled on ice. Three samples were run for each primer set: the patient PCR product, the control PCR product, and the patient plus control PCR products. Denatured samples were run through a 10% (49:1) acrylamide:bis-acrylamide gel (National

Diagnostics) with 1× Tris-borate EDTA (TBE) and 10% glycerol either at 8 Watts for 5 hours at 4°C or at 3 Watts for 16 hours at 4°C after a 30-minute prerun. Gels were stained in SYBR Gold (Molecular Probes) diluted 1:10,000 in 1x TBE, in accordance with the manufacturer's protocol.

Expression Vector Construct and Transfection

Two mammalian expression vectors containing a FLAG tagged *CISD2* cDNA were constructed, with one having the FLAG on the N-terminus and the other on the C-terminus. The FLAG tags with 5' overhang restriction enzyme ends were generated using oligonucleotides and inserted into the destination vector pDEST26 (Invitrogen). For the N-terminus FLAG tag, the primers were 5'-GGACCATGGCGTACTACGACTACAAAGACGATGACGACAAGT-3' and 5'-GCGGACCATGGCGTACTACGACTACAAAGACGATGACGACAAGTCTAG-3' which create a *SacII* site at the 5' end and an *XbaI* site at the 3' end. For the C-terminus FLAG tag, the primers were 5'-GTACAAAGTGGTTGACTACAAAGACGATGACGACAAGTGAGACGT-3' and 5'-AAAGTGGTTGACTACAAAGACGATGACGACAAGTGAG-3', which create a BsrGI at the 5' end, then an attB2 site which is upstream of the FLAG sequence, followed by a stop codon, and an *AatII* site at the 3' end.

For the N-terminus FLAG construct, the FLAG tag sequence was cloned into pDEST 26 using *SacII* and *XbaI* sites. For the C-terminus FLAG-tag construct, a fragment from pDEST 26 was excised using *SalI* and *HindIII* and was cloned into pBluescript KS (Stratagene); then, the C-terminus FLAG tag was cloned into the pDEST 26 fragment using the *BsrGI* and *AatII* sites; and, finally, the pDEST26 fragment containing the FLAG tag was cloned back into the *SalI* and *NheI* sites of the pDEST 26 vector.

CISD2 cDNA was obtained from IMAGE clone 5105935 (Invitrogen). It was subcloned into the *EcoRI* and *Xho* I sites of the entry vector pENTR3C (Invitrogen) creating pENTR5105935. For the vector with the FLAG tag at the C-terminus, a *CISD2* cDNA without a stop codon was generated by PCR using the primers pENTR3C-F2 (5'-TGGCTTTTTTGCGTTTCTAC-3') and pogo3'no stop Xho R (5'-GCCGCTCGAGGCTACTTCTTTCTTCTTCAGTATTAGTG-3') using pENTR5105935 as a template, and then this fragment was cloned into the *EcoRV* site of pBluescript SK (Stratagene). The integrity of the cone was checked by sequencing, and then subcloned into the pENTR3C EcoRI/XhoI sites.

The *CISD2* cDNA and the *CISD2* no stop cDNA in the pENTR3C vectors were cloned into the N-terminus FLAG tag pDEST26 vector and the C-terminus FLAG tag pDEST26 vector respectively via lambda-recombination (LR) reaction using the Gateway LR Clonase II kit (Invitrogen). The sequences of the expression constructs were confirmed by sequencing. pN-FLAG CISD2 or pC-FLAG CISD2 were transfected into either P19 cells or HEK293 cells using Lipofectamine 2000 (Invitrogen) according to the manufacturer's protocol.

Confocal Immunofluorescence Microscopy

HEK293 and P19 cells (1×10^4 cells) were grown on 4-well chambered slides (Lab-tek) overnight. Then they were transfected using 2.4 µl lipofectamine 2000 in 50 µl serum free medium mixed with 0.8 µg of either pN-FLAG CISD2 or pC-FLAG CISD2 in 50 ul serum free media and incubated overnight. Cells were fixed in 4% paraformaldehyde in phosphate-buffered saline (PBS) for 20 minutes at room temperature. After washing once with PBS, cells were permeablized with 0.2% Triton X-100 in PBS for 10 minutes at room temperature. Cells were

blocked with 1% bovine serum albumin (BSA) in PBS for 30 minutes at room temperature. Cells were then incubated with either anti-calnexin antibody (Santa Cruz) or anti-FLAG M2 monoclonal antibody (SIGMA) or both at a dilution of 1:250 in 5% BSA in PBS for 1 hour at room temperature. After washing twice in 1% BSA in PBS, cells were incubated with either Alexa fluor 488 anti-mouse (Invitrogen) or Alexa fluor 568 anti rabbit (Invitrogen) or both at a dilution of 1:250 in 5% BSA in PBS for 30 minutes in room temperature. Cells were washed three times in PBS and twice in 5% BSA in PBS, and were equilibrated in the pH Equilibration solution from SlowFade® Antifade Kit with DAPI (Invitrogen) for 10 minutes. DAPI mounting medium with SlowFade were added to the cells. Confocal microscopy images were obtained using a Leica TCS SP2 AOBS confocal microscope with LCS software.

Protein Extraction and Western Blot Analysis

Upon 90% confluence, cells were harvested by washing with 1× PBS and briefly treated with 0.25% trypsin-EDTA (Invitrogen). Cell were centrifuged at 800 rpm for 5 minutes, followed by three washes in 1x ice cold PBS. Cell pellets were lysed in a radioimmunoprecipitation (RIPA) buffer (50 mM Tris-HCl, pH 7.4, 10 mM NaCl, 3 mM $MgCl_2$, 1% NP-40, 0.25% Na-deoxycholate) with 40 µl/ml protease inhibitor cocktail (SIGMA). Lysates were cleared by centrifuged at 5000 rpm for 10 minutes at 4°C. SDS loading buffer (2×) was added to the supernatant in a 1:1 ratio. The lysate was then denatured at 55°C for 30 minutes.

The lysates were separated on 10% or 12% SDS-polyacrylamide gels and electroblotted onto a PVDF membrane (BioRad), at 100 volts for 1.5 hours. The membranes were blocked for 1 hour at room temperature or overnight at 4°C in 5% nonfat dry milk or 5% BSA dissolved in Tris-buffered saline solution containing 0.1% Tween-20 (TBST) followed by 3× washes in

TBST for 10 minutes each. The membranes were then incubated with the primary antibody for 1 hour at room temperature or overnight at 4°C in 5% nonfat dry milk or 5% BSA dissolved in TBST. Primary antibodies that were used include mouse anti-FLAG (1:1000, SIGMA), rabbit anti-WFS1 (1:2,000, NOVUS), rabbit anti-CISD2 (1:1,000, ProteinTech), rabbit anti-BiP/GRP78 (1:1,000,Santa Cruz), rabbit anti-p-eIF2α (1:500, Cell Signalling), rabbit anti-GRP94 (1:1,000, SIGMA), rabbit anti-LC3 (1:1,000, NOVUS), rabbit anti-BAX (1:1,000, BD Pharmingen), and anti-nitrotyrosine (1:1,000, Millipore). Mouse anti-α-tubulin (3µg/ml, SIGMA) was included as an internal control. The appropriate secondary antibody was then added at a dilution of 1:10,000 for the anti-mouse antibody and 1:20,000 for the anti-rabbit antibody in 5% milk in TBST for 30-45 minutes at room temperature. Visualization of the immunoreactive proteins was performed using Western Lightning chemiluminescence reagent plus (PerkinElmer). For quantification of protein expression, spot densitometry was used by normalization to α-tubulin expression.

Immunoprecipitation

Whole cell lysates were prepared as described above. For the CISD2-WFS1 immunoprecipitation (IP), 5µg/ml of primary antibody, either anti-FLAG or anti-WFS1, was added to the whole cell lysate and left on ice for 2 hours with periodic agitation. Then, 50 µl of prewashed protein A sepharose beads (Amersham) were added to the antibody and cell lysate mixture and incubated overnight at 4°C with agitation. Beads were pelleted by centrifugation at 5000 rpm for 3 minutes at 4°C and the supernatant was discarded. For the nitrotyrosinated proteins IP, 10 µl anti-nitrotyrosine and 20 µl Agarose A beads (SIGMA) were added to the whole cell lysates and incubated overnight at 4°C. The next day, for both IPs, the beads were washed three times with RIPA buffer and resuspended in 18µl of 2x SDS loading buffer and denatured at 55°C for 30

minutes. The denatured samples were centrifuged for 3 minutes at room temperature, the supernatant was loaded onto a 10% SDS-polyacrylamide gel and the proteins were analyzed by western blot analysis.

RT-PCR, Semi-quantitative RT-PCR and quantitative real-time PCR analysis

Total RNA was extracted from cells using Trizol (Invitrogen) according to the manufacturer's protocol. Total RNA was treated with 20 units of RQ1 DNase in $1\times$ RQ1 buffer to remove DNA contamination as recommended by the manufacturer (Promega). RNA yield and purity were determined spectrophotometrically at 260/280 nm and the integrity of RNA was checked by electrophoresis on agarose gels. First-strand cDNAs were generated from 500 ng of total RNA with 5ng/ul of both oligo dT and random primers, and 0.5 mM dNTPs then heated to 65°C for 5 minutes and cooled immediately afterwards on ice. First-strand buffer ($1\times$), 0.01 M DTT, and 40 U RNase inhibitor (Promega) was then added and the mixture is incubated at 37°C for 2 minutes. Two hundred units of Moloney murine leukemia virus reverse transcriptase M-MLV-RT (Invitrogen) was added and the reaction was allowed to take place at 37°C for 50 minutes followed by a final incubation at 70°C for 15 minutes.

For RT-PCR to check the differential tissue expression of *CISD2*, the transcript-specific primers were used for amplification of *CISD2* cDNA were: pogo.a RT F, 5'-GCTCGGGAGAGGAGTGGA-3' and pogo.a RT R, 5'-TGCAGGAAGAAAATAAATTGGAA-3'. GADPH primers used were GADPH F, 5'-ACTTCAACAGCGACACCCACTC-3' and GADPH R', 5'-CCCTGTTGCTGTAGCCAAATTC-3'. PCR was performed in 12.5 μl reactions with 1.25 μl of

cDNA, 1× PCR buffer (GeneChoice), 0.2 mM dNTPs, 0.26 pmol/μl of each primer, and 0.25 U of Taq polymerase (GeneChoice). PCR cycling conditions were denaturation of 1.5 minutes, followed by 30 cycles of 94°C for 30 seconds, 63°C for 30 seconds, and 72°C for 30 seconds, and finally extension at 72°C for 7 minutes. PCR products were separated on 6% polyacrylamide gels and stained with ethidium bromide for visualization.

Semi-quantitative RT-PCR was used to screen *Cisd2* knockdown cell lines and to measure the relative expression of spliced *XBP-1 (XBP-1s)*. In both instances, *GADPH* was used as an internal control. Exponential phase amplification was determined by performing PCR at different number of cycles. The sequence, the expected size, annealing temperature, and number of cycles of each primer pair are provided in Table 2.

Real-time quantitative RT-PCR for measuring gene expression levels was performed in triplicate using Applied Biosystems (ABI) PRISM 7900 HT. Primers were designed using the Primer 3 program (v.0.4.0; Rozen & Skaletsky, 2000), and optimized using standard PCR. Primer information including sequence, expected size, annealing temperature, and number of cycles are shown in Table 3. For each experimental sample, *GADPH* was also run as an internal control. Reactions were set up with 1.5 μl cDNA, 0.1 pmol/ μl primers and 10 μl of 2× PerfeCTA SYBR Green SuperMix, ROX (Quanta Biosciences) in a total volume of 20 μl. Output was analyzed using SDS software version 2.2 (ABI).

Table 2: Primers used for semi-quantitative RT-PCR

Gene (species)	Sequence (5'→3')	Size (bp)	Annealing Temp / Number of Cycles
XBP-1 (human)	F: GGAGTTAAGACAGCGCTTGG R: TGCCCAACAGGATATCAGAC	225/199*	63˚C/25cycles
*GAPDH*** (human)	F: ACAGTCAGCCGCATCTTCTT R: ACGACCAAATCCGTTGACTC	94	60˚C/20cycles
*Cisd2*** (mouse)	F: CCCAAGGTGGTGAATGAGAT R: GGATGAGAGGACCCACGTTA	151	60˚C/20 cycles
Xbp-1 (mouse)	F: GATCCTGACGAGGTTCCAGA R: CCAGAATGCCCAAAAGGATA	204/178*	60˚C/22 cycles
*Gapdh*** (mouse)	F: TGGCAACAATCTCCACTTTGC R: AGCCTCGTCCCGTAGACAAA	111	60˚C/18 cycles
*Cisd2*** (rat)	F: CCCAAAGTGGTGAACGAAAT R: GGATGAGAGGACCCACGTTA	213	60˚C/23cycles
Xbp-1 (rat)	F: GGAGTTAAGGACACGCTTGG R: AGAGCCAACAGCGTCAGAAT	201/175*	60˚C/23cycles
*Gapdh*** (rat)	F: ATGACAACTTTGGCATCGTG R: GGATGCAGGGATGATGTTCT	136	60˚C/18cycles

*For XBP-1 PCR product sizes, the first number indicates the size of the unspliced variant, and the second number indicates the size of the spliced variant
**Also used in Real-Time quantitative PCR

Table 3: Primers used for Real-Time quantitative PCR

Gene (species)	Sequence (5'→3')	Size (bp)	Annealing Temp
SOD1 (human)	F: GAAGGTGTGGGGAACCATTA R: ACATTGCCCAAGTCTCCAAC	174	60˚C
SOD2 (human)	F: GGACAAACCTCAGCCCTAACG R: TTTGATGGCTTCCAGCAACTC	64	60˚C
NeuroD1 (mouse)	F: GCTCCAGGGTTATGAGATCG R: CTCTGCATTCATGGCTTCAA	205	60˚C
Grin1 (NMDA1) (mouse)	F: ACTCCCAACGACCACTTCAC R: GTAGACGCGCATCATCTCAA	186	60˚C
Sod1 (mouse/rat)	F:CGGATGAAGAGAGGCATGTT R: CACCTTTGCCCAAGTCATCT	165	60˚C
Sod2 (mouse/rat)	F:GGCCAAGGGAGATGTTACAA R:GCTTGATAGCCTCCACGAAC	149	60˚C
Ddit3/CHOP (rat)	F:GCAGCTGAGTCTCTGCCTTT R:AGGTGCTTGTGACCTCTGCT	223	60˚C
Gapdh (rat)	F: ATGACAACTTTGGCATCGTG R: GGATGCAGGGATGATGTTCT	137	60˚C

Creation of stable *Cisd2* knockdowns in INS1, N1E115, and P19 cell lines

To create *in vitro* models of WFS2, RNA silencing technology using the pSUPER RNAi system (oligoengine) was used to knockdown *Cisd2* in three cell lines. The cell lines used were INS1, rat insulinoma cells derived from a tumor of pancreatic β-cells, NIE115, neuroblast cells derived from a mouse brain neuroblastoma, and P19, a murine embryonic carcinoma cell line that can be induced to differentiate into neuronal cells. A mRNA BLAST search using the known murine *Cisd2* transcript helped identify the predicted rat *Cisd2* transcript (RGD1566242). RT-PCR analysis showed expression of *Cisd2* in both cell lines.

To knockdown *Cisd2* in these cell lines, two sets of 60-nt oligonucleotides were designed for each species that contain the sense (forward) and antisense (reverse) orientation of a 19-nt target sequence derived from the mRNA transcript of *Cisd2*. The target sequences were chosen in accordance with published experimental strategies (Sui et al., 2002) and were analyzed using BLAST against the transcriptome of the relevant species to ensure target specificity. Target sequences of rat *Cisd2* are gtggtgaacgaaataaaca, which starts at position 243 from the translational start site and is located in the coding region, and atgacaacagggtattaag, which starts at position 1195 from the translational start site and is located in the 3'UTR. The mouse *Cisd2* target sequences are gaagcaacagaaggatagc, which starts at position 189 from the translational start site and is located in the coding region, and gagcactcatgaactagag, which starts at position 1146 from the translational start site and is located in the 3'UTR. Using the target sequences, oligonucleotide inserts were designed (Table 4) following the manufacturer's protocol. Additional oligonucleotides were designed using scrambled versions of the upstream target sequences (Table 4).

Table 4: Sequence of oligonucleotides designed for use with pSUPER RNAi system to generate Cisd2 knockdown stable cell lines.

Oligo* (species)	Sequence (5'→3')
pSR-189 F (mouse)	GATCCCCGAAGCAACAGAAGGATAGCTTCAAGAGAGCTATCCTTCTGTTGCTTCTTTTTA
pSR-189 R (mouse)	AGCTTAAAAAGAAGCAACAGAAGGATAGCTCTCTTGAAGCTATCCTTCTGTTGCTTCGGG
pSR-1146 F (mouse)	GATCCCCGAGCACTCATGAACTAGAGTTCAAGAGACTCTAGTTCATGAGTGCTCTTTTTA
pSR-1146 R (mouse)	AGCTTAAAAAGAGCACTCATGAACTAGAGTCTCTTGAACTGTAGTTCATGAGTGCTCGGG
pSR-MSCR F (mouse)	GATCCCCGGAATAGCACACGAGAAGATTCAAGAGATCTTCTCGTGTGCTATTCCTTTTTA
pSR-MSCR R (mouse)	AGCTTAAAAAGGAATAGCACACGAGAAGATCTCTTGAATCTTCTCGTGTGCTATTCCGGG
pSR-243 F (rat)	GATCCCCGTGGTGAACGAAATAAACATTCAAGAGATGTTTATTTCGTTCACCACTTTTTA
pSR-243 R (rat)	AGCTTAAAAAGTGGTGAACGAAATAAACATCTCTTGAATGTTTATTTCGTTCACCACGGG
pSR-1195 F (rat)	GATCCCCATGACAACAGGGTATTAAGTTCAAGAGACTTAATACCCTGTTGTCATTTTTTA
pSR-1195 R (rat)	AGCTTAAAAAATGACAACAGGGTATTAAGTCTCTTGAACTTAATACCCTGTTGTCATGGG
pSR-RSCR F (rat)	GATCCCCGAAAGGGACTGACAAATATTTCAAGAGAATATTTGTCAGTCCCTTTCTTTTTA
pSR-RSCR R (rat)	AGCTTAAAAAGAAAGGGACTGACAAATATTCTCTTGAAATATTTGTCAGTCCCTTTCGGG

*Oligos are named according to the number of base pairs from the translational start site of *Cisd2*, and "SCR" denotes scrambled versions of the upstream target sequences

Three micrograms each of the forward and reverse oligos were added to 48 μl of annealing buffer (100 mM NaCl and 50 mM HEPES pH 7.4) and were denatured at 100˚C for 4 minutes and then allowed to anneal by cooling accomplished by simply turning off the water bath overnight. Oligonucleotide pairs were then cloned into the pSUPER.retro.neo+GFP (pSP) vector (Oligoengine) linearized with HindII and BglII. The vector also contains a neomycin resistance gene for positive selection and an *EGFP* gene for GFP reporter expression. Proper insertion was confirmed by restriction-enzyme digest and sequencing of all targeting vectors. Prior to transfection, cells were grown to ~75% confluency in 6 well plates (23.1mm diameter).

For transfection, 4 μg of plasmid DNA was diluted in 250 μl of antibiotic and serum free media, and 12 μl of Lipofectamine 2000 (Invitrogen) was diluted in 250 μl antibiotic and serum free media. The two solutions were then combined and incubated at room temperature for 20 minutes, then added to the cells. After 4 hours incubation at 37˚C in 5% CO_2, the media was replaced with antibiotic free media. After 48 hrs, cells were transferred to 150 mm diameter plates in media containing Geneticin (Invitrogen) to select for cells with the neomycin resistance gene. Kill curves for the cell lines have been previously carried out and the optimal concentration of geneticin for selection was determined to be 200 μg/ml for INS1 cells, 300 μg/ml for N1E115 cells, and 150 μg/ml for P19 cells. Untransfected cells were also transferred and treated with the selective media to act as a negative control. Cells were monitored for growth for 10-15 days, with media being changed every 3 days. Once colonies from single transfected cells were formed, they were isolated, expanded, and screened for *Cisd2* knockdown by semiquantitative RT-PCR and/or Real-Time quantitative PCR. High level of knockdown in cell lines was confirmed using Western blot analysis.

Reagents used for cell treatments

Cells were treated with a variety of different reagents and chemicals to induce different cellular responses. Thapsigargin (SIGMA) was solubilized in Dimethylsulfoxide (DMSO; Fisher). Hydrogen peroxide (SIGMA), D-Glucose (SIGMA), and paraquat (SIGMA) were solubilized in water. All solutions were prepared freshly prior to use except D-Glucose.

Annexin V and 7-AAD Cell Death Assay

For Annexin V and 7-AAD staining, the PE Annexin V Apoptosis Detection Kit I (BD Pharmingen) was used according to the manufacturer's protocol. Briefly, upon completion of stressor treatment or when cells were 80-90% confluency, cells were harvested as described above. Cells were washed twice with ice cold PBS and then resuspended in $1\times$ Annexin V Binding Buffer at a concentration of 1×10^6 cells/ml. One hundred microliters of resuspended cells (1×10^5 cells/ml) was transferred to a 5 ml culture tube. Then, 5 µl of PE Annexin V reagent and 5 µl of 7-AAD reagent were added to each experimental sample, mixed gently and incubated for 30 minutes at room temperature in the dark. Following the incubation, 500 µl Annexin V Binding Buffer was added to each tube and the samples were immediately analyzed by flow cytometry using Beckman Coulter EPICS XL-MCL benchtop flow cytometer.

Cell viability and metabolic rate

The 3-[4,5-dimethylthiazol-2-yl]-2,5-diphenyltetrazolium bromide (MTT, EMD Biosciences) assay was used to assess INS1 metabolism and viability. INS1 cell lines (1×10^5 cells/well) were seeded into 24-well plates in triplicates and incubated under normal conditions. After 2 days, 4 days, and 6 days, cells were washed once with PBS, then MTT, previously dissolved in PBS (5

mg/ml), was diluted 1:10 with cell media and 0.5 ml is added to each well. The cells were incubated for 4 hrs after which the MTT/media solution was removed and 0.5 ml DMSO was added to solubilize the dye. Then, 200 ul of the solubilized dye from each well was transferred to a 96 well plate, and the absorbance of each sample was measured at 600 nm in a spectrophotometer plate reader.

To measure differences in metabolic rate between cell lines, trypan blue exclusion was carried out in parallel to the viability assay. Briefly, INS1 cell lines were plated in 24 well plates as described above. After 2 days, 4 days, and 6 days, cells were harvested as previously described, Trypan Blue stain (Invitrogen) was added at a 1:1 dilution for 2 minutes and live cells were counted by using a hemocytometer (Fisher).   To quantify relative metabolic rate, absorbance values from the MTT assay were divided by the number of viable cells.

In-Gel SOD Activity Assay

Cells were haravested and collected by trypsinization and centrifugation as described above and 200 μl 1X SOD Isolation Buffer (5X: 250 mM KPO4 (monobasic), 0.5 mM EDTA, 10% v/v Triton-X 100, pH 7.8) was added to each cell sample. Cells were sonicated using a probe sonicator at 4°C for 20 seconds, centrifuged briefly to collect lysates, and then incubated on ice for 45 minutes. Then, samples are centrifuged at 14,000 rpm for 15 minutes at 4°C and the supernatant is transferred to a new tube. Protein concentrations is then determined using the Lowry Assay (BioRad). One hundred micrograms of each cell lysate in 1:1 sample buffer (2X sample buffer: 0.125 ml/ml 0.5 M Tris-HCl at pH 6.8, 0.5 ml/ml, glycerol, 0.02 ml/ml 0.5% bromophenol blue) was loaded on to a 15% polyacrylamide gel for separation at 180 Volts until

bands enter resolving and then at 110 Volts until dye marker reaches end of gel followed by an additional 30 minutes at the same voltage, all takes place at 4°C in the cold room.

After electrophoresis, gel is soaked in 25 ml of SOD activity Solution 1 (2.45mM NBT in 50 mM Potassium Phosphate Buffer pH 7.8) for 20 minutes in the dark with gentle agitation. Gel is then washed in 50 mM Potassium Phosphate Buffer for 5 minutes. Then gel is soaked in 25 ml of SOD activity Solution 2 (28 μM riboflavin, 28 mM TEMED in 50 mM Potassium Phosphate Buffer) for 15 minutes in the dark with gentle agitation, followed by washing in 50 mM Potassium Phosphate Buffer for 5 minutes. The gel is then exposed to white light on a light box until maximum contrast between achromatic zones and formazan is achieved, usually by 15-20 minutes after exposure, and the gel is photographed. To determine SOD levels for each sample, spot densitometry measurements were made and SOD activity index was calculated by Integrated Density Value (IDV) divided by μg protein.

Statistical analysis

When comparing means of multiple samples, analysis of variance (ANOVA) was used to determine overall differences in means followed by either Dunnett's test which was used to evaluate the differences between each group and the control group (reference group), or Tukey's multiple comparisons test to evaluate differences between all groups. When comparing the means of two samples, equality of variance was determined using an F-test followed by unpaired student's t-test which was used to test for significant differences between the two groups. A p-value less than 0.05 was considered statistically significant.

CHAPTER 3

A HOMOZYGOUS MUTATION IN A NOVEL ZINC FINGER PROTEIN, ERIS, IS RESPONSIBLE FOR WOLFRAM SYNDROME 2

3.1 Introduction

Wolfram syndrome (WFS [MIM 222300]) is an autosomal recessive disorder with severe neurodegeneration. Affected individuals present with juvenile onset insulin-dependent diabetes mellitus (DM) and optic atrophy (OA) (Wolfram & Wagner, 1938; Blasi *et al*., 1986). Other neurological and endocrine manifestations include diabetes insipidus (DI), sensorineural deafness, dementia, psychiatric illnesses, renal tract abnormalities and bladder atony (Cremers *et al*., 1977; Minton *et al*., 2003). One gene for the disorder, designated as *WFS1*, on chromosome 4p16.3, has been identified and encodes a novel transmembrane protein located in the endoplasmic reticulum (ER) and may play a role in calcium (Ca^{2+}) homeostasis (Inoue *et al*., 1998; Strom *et al*., 1998; Takeda *et al*., 2001; Osman *et al*., 2003). In addition, dominant mutations in the *WFS1* gene have been shown to play a role in low frequency sensorineural hearing loss, progressive hearing loss and deafness with optic atrophy (Bespalova *et al*., 2001; Young *et al*., 2001; Eiberg *et al*., 2006).

The WFS2 locus (MIM 604928) was mapped to chromosome 4q22-24 between markers D4S1591-D4S3240 in three large consanguineous Jordanian families (El-Shanti *et al*., 2000). Although the families are not related, haplotype analysis shows a common affected haplotype between families. An extensive phenotypic analysis showed additional symptoms in individuals with WFS2 such as significant bleeding tendency, as well as a defective platelet aggregation with collagen (Al-Sheyyab *et al*., 2001) which has not been previously reported in WFS families. In

addition, a considerable number of the patients had peptic ulcer disease that was compounded by the bleeding tendency causing gastrointestinal tract bleeding (Ajlouni *et al*., 2002).

In this study, we identify a mutation causative for WFS2 in a novel, highly conserved, zinc finger gene, *CISD2* that is located within the gene critical region. In addition, evidence of the pathogenetic nature of the mutation is revealed. Further studies of this novel gene include the characterization of its protein domains, expression and cellular localization and studies to determine if there is a role of this gene in calcium homeostasis. To determine if the WFS2 gene is also associated with nonsyndromic hearing loss, mutation analysis in a large cohort of hearing loss individuals was also performed.

3.2 Results

3.2.1 Clinical Update

The three Jordanian consanguineous families from the El-Shanti *et al*., (2000) study had 16 individuals affected with Wolfram Syndrome that linked to the WFS2 locus (Families WS-2, WS-3, and WS-4). One family in that study, family WS-1, showed linkage to the WFS1 region. Of the 16 WFS2 affected individuals, 14 individuals were previously described in El-Shanti *et al*., (2000). In summary, all but three of the individuals presented with DM and all presented with OA. Other common clinical manifestations include sensoneural hearing loss (13/14), urinary-tract dilation (7/14), and peptic ulcer (11/13) (El-Shanti *et al*., 2000).

Family WS-2 - Individual II-2, who was affected, committed suicide about 5 years ago after battling with depression for a long time. Individual II-9 developed high frequency sensorineural hearing loss although it is not as severe as his siblings.

Family WS-3 - Individual II-3 died about 7 years ago (after the publication of the original linkage article) from complications of dialysis. He developed renal failure and bleeding during dialysis. Individual II-9 died 5 years ago and the cause of death is unknown.

Family WS-4 - All affected family members now have DM, OA and high frequency sensorineural hearing loss. The DM is mild and easily corrected with low doses of insulin. The hearing loss is currently symptomatic in all four affected individuals.

3.2.2 Mutation Detection

The WFS2 gene critical region, between markers D4S591 and D4S3240, is a large region representing 7.1 cM. To narrow down the gene critical region, additional markers within the region were genotyped in the families. These include markers D4S2961, D4S3043, D4S1572, Wpoly2, D4S2913, D4S411 and D4S1531 at the proximal end and D4S2917 and Wpoly5, Wpoly6 and Wpoly7 at the distal end. The Wpoly markers are new microsatellite polymorphisms identified by Sputnik, a program which scans genomic DNA and identifies microsatellite stretches within the DNA and evaluates their polymorphic potential. These markers were either uninformative in the families or did not cross the recombination breakpoint, thus the gene critical region could not be reduced (data not shown).

The gene critical interval contains 62 transcripts including known genes, full-length cDNAs, ESTs and predicted proteins. To reduce the gene list, predicted proteins without a start and stop codon were not studied. In addition, homology searches of the translated sequences using BLAST were also performed which eliminated additional putative genes. This left 42 transcripts in the region to be studied including an excellent candidate gene, BANK1, known to induce Ca^{2+} mobilization in B-cells (Yokoyama *et al*., 2002). All of the genes in the region have been screened

either by direct sequencing or SSCP analysis starting with known genes and full-length cDNAs. In table 5, known genes, expressed sequence tags and predicted genes are listed in order of the markers on chromosome 4q22-24. Additional information is also provided including NCBI accession number, protein information, and whether mutation analysis (SSCP and/or sequencing) was carried out. Protein information includes predicted start and stop codons for putative proteins, known function of proteins, and known or predicted conserved domains in proteins and predicted proteins.

Various polymorphisms were identified but only one nucleotide change in a novel predicted gene *CISD2* was found to be the WFS2 mutation in these families. A G to C transversion in nucleotide 109 (109G>C) is predicted to change amino acid 37 from a glutamic acid to a glutamine (E37Q) (Figure 3A). This same mutation is found in all three families. The families are not known to be related but haplotype analysis had revealed a common haplotype in the linked region (El-Shanti *et al*., 2000) which would indicate a common ancestor for this mutation. This change disrupts an *Xmn I* restriction enzyme site which was used to genotype the family members. The mutation completely segregates with the phenotype in all three Jordanian families (Figure 3B). The mothers from all three pedigrees are shown to be obligate carriers and the same is assumed for the fathers though no samples were ever obtained from those individuals. Of the 20 original samples obtained for the children in the three families, only 16 samples were still currently available to test. The original blood spots of the four individuals not tested did not yield any appreciable DNA and new samples were not able to be obtained.

Table 5: List of genes and predicted genes analyzed in WFS2 critical region

Marker	Locus	Name/Accession #	Protein and Functional Information	Analysis
Wpoly3 D4S1591				
	AK124002	Hypothetical protein FLJ42008		Yes
	PPP3CA (exon 1 only)	Protein phosphatase 3 (formerly 2B), catalytic subunit, alpha isoform (calcinerin A alpha)/AL353950	Serine/Threonine phosphatase	Yes
	AK091523			Yes
D4S2961	BANK1	B-cell scaffold protein w/ankrin repeats/AK091523	Interacts with IP3R & affects calcium homeostasis	Yes
	NT_016354.436	predict-extends BANK1 5', internal, 3'		
	SLC39A8 (BIGM103)	solute carrier family 39 (zinc transporter), member 8 /AB040120	zinc transporter/bacillus Culmet Guillen-cell wall skeleton (BCG-WVS) induced integral membrane protein in monocytes	Yes
	neygo.aNov4	AW959279 spliced EST	weakly similar to neuronal thread protein/ Alu sequences/ no Met	No
	neygo.bNov4	BQ082187		No
	NFKB1	nuclear factor kappa light polypeptide gene enhancer in B-cells 1 (p105) /BC057165	transcription factor	Yes
D4S3043	MANBA (HGNC)	mannodisase, beta A, lysosomal/BC015743	removes N-linked mannose during glycoprotien catabolism; thought to cause beta-mannosidosis	Yes
	UBE2D3	ubiquitine-conjugating enzyme E2D3(homologous) /BC037894	ubiquitination of cellular proteins	Yes
D4S1572 (afm265va9)				
	pogo.aNov04	(BC032300 /LOC285553) spliced EST	Met downstream	Yes
	LOC150159.aNov04	AF447585	unknown function / methionine not first base	Yes
	LOC150159.hNov04	BC022079		No

	LOC133308	BC009732	Na/H antiporters, maintain pH of actively metabolizing cells	see next
	LOC133308	BC047447	Same as BC009732 with more exons	Yes
	DHRS6 (SDR4)	dehydrogenase/reductase (SDR family) member 6 /BC001953	Member of the short-chain and glucose/ribitol dehydrogenase family; involved in retinoid, NAD(P)H, steroid biosynthesis	Yes
	CENPE	centrosome associated protein E /Z15005	kinesin-like motor protein important for mammalian chromosome movement or spindle elongation	Yes
	CB116995	spliced EST	not in Unigene/no methionine	No
	peygo.aNov04	peygo.aNov04 (BG209440) spliced EST	no library information	Yes
Wpoly1 afma070TH5	TACR3	tachykinin receptor 3	receptor for the tachykinin neurokinin 3 or B	Yes
	Porgo	Porgo (BG717053) spliced EST	no stop codon	No
Wpoly2 D4S2913 D4S2907				
	jeybobo	Jeybobo (CD512067)		Yes
	CXXC4 (IDAX)	CXXC finger 4 (dishevelled (Dvl)-binding protein) /AF272159	inhibition of the Dvl and Axin complex or wnt signalling; induces ventralization	Yes
	mosare	mosare (AK094561) mRNA, overlaps IDAX in opposite orientation	not in Unigene; no methionine or stop codon	No
D4S1570 (afm150yh6)	korsnarby	(CD707196) spliced EST		Yes
	slyfloy.cNov04	slyfloy.cNov04 (AI761223)		Yes
	FLJ20032	(AK055149)		Yes
	KIAA1546	AB046766/BC019007	similar to yeast protein kinase CLA4; important in G1 progression	Yes
D4S3026	PPA2 (SID6-306)	inorganic pyrophosphatase 2 /AK000466		Yes

	FLJ20184	hypothetical protein; hom mouse proline rich/ dros son of sevenless/ AK000191	similar to guanine nt exchange factors family of rho sub fam of ras-related GTP binding proteins	Yes
	PHF22	PHD finger protein 22 SBBI22/LOC57117(sts G4511)	zinc finger domain	Yes
	LOC401147.aNov04	spliced EST	Predicted start not Met	Yes
	FLJ13273	BC032942	GST-domain	Yes
	rorgo.aNov04	AI424808 spliced EST w/mer repeat within FLJ13273 in opposite direction	small overlap w/BF222990	Yes
	rorgo.dNov04	has met & stop but different exons than a. coding is not until 6 (last) exon, BF222990	small overlap w/AI424808, part of last exon only	Yes
	warsnarby			Yes
	sugo.aNov04			No
	NPNT	LOC255743 (POEM) /AL832465	similar to mus nephronectin short isoform; hum EGF-like protein 6; ECM adhesion molecule & interacts w/integrin in kidneys	Yes
	MGC16169	AF161420/1 more exon in AK074305	protein kinase domain, TBC, GTP-activator activity	Yes
	SCYE1, p43, EMAP2, AIMP1	small inducible cytokine subfamily E, member 1 /BC014051	tRNA binding domain	Yes
D4S1531 (UT2021)	bagee.Nov04	AW471226/spliced EST/very small protein		No
D4S3256	DKK2/ BU902436 (stSG48492)	dickkopf (Xenopus Laeris) homolog-2	associates w/ LRP6, Wnt8 inhibition of beta catenin signaling	Yes
	bygee	spliced EST AW972978 /BX093744		No
D4S1564				
	PAPSS1 (SHGC-7493)	3' phosphoadenosine 5' phosphosulfate synthase 1	ATP sulfurylase and adenosine 5' phosphosulfate kinase activities, required for the synthesis of sulfonate donor 3'-phosphoadenosine 5'-phosphosulfate. Donates sulfate for sulfatransferases, Important in skeletal development	Yes
D4S2917				

	BI821015	spliced EST	extends MGC26963 3'	
	SMS2 /MGC26963	Sphingomyelin synthase 2 /Phosphatidylcholine:ceramide cholinephosphotransferase 2 /BC041369	Bidirectional lipid cholinephosphotransferases capable of converting phosphatidylcholine (PC) and ceramide to sphingomyelin (SM) and diacylglycerol (DAG) and vice versa	Yes
	bogee.aNov04	AK123292 spliced EST/no met but has stop		Not Done
	bogee.bNov04	BM931739 spliced EST		Yes
	CYP2U1*	cytochrome p450 /AY343323	hydroxylase metabolizes arachidonic acid and other long chain fatty acids; ER membrane bound	Yes
	AL359563 (stAL359563)	LOC153077		
	HADHSC (stSG9749)	L-3-hydroxyacyl-Coenzyme A dehydrogenase, short chain	lipid metabolism, energy generation in mitochondria	Yes
Wpoly5	LEF1	lymphoid enhancer binding factor-1 /AF288571	expression activated by Wnt3a-beta catenin signaling. Is a transcription factor & related to HMG proteins	Yes
	AA769836	extends LEF1 3'		
	snosnarby	AW850300		Not Done
Wpoly6				
Wpoly7				
Wpoly4b				
	FLJ37673.a	AK094992	similar to ubiquitously expressed tetratricopeptide repeat gene on Y chromosome	
	RPL34	ribosomal protein L34 family /BC001773	60S subunit component; cytoplasm	Yes
	DC2	Hydrophobic protein HSF-28 /BC016321		Yes
	AGXT2L1	alanine-glyoxylate aminotransferase 2 homolog 1, splice form 1 /BC022526	4-aminobutyrate aminotransferase, acetyl ornithine aminotransferase	Yes
D4S3240	COL25A1(last 18 exons)	collagen-like Alzheimer amyloid plaque component type II /BC036669/LOC84570	novel type II transmembrane protein	Yes

The amplified region containing the mutation was sequenced in at least one affected individual in each family and all showed the 109G>C mutation. This change is not found in the SNP (signal nucleotide polymorphism) database (http://www.ncbi.nlm.nih.gov/SNP/). Custom TaqMan SNP genotyping for the mutation was used to screen for this change in a large number of control individuals from various populations. Only one chromosome was identified to have the change in the ethnically matched control population. One individual from the affected Jordanian families is part of the Jordanian control panel. Since the panel is anonymous it is unknown which individual from the families is included in the control panel. The allele frequency for this change is 0.08% in the Jordanian population and not found in other populations after assessing 2,004 chromosomes. Since this is an autosomal recessive condition, a very small portion of the population may very well carry this change in a heterozygous state, though in our panel the single mutation carrying the change could be a carrier from the families studied.
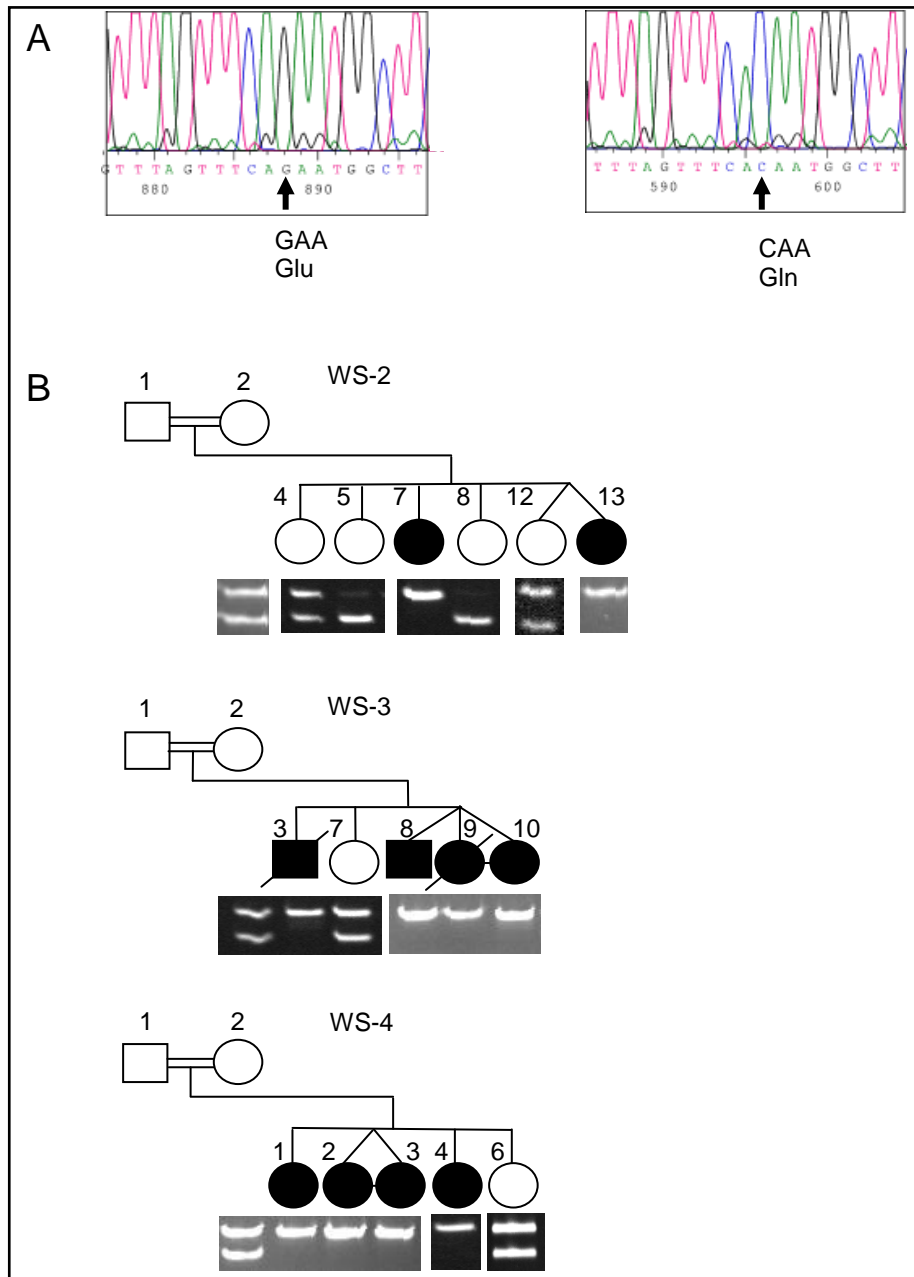
Figure 3. Identification of a single base pair change causative for WFS2. A, Sequencing results from a control individual (left panel) with a G at nucleotide 109 in exon 2 of the *CISD2* gene which codes for glutamic acid while the right panel shows sequence from an affected individual with a homozygous C at the same position which changes the amino acid to glutamine. B, Truncated pedigrees of WFS2 families with genotyping of the mutation is shown below. All pedigrees represent consanguineous matings. Only children with DNA samples are shown. Children are numbered using designations from the original published pedigree[12]. The mutation disrupts an *Xmn I* restriction enzyme site (GAANNNNTTC) and homozygous affected individuals show a 249 bp fragment while the wild type allele is cut into a 210 bp and 39 bp (not shown) fragment.

3.2.3 Protein Analysis

The *CISD2* gene codes for a very small 135 amino acid protein with the molecular weight estimated to be 15,278 KDa (Figure 4). It has a single predicted transmembrane domain and a single zinc finger domain of the CDGSH type located close to the carboxy terminus. The predicted zinc finger domain has been more recently identified to be a conserved iron sulfur binding domain (Wiley *et al*., 2007; Conlan *et al*., 2009), to which the gene name refers to: conserved iron sulfur domain 2 (CISD2). This zinc finger is similar to domains in another human gene (*CISD1*) and proteins in many single cell organisms, all of unknown function. ERIS homologues from dog, mouse, rat, chicken, two frog species, two fish species and *Drosophila melanogaster* have been identified. The protein is highly conserved and is 70% identical and has 82% similarity across all of the vertebrate species (Figure 4). The human and *Drosophila* protein are 46% identical and 68% similar. Several serine/threonine and one tyrosine phosphorylation sites were identified in the human protein though only four serine/threonine sites are conserved in all species including *Drosophila* (Figure 4). The protein has a single β-adrenergic receptor kinase site at amino acids 25-29 ([E/D][S/T]XXX) (Onorato *et al*., 1991), two PKA/PKC kinase motifs at amino acids 32-34 and 67-69 ([R/K]X[S/T]) (Pearson & Kemp, 1991) and a single CK2 (formerly casein kinase 2) phosphorylation site ([S/T]XX[D/E]) (Kuenzel *et al*., 1987) located at amino acid 34 to 37, which encompasses the site of the mutation in the last position.

```
                              1                            ▽   ↓          47
Homo sapiens              MVLESVARIVKVQLPAYLKRLPVPESITGFARLTVSEWLRLLPFLGV
Canis familiaris          ----------------------------------------------
Rattus norvegicus         ---D--------------Q--L-D----------A-----------
Mus musculus              ---D--------------Q----D----------D-----------
Gallus gallus             -----L------------L---VG--L-------------------
Xenopus laevis            -----I--VL---------I-D--A—I-------------------
Xenopus tropicalis        -----I--VL---------I-D--A—I-------------------
Danio rerio               -----I---I-I-------K--L--T-G--------------L--I
Tetraodon nigroviridis    ---DTISK-I----------L--T-G--------------L--I
Drosophila Melanogaster   -**-PISHL--SS--N--SS----D--G-WFK-SFKD--A-I-PTV-


                          48
90
Homo sapiens              LALLGYLAVRPFLPKKKQ***QKDS*LINLKIQKENPKVVNEINIED
Canis familiaris          --------I----------***----*-------------------
Rattus norvegicus         -----------F-----***----*-------------------
Mus Musculus              -----------F-----***----*-------------------
Gallus gallus             -----------------***----*-------------------
Xenopus laevis            --------I----L----***----*-------------------
Xenopus tropicalis        --------I---------***----*-------------------
Danio rerio               -------TI--------K***-R--*----------------D---
Tetraodon nigroviridis    -------TI--------K***-R--*----------------D---
Drosophila melanogaster   V-G---T-YLAYC-AARASCAA-N-GRC-NH-R-NE----DM-DV--


                          91                   ▽                        135
Homo sapiens              LCLTKAAYCRCWRSKTFPACDGSHNKHNELTGDNVGPLILKKKEV
Canis familiaris          ---------------------------------------------
Rattus norvegicus         -N-------------------------------------R----
Mus Musculus              ---------------------------------------------
Gallus gallus             -----*------------V-------------------------
Xenopus laevis            -H-A--------------V-------------------------
Xenopus tropicalis        -H-A--------------V-------------------------
Danio rerio               -RTPNVC----------V--K--I-----------------TL
Tetraodon nigroviridis    -NS-NVC----------V--K--L-----------------I*
Drosophila melanogaster   I*AE---F----KT-NW-Y-----GE--KQ-------IVI--***
```

Figure 4. Comparison of amino acid sequence of ERIS in nine species. The human sequence is shown and amino acid identities in other species are represented with a dash. Asterisks represent a missing amino acid in that species. The bold amino acids signify predicted conserved phosphorylation sites (β-adrenergic receptor kinase substrate 25-29; PKA/PKC kinase substrate motif 32-34, 67-69; CK2 substrate motif 34-37). The glutamic acid that is mutated in ERIS in the Jordanian families is indicated by an arrow. The underlined amino acids represent a putative transmembrane domain. The double-underlined amino acids highlight the zinc finger domain of the protein. The open arrowheads indicate the region corresponding to splice junctions in the cDNA.

57

3.2.4 Hearing Loss Mutation Screen

Though WFS is a recessive disorder, dominant mutations in the *WFS1* gene have been associated with nonsyndromic hearing loss and OA with hearing impairment (Bespalova *et al*., 2001; Young *et al*., 2001; Eiberg *et al*., 2006). Six families with *WFS1* mutations have low frequency sensorineural hearing loss (Bespalova *et al*., 2001) and one additional family had progressive hearing loss with mild hearing loss in the low frequency range but advanced to moderate to severe hearing loss across all frequencies (Young *et al*., 2001). Hearing loss in WFS mostly involves high frequencies which is also observed in WFS2 families (Cremers *et al*., 1977; El-Shanti *et al*., 2000). To determine if *CISD2* is involved in deafness in a general hearing loss population, we screened 377 probands for mutations in *CISD2*. These probands represent individuals that presented with hearing loss but did not have a positive hit on a panel of previously identified mutations for hearing loss. No mutations were identified in this cohort so it seems that *CISD2* is not commonly involved in nonsyndromic deafness. Only one proband had low frequency sensorineural hearing loss so it remains to be determined if *CISD2* is involved in this subset of hearing loss.

3.2.5 Expression Studies

Using RT-PCR on RNA from a variety of human tissues including brain, testis, small intestine, heart, kidney, lung, skeletal muscle, fetal liver, cartilage, liver, and pancreas. Expression of CISD2 was observed in the majority of tissues including brain and pancreas which are the two organs first affected in WFS. Expression was not observed in cartilage, fetal liver and skeletal muscle (Figure 5A). The expression of CISD2 in a variety of tissues suggests a possible important function of *CISD2* in the cell especially in cells of the brain and pancreas.

3.2.6 Disease Pathogenesis

The mutated glutamic acid is conserved in all species except in mouse where there is an aspartic acid residue in its place (Figure 4). The replacement of the glutamic acid residue at position 37 with aspartic acid does not disrupt the CK2 phosphorylation site. This site is also found in *Drosophila* though the sequence is divergent (SFKD). The mutation changes the conserved glutamic acid from the single conserved CK2 site which would abolish phosphorylation at this site. It would be logical to conclude that the disruption of a functional domain would be indicative of disease pathogenesis but in actuality, the mutation also creates a splice site mutation.

The mature cDNA is derived from three exons. The mutated base is located close to the 5' end of exon 2, six bases from the intron/exon junction. Performing RT-PCR with primers that would amplify the full-length cDNA on templates derived from lymphoblastoid RNA from an affected individual and two controls showed a 336 bp product in the affected individual and a 551 bp product of expected size in controls (Figure 3B). Sequencing the RT-PCR products showed that the 336 bp product is due to exon 2 being skipped in the final transcript (Figure 5C). This smaller RT-PCR product is not observed in RNA from other tissue types and likely not a splice variant (data not shown).

The aberrant splice product would code for the 34 amino acids of exon 1 but the frame shifts in exon 3 would create a premature stop codon after eight additional amino acids. This would eliminate 75% of the protein including the transmembrane and zinc finger domains. This particular nucleotide change does not reside in any known splice acceptor or donor regions and thus it is likely that this change disrupts an exonic splice enhancer (ESE).
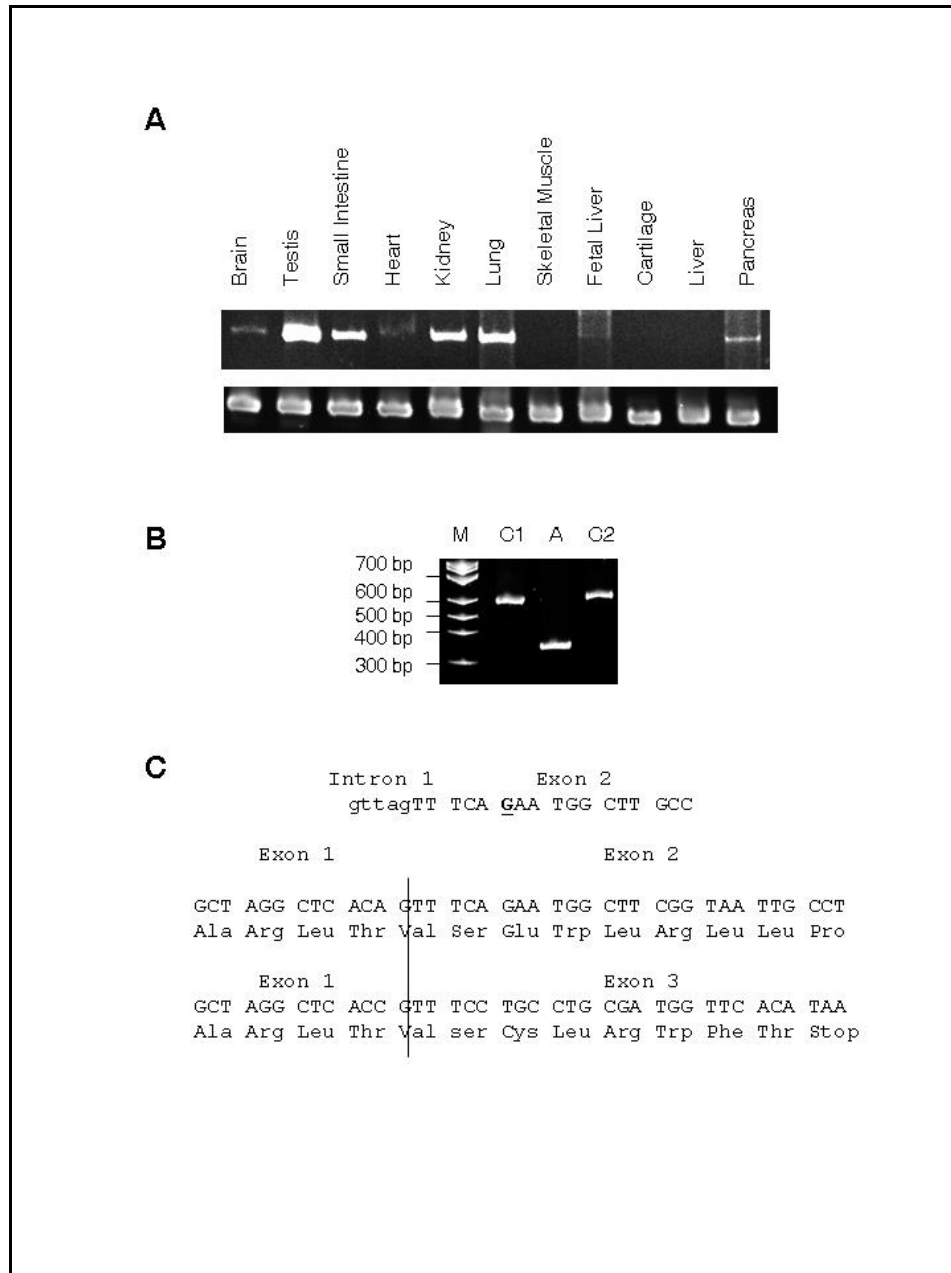
Figure 5. *CISD2* **expression and WFS2 disease pathogenesis.** (A)*CISD2* is expressed in a wide variety of human tissues including the pancreas and brain. RT-PCR of the WFS2 gene, *CISD2*, in a variety of tissues is shown in the top row and the bottom row shows the *GADPH* control. (B)Single base change mutation in WFS2 patient causes a splicing error. RT-PCR of lymphoblastoid RNA from two control individuals (C1, C2) and an affected individual using human *CISD2* cDNA primers. The primers amplify the full-length cDNA and the large band is 551 bp and the smaller band is 336 bp. (C) Sequencing affected individual's CISD2 cDNA reveals splicing error. Genomic sequence of the intron/exon boundary shows that the mutation (shown in bold and underlined) is within 6 bp of the 3' splice acceptor site. Below cDNA and amino acid sequences are shown at the boundary between exon 1 and exon 2 as compared to the premature stop codon when exon 1 and exon 3 are spliced together in an affected individual.

3.2.7 ERIS Cellular Localization

To determine the cellular localization of *CISD2*, the human gene was tagged with FLAG on the amino (N-FLAG) or carboxy (C-FLAG) terminus and expressed in mouse P19 and human HEK293 cells. N-FLAG ERIS is localized to the ER as it colocalizes with calnexin a known ER marker (David *et al.*, 1993) (Figure 6A). Due to the protein's predicted domains and cellular localization, we have named the *CISD2* protein, ERIS for Endoplasmic Reticulum Intermembrane Small protein. This finding suggests a possible role of ERIS in a role related to the function of the ER such as, but not limited to, ER calcium homeostasis or the ER unfolded protein response (UPR).

3.2.8 ERIS does not interact with wolframin

To determine if ERIS interacts directly with the WFS1 protein, wolframin, co-immunoprecipitation studies were performed in cell lines expressing N-FLAG and C-FLAG ERIS. wolframin did not co-precipitate with ERIS (Figure 6B). This finding suggests that the two proteins do not have a strong direct interaction, however, there may be an indirect or weaker interaction between the two proteins that was not detected in the co-immunoprecipitation of the two proteins.

3.2.9 Calcium Measurements

$[Ca^{2+}]i$ was measured using a Ca^{2+} sensitive dye, fura-2-AM. Ca^{2+} values were determined from the fluorescence ratio of Ca^{2+} bound fura-2 (340 nM) to unbound fura-2 (380 nM) in single cells from blinded tests. Resting $[Ca^{2+}]i$ levels were not significantly different in a

61

lymphoblastoid cell line derived from an affected individual when compared to an unaffected control (Figure 7A). When stimulated by TG, a known stimulator for ER Ca^{2+} release, there was significantly more intracellular Ca^{2+} release in the affected cell line (Figure 7B-D). This finding points to a possible role of ERIS in ER Ca^{2+} homeostasis by having greater calcium accumulation in the ER during resting conditions, or having abnormally greater calcium release from the ER upon stimulation of ER calcium release.
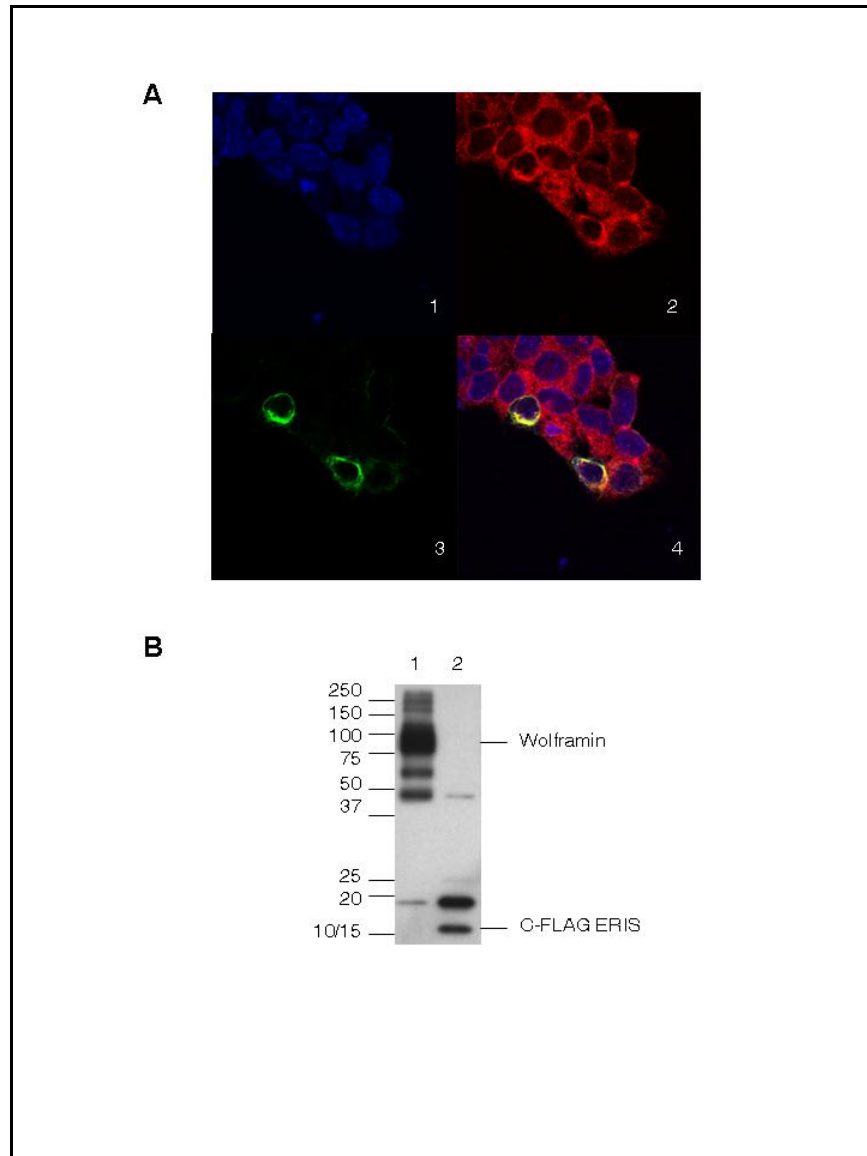
Figure 6. Localization and immunoprecipitation of ERIS. (A) FLAG tagged ERIS colacalizes with the ER marker calnexin. P19 cells transfected with pN-FLAG ZCD2. In panel 1, the transfected cells were stained with DAPI. Panel 2 shows the ER marker calnexin in red. Panel 3 shows pN-FLAG ZCD2 in green. Only a proportion of the cells that were transfected showed pN-FLAG ZCD2 expression. Panel 4 shows the merged picture with pN-FLAG ZCD2 colocalizing with calnexin in the ER. (B)FLAG tagged ERIS does not co-immunoprecipitate with WFS1 protein. Cell lysates from HEK293 cells transfected with pC-FLAG ZCD2 were immunoprecipitated using anti-WFS1 antibodies (lane 1) and anti-FLAG antibodies (lane 2). The top half of the blot was probed with anti-WFS1 antibodies and the bottom half with anti-FLAG antibodies. Lane 1 shows a strong wolframin band at 100 kDa but did not pull down pC-FLAG ZCD2 (17.5 kDa). pC-FLAG ZCD2 is observed in lane 2 with no wolframin. The 19 kDa band represents IgG while other bands represent nonspecific binding of the antibodies. The same results were observed when the experiment was performed with pN-FLAG ZCD2 (data not shown).

63
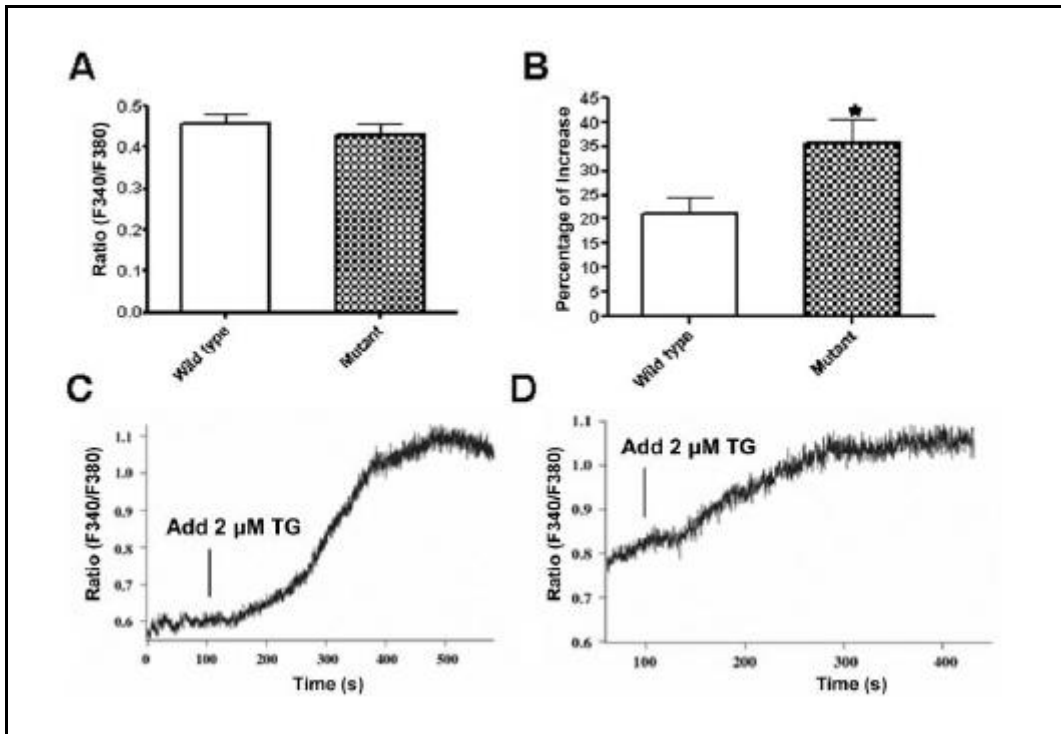
Figure 7. Intracellular Ca^{2+}measurements. (A) Resting intracellular Ca^{2+} levels are similar in wild type and WFS2 (mutant) lymphoblastoid cells. No difference in the mean basal $[Ca^{2+}]$i levels is observed between wild type and mutant cells (n = 30-37; p = 0.49). (B)Greater increase of $[Ca^{2+}]$i in WFS2 mutant lymphoblastoid cells compared with wild type. The mean $[Ca^{2+}]$i increase is significantly greater in mutant versus wild type cells when stimulated with 2 μM TG (n = 8, *p = 0.03). Representative single cell measurements of $[Ca^{2+}]$i changes in mutant (C) and wild type (D) cells when stimulated by TG are shown. (This experiment was carried out by our collaborators in the Satin Lab)

3.3 Discussion

The majority of Wolfram syndrome cases seem to be caused by mutations in the WFS1 gene but in many studies, there has been evidence of genetic heterogeneity (El-Shanti *et al*., 2000; Collier *et al*., 1996; Gomez-Zaera *et al*., 2001; Khanim *et al*., 2001). We have shown that a mutation in a zinc finger gene, *CISD2*, also causes Wolfram syndrome. The same missense mutation was identified in all three unrelated consanguineous Jordanian families. Through haplotype analysis, it is clear that these families share a common ancestor (El-Shanti *et al*., 2000). Though the missense mutation occurs at a conserved amino acid, the actual pathogenesis of the nucleotide change has been shown to affect mRNA splicing. The mutation causes exon 2 to be skipped which results in a frame shift leading to a premature stop codon resulting in over 75% of the protein to be missing including a putative transmembrane domain and the zinc finger domain. Although the mutation functionally affects splicing, the 10 bp surrounding the mutation site does not demonstrate any consensus for ESEs. Some of the best-defined ESEs share one of two features. One class of ESEs shows high purine content (≥80%) though specific sequences within that region are known to be important and the second class is A/C rich (ACE) (Cooper & Mattox, 1997). *CISD2* has 60% purines in the sequence adjacent to the mutation and the region is not particularly AC rich. In fact, the mutation replaces a G with a C. It is well known that a large number of sequences can function as ESEs but do not conform to any specific sequence. We have identified a functional ESE in *CISD2* that does not conform to a known class of ESEs.

We did not identify mutations in *CISD2* in a large cohort of 377 individuals from multiplex families with nonsyndromic deafness. Dominant mutations, in the WFS1 gene, have been reported in DFNA6/14 families with low frequency sensorineural hearing loss or progressive hearing loss (Bespalova *et al*., 2001; Young *et al*., 2001). Of the 377 probands, 240 had autosomal recessive

65

inheritance, 84 had dominant hearing loss and 53 were heterozygous for a single change in the GJB2 gene. Although the majority had severe to profound hearing loss, 14 had high frequency hearing loss but only one individual had low frequency hearing loss. *CISD2* does not seem to be generally associated with nonsyndromic hearing loss but it remains to be determined if it is specifically associated with low frequency hearing loss similar to the *WFS1* gene.

CISD2 has a fairly wide expression profile including the pancreas and brain, two tissues affected by the disorder. Since the transcript could be amplified from RNA derived from lymphoblastoid cells it may be also expressed in blood cell lineages. Expression studies using mass spectrometry listed in the Human Protein Reference Database (HPRD 17413) show the presence of *CISD2* transcripts in platelets (Peri *et al*., 2003). This would correlate with the bleeding phenotype described in these families.

Though we did not perform *in-situ* hybridization on tissue sections, these experiments were performed on sagittal sections with the mouse *Cisd2* transcript (1500009M05Rik) as part of the Allen Brain Atlas project (Lein *et al*., 2007). Expression of the gene in adult mouse brain is observed in a wide variety of structures including the cerebral cortex, piriform area, pyramidal cells of the hippocampus, and the central amygdalar nucleus, the medulla, pons, thalamus, inferior and superior colliculus of the brainstem and the Purkinje cell layer and dentate nucleus of the cerebellum. Interestingly, there is substantial overlap of expression of *Cisd2* in mice and *Wfs1* in rat brain (Takeda *et al*., 2001). These brain regions primarily control memory, emotions and motor skills. Affected individuals with WFS are known to have neurological complications such as cerebellar ataxia and myoclonus as well as psychiatric illness (Minton *et al*., 2003).

MRI studies of individuals living with WFS show degeneration of the brainstem, cerebellum, optic nerve, tracts and chiasm (Barrett *et al*., 1997*)*. A small number of WFS

affected brains have been studied post-mortem. These studies show the degeneration of specific brainstem structures and also show a much wider pathology (Carson *et al*., 1997; Genis *et al*., 1997). Neural degeneration of many other areas where *Cisd2* is expressed is also observed. These include the superior and inferior colliculi and thalamus (brainstem) as well as the pontine nuclei, Purkinje cells, and pons. Loss of the cochlear nerves and mild loss of cochlear nuclei has also been observed. In general, it appears that neurodegeneration in WFS is correlated with the spatial expression of *CISD2*. As it is the loss of sensory neurons, pancreatic beta cells, absence or hypoplasia of the hypothalamus that could explain the main clinical symptoms, *CISD2* expression in these tissues needs to be examined further.

ERIS is an extremely small but well-conserved protein. Indirect immunofluorescence studies show that the protein is localized to the ER. ERIS does not have a predicted ER signal sequence at the amino terminus but it has a single transmembrane domain. Transmembrane proteins have been shown to use their first transmembrane domain to be directed into the ER (Kanner *et al*., 2002). The other major predicted domain is a zinc finger domain of the CDGSH type with a CCHH finger. Zinc finger domains are now known to be able to bind nucleic acids, lipids and proteins (Mackay & Crossley, 1998). Wolframin co-immunoprecipitation studies performed in cell lines expressing N- or C-FLAG ERIS revealed that wolframin does not co-precipitate and interact with ERIS.

Wolframin has been well studied and has been shown to localize to the ER and play a role in modulating $[Ca^{2+}]i$. Though $[Ca^{2+}]i$ between WFS2 affected and control lymphoblastoid cells were not significantly different, a significantly greater increase in $[Ca^{2+}]i$ in affected cells was observed when stimulated with TG. TG is a known inhibitor of the sarco(endo)plasmic reticulum $Ca^{2+}ATPase$ (SERCA) which results in ER Ca^{2+} efflux (Lytton *et al*., 1991). This is consistent with

a role of ERIS in $[Ca^{2+}]$i homeostasis in cells expressing the gene. Recently it has been shown that knockdown of WFS1 in HEK293 cells showed lower increases in Ca^{2+} when TG was added to the media suggesting lower $[Ca^{2+}]_{ER}$ in cells without wolframin (Takei *et al*., 2006). Measuring the rate in which Ca^{2+} moves back into the ER showed that this rate was impaired indicating a role for Wolframin in ER Ca^{2+} uptake (Takei *et al*., 2006). Additional studies need to be undertaken to determine if greater TG Ca^{2+} release in WFS2 affected cells is due to higher $[Ca^{2+}]_{ER}$.

The symptoms of this disorder are caused by degeneration of neurons and pancreatic β cells. $[Ca^{2+}]_{ER}$ is not only important for signaling but also for the folding and processing of newly synthesized proteins which have shown to be Ca^{2+}-dependent reactions (Kuznetsov *et al*., 1992; Lodish *et al*., 1992). Cell lines and animals with WFS1 insufficiency have shown ER stress which triggers the unfolded protein response (UPR), impairs cell cycle progression, and increases apoptosis in pancreatic β cells (Fonseca *et al*., 2006; Yamada *et al*., 2006). Wolcott-Rallison syndrome (MIM 226980), a rare autosomal recessive disorder with infancy-onset diabetes as one of its symptoms, is caused by mutations in *EIF2AK3* (translation initiation factor 2-alpha kinase 3, also known as *PERK*), a kinase important in the UPR (Delepine *et al*., 2000). Folding and processing of newly synthesized proteins require high Ca^{2+} levels thus higher than normal $[Ca^{2+}]_{ER}$ may not impair protein folding and trigger the UPR.

High $[Ca^{2+}]_{ER}$ has been shown to have a number of different cellular effects. It can increase the Ca^{2+} release rate constant in cardiomyocytes (Han *et al*., 1994; Bassani *et al*., 1995), affect the sensitivity of the ryanodine receptor, a major ER Ca^{2+} release channel (Gyorke & Gyorke, 1998; Gyorke *et al*., 2004) and can inhibit Ca^{2+} uptake and affect the velocity of uptake in mouse pancreatic acinar cells and sensory neurons from dorsal root ganglia of rats (Mogami *et al*., 1998; Solovyova *et al*., 2002). Interestingly, knockin of presenilin-1 Alzheimer mutations in mice show

increased $[Ca^{2+}]_{ER}$ (Leissring *et al.*, 2000). In hippocampal neurons from these mice, glutamate-induced oxidative stress and mitochondrial dysfunction is enhanced resulting in a lower threshold for excitotoxic neuronal necrotic cell death (Guo *et al.*, 1999). The mitochondria is also an important component in Ca^{2+} signaling as it can rapidly sequester Ca^{2+} after an initial Ca^{2+} pulse and slowly releases it during the recovery phase through a permeability transition pore (PTP) (Jouaville *et al.*, 1995; Collins *et al.*, 2000). Overloading the ER with Ca^{2+} enhances sensitivity of ceramide induced apoptosis through the overload of Ca^{2+} in the mitochondria and release of cytochrome c through the formation of the PTP (Shimizu *et al.*, 1999; Pinton *et al.*, 2001). Disturbing Ca^{2+} homeostasis seems to predispose cells to multiple forms of cell death.

WFS has now been shown to be caused by at least two different genes, *WFS1* and *CISD2*. They are both ER proteins and seem to affect cellular Ca^{2+} homeostasis. *WFS1* has also been implicated in nonsyndromic hearing loss and OA. *CISD2* could also be important in isolated cases of these disorders. It remains to be determined if the two genes reside in the same pathway and what specific mechanism each gene uses that leads to nerve and pancreatic degeneration.

CHAPTER 4

CHARACTERIZATION OF THE CELLULAR PATHOGENESIS IN WFS2 USING AN

IN VITRO MODEL

4.1 Introduction

Neurodegeneration and diabetes mellitus, two characteristic manifestations in Wolfram syndrome, arise from a progressive loss or dysfunction of neurons (Mayeux, 2003), and β-cells (Donath & Halban, 2004) respectively. Cell death, in both diabetes and neurodegeneration, is a key driver of the progression of the disease. Loss of these types of cells is attributed to apoptotic, necrotic, or autophagic pathways of cell death. Cell death pathways are triggered by several types of cellular stress including ER stress and oxidative stress, which in turn activate converging downstream pathways. After exposure to these types of stress, cellular responses initially attempt to restore cellular viability and homeostasis, but under persistent insult, eventually give in to cell death pathways.

Post mortem and MRI studies of WFS patients showed loss of neurons in various brain regions, atrophy of optic nerves, diffuse neurodegeneration throughout the brain, and selective loss of pancreatic β-cells (Genis *et al*., 1997; Rando *et al*., 1992). A mouse knockout of the first gene identified for Wolfram syndrome, WFS1, showed impaired glucose homeostasis and progressive β-cell loss via apoptosis (Ishihara *et al*., 2004), such as seen in Wolfram Syndrome patients.

Additionally, *WFS1* has increased levels of expression in isolated pancreatic islets (Yamaguchi *et al.*, 2004), human fibroblasts (Ueda *et al.*, 2005), pancreatic β-cell derived MIN6 cells (Ueda *et al.*, 2005), and Ins2 $^{96Y/Y}$ cells derived from a juvenile diabetes mouse model

(Ueda *et al.*, 2005), in response to ER stress inducing chemicals, such as thapsigargin and dithiothreitol, in the former three cell types and increased insulin expression in the Ins2 $^{96Y/Y}$ cells. Ueda *et al.* (2005) also carried out *WFS1* promoter luciferase reporter assays that revealed increased *WFS1* promoter activity in response to the aforementioned ER stressors. Furthermore, Fonseca *et al.* (2005) showed that mouse fibroblasts with homozygous mutations in either one of two major regulatory UPR proteins, *Ire1α* or *Perk*, resulted in attenuation of *Wfs1* induction by ER stressors. In addition, *Wfs1* knockdown in a β-cell line, INS-1 832/13, resulted in increased expression of several UPR markers including BiP, ERO1α, spliced *Xbp-1*, and total *Xbp-1* mRNA (Fonseca *et al.*, 2005). Similar results were seen in pancreatic islets derived from *Wfs1*-deficient mice and *Wfs1*-deficient MIN6 clonal β-cells along with increased apoptosis, reduced BrdU incorporation, and increased expression of the cell cycle inhibitor p21^{CIP1} (Yamada *et al.*, 2006). Taken together, this data suggests that *WFS1* plays a role in ER homeostasis in cells (Yamaguchi *et al.*, 2004; Ueda *et al.*, 2005; Fonseca *et al.*, 2005; Yamada *et al.*, 2006), particularly pancreatic β-cells, and is an important regulator of the UPR (Fonseca *et al*, 2005, Yamada *et al.*, 2006). Thus, homozygous mutations in *WFS1* lead to an inability to cope with chronic ER stress resulting in impaired function and proliferation, and increased apoptosis in β-cells which, in turn, contribute to disease pathogenesis (Yamada *et al.*, 2006).

As our previous results showed, the newly identified Wolfram syndrome gene, *CISD2*, translates into a protein, ERIS, which is localized in the ER but does not interact directly with WFS1. It is expressed in most tissues, notably the brain and the pancreas. Protein analysis showed that *CISD2* contains a conserved zinc finger domain, referred to as CDGSH zinc finger domain. In a previous study, another protein containing the same conserved zinc finger domain, called MitoNEET, was found to be a target of the diabetic insulin sensitizer drug, pioglitazone

(Coleca *et al*., 2004). It was Wiley *et al*., (2007), however, who identified mitoNEET as a member of the CDGSH zinc finger family, along with ERIS (referred to as Miner1) and a third protein, Miner2. MitoNEET was shown to be an outer mitochondrial membrane protein that binds to iron, not zinc, which prompted the authors to suggest that ERIS and Miner2 are also iron-containing proteins (Wiley *et al*., 2007). The gene name of *CISD2* was appropriately changed to conserved iron sulfur domain 2 (*CISD2*), which will be used henceforth. Wiley *et al*. (2007) showed that loss of MitoNEET expression in mice resulted in a decrease in the maximal capacity of heart mitochondria to carry out electron transport and oxidative phosphorylation and highlighted the idea that MitoNEET plays an important role in mitochondrial function.

The goal of our study is to create *in vitro* models of WFS2 to study cellular and molecular pathogenesis by knocking down *Cisd2* in cell lines derived from tissues most affected by the disease. Cell lines utilized in the study were the rat pancreatic insulinoma cell line (INS1), the mouse neuroblastoma cell line (N1E115), and the mouse embryonic stem cell like cell line (P19) which can be differentiated into neurons. The lymphoblastoid cell line derived from a WFS2 affected individual was also used. To characterize WFS2 pathogenesis, cell death was assessed in INS1 *Cisd2* knockdown cell lines and the levels of apoptotic and autophagic markers were examined. Due to the intimate relationship of WFS1 with the UPR, activation of UPR markers was assessed in INS1 and N1E115 *Cisd2* knockdown cells as well as affected lymphoblastoid cells. *Cisd2* levels were determined in INS1 and N1E115 wild type cells in response of ER stress in the form of thapsigargin. Furthermore, another route for disease pathogenesis, oxidative stress, was investigated by measurement of levels of antioxidant enzymes and global protein nitration in INS1 *Cisd2* knockdown cells, and an exacerbated cell death response due to treatment with oxidative stressors. Metabolic activity is assessed in INS1

Cisd2 knockdown cells to investigate whether cells had a higher demand for energy or had to work harder due to *Cisd2* knockdown. In light of recent reports on the function CISD2, the autophagic response in the INS1 *Cisd2* knockdown model is also looked at, where cells were starved and the autophagy marker LC3-II was measured. P19 *Cisd2* knockdown cells were utilized to study the role of *CISD2* in neuronal differentiation. Through these different strategies, our aim was a greater understanding of how WFS2 developed at a cellular and molecular level.

4.2 Results

4.2.1 Creation of Stable Cisd2 knockdown cell lines

To create an *in vitro* model of WFS2, stable *Cisd2* knockdown cell lines were established in three cell lines using the pSUPER RNAi system: rat insulinoma cells (INS1), mouse neuroblastoma cells (N1E115), and mouse embryonic stem cell like cells (P19). INS1 and N1E115 cell lines were used because they are derived from tissues that are primarily affected in Wolfram syndrome, namely pancreatic β-cells and neurons respectively. The P19 cell line was used because of its ability to be differentiated into neurons and glial cells. In addition, a fourth cell line, human lymphoblastoid cell lines, were derived from an unaffected control (W1) and an affected member from one of the Jordanian families (W2). The W2 cell line is a natural knockout of the CISD2 gene but lymphoblastoid cells are not derived from tissues most affected in the disease. Before carrying out knockdown experiments, semi-quantitative RT-PCR using *Cisd2* species-specific primers were used to determine that *Cisd2* is expressed in all lines (data not shown).

After screening several colonies by semi-quantitative RT-PCR followed by Real-Time quantitative RT-PCR (qRT-PCR), several colonies from each cell line showed knockdown of

Cisd2. qRT-PCR analysis revealed that the N1E115 knockdown cells M1-2 and M2-4 showed modest levels of knockdown (Figure 8A), while the P19 knockdown cells P19 1-5 and P19 2-12 (Figure 8B) and INS1 knockdown cells R1-2, R1-3, and R1-4 (Figure 8C) showed more substantial knockdown. Western blot analysis using the CISD2 antibody confirmed robust knockdown of *Cisd2* knockdown in INS1 cells (Figure 8D lower panel) and in P19 1-5 cells (Figure 8D, upper panel). P19 2-12 cells did not show knockdown at the protein level. Vector only control cells were created for the P19 (P19 VO-4), and INS1 (RVO-2) cell lines and scrambled control cells (RSCR-1) were created for the INS1 cell line, all of which showed comparable *Cisd2* expression to wild-type cells (Figure 8B, C, D). For all experiments the INS1 knockdown cells were used as it had the greatest levels of knockdown, complete set of controls, and most resembles the tissue it was derived from. Other knockdown cells were used in adjunct to the INS1 cells, except for the P19 differentiation experiments which were carried out with the P19 cells only.

4.2.2 Increase levels of apoptosis in Cisd2 knockdown INS1 cells

β-cell loss is observed in postmortem tissue of WFS patients (Genis *et al*., 1997). Additionally, *Wfs1* knockout mice exhibit loss of β-cells through apoptosis (Ishihara *et al*., 2004). To determine whether apoptotic pathways are activated in WFS2 patients, we carried out Annexin V/7AAD apoptosis assay in INS1 *Cisd2* knockdown cells. Annexin V has a strong, specific affinity to phosphatidylserine, which is translocated from the cytoplasmic side of the plasma membrane to the outer side after the induction of apoptosis. 7AAD is a fluorescent chemical compound with a strong affinity for DNA, but can only enter the cell if the cell membrane is permeabilized or disrupted as is the case with dying or dead cells. Thus, Annexin
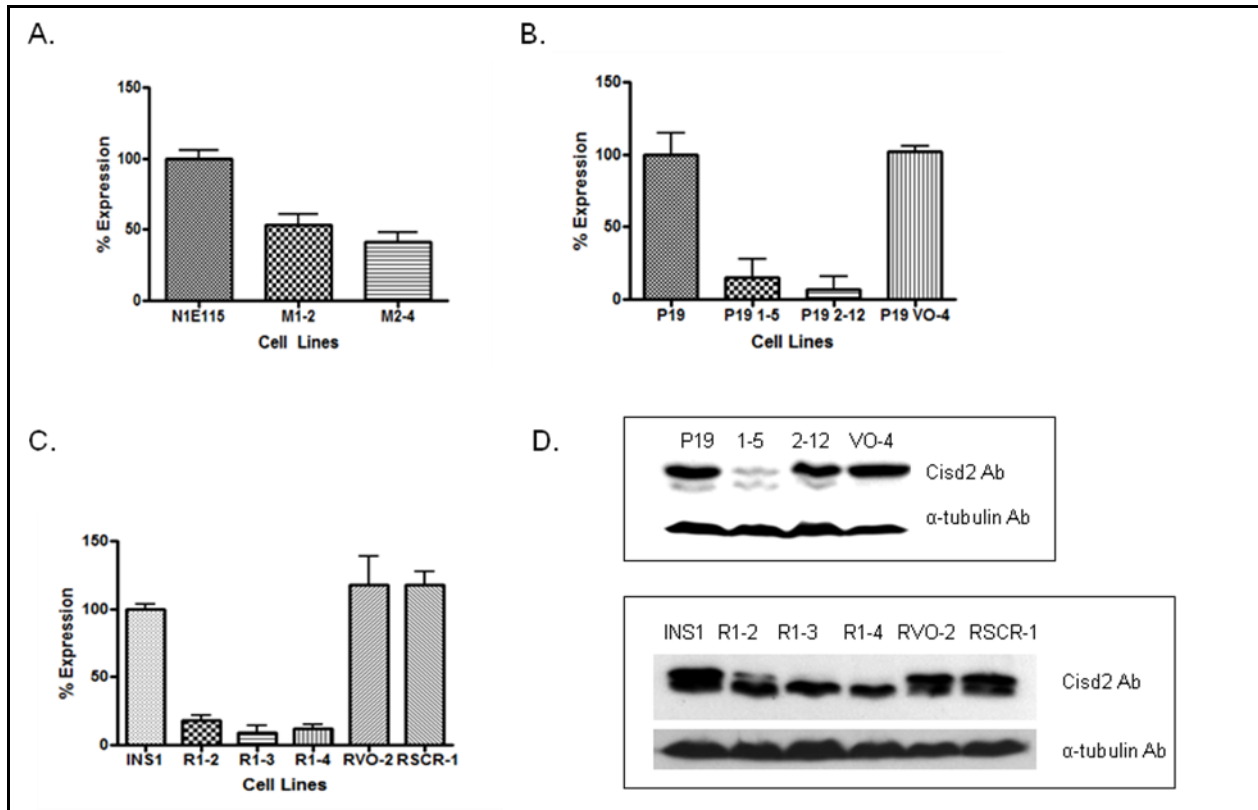
Figure 8. qRT-PCR and Western blot analysis of stably transfected *Cisd2* knockdown cells.
(A) N1E115 cells M1-2 and M2-4 show 46.8% and 58.9% knockdown respectively. (B) Two
P19 cell lines show high levels of *Cisd2* knockdown using different targets in each cell line: 1-5
(85.1%) and 2-12 (93.1%). (C) INS1 cells show high levels of *Cisd2* knockdown with R1-2 at
81.8% knockdown, R1-3 at 90.6% knockdown, and R1-4 at 87.6% knockdown, compared with
the untransfected INS1 cells. Vector only controls for P19 cells and vector only and scramble
controls for INS1 cells did not show *Cisd2* knockdown. (D) Western blot analysis shows
knockdown of *CISD2* (15.2 KDa) in P19 1-5 cells but not in P19 2-12 cells (upper panel), and
effective knockout in R1-3 and R1-4, and moderate knockout in R1-2 (lower panel). The lower
band seen when blotting with CISD2 antibody corresponds to CISD1 protein (12.5 KDa) which
shares a high degree of homology to CISD2 protein. In all qRT-PCR experiments GAPDH was
used as an internal control, and in all Western blot analysis α-tubulin was used as an internal
control. Data in graphs represented as means + SEM.

V/7AAD allows for detection of apoptosis at all stages from earlier events such as phosphatidylserine translocation to late events such as disruption of the cell membrane. After staining with Annexin V and 7AAD, cells were analyzed by flow cytometry (Figure 9). Two of the three knockdown cell lines, R1-3 and R1-4, showed significantly greater levels of Annexin V/7AAD staining compared with wild-type INS1 cells, while both vector only and scrambled control cells showed no difference (Figure 9). Although the R1-2 did not show a significant difference in percentage of cell death compared with wild type INS1 cells, it did show a significant difference in percentage of cell death compared with both RVO-2 and RSCR-1 control cells.

To further investigate the activation of apoptotic pathways in *Cisd2* knockdown cells, we set out to measure the expression of well studied molecular markers of apoptosis, namely *CHOP/GADD153* and BAX. The stress inducible transcription factor CHOP (C/EBP homologous protein), also known as growth arrest and DNA damage-inducible gene 153 (GADD153), is a transcriptionally regulated pro-apoptotic molecule (Oyadomari & Mori, 2004). The BCL2-associated X protein (BAX) is also a well known proapoptotic molecule that plays a role in the mitochondrial intrinsic apoptosis pathway (Chipuk & Green, 2005). We measured expression levels of these two apoptosis markers in INS1 *Cisd2* knockdown cells by using qRT-PCR to measure the transcriptional expression of *Chop* and Western blot analysis to measure the translational expression of BAX. In *Cisd2* knockdown cells, *Chop* transcription increased 16-fold in R1-2, 12-fold in R1-3, and 16-fold in R1-4 compared with wild-type INS1 cells. This was significantly greater than the 6-fold and 4-fold increase of *Chop* expression seen in the control cells RVO-2 and RSCR-1 respectively (Figure 10A). Additionally upregulation of BAX protein levels was detected in *Cisd2* knockdown cells compared with control cells (Figure 10B). These
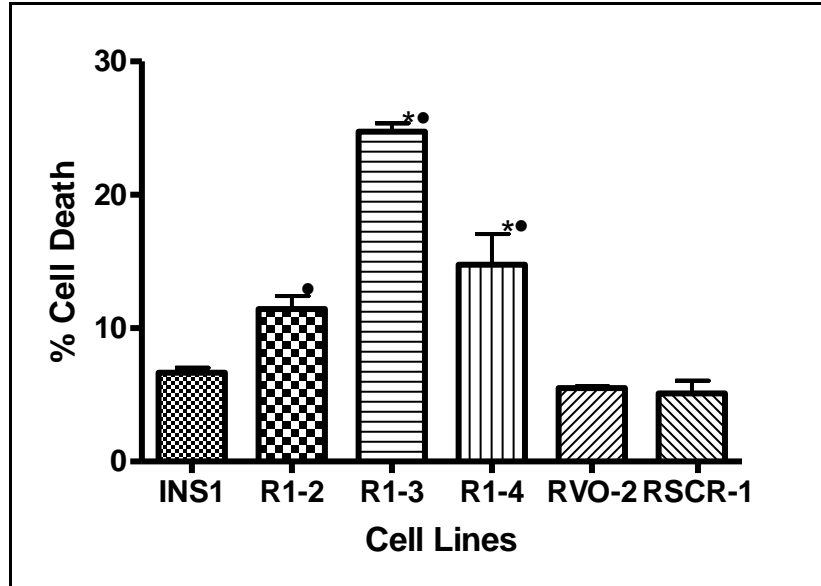
Figure 9. Apoptotic cell death increases in INS1 *Cisd2* knockdown cells compared with control lines. Annexin V/7AAD staining of INS1 cell lines (n = 2) reveal a significantly greater percentage of cell death in the knockdown cells R1-3 (24.3% ± 0.9) and R1-4 (14.8% ± 3.3) compared with wild type INS1 cell (6.7% ± 0.5). R1-2 cells (11.45% ± 1.4) did not show a significant difference compared with INS1 cells, but did show a significant difference with both control cells RVO-2 (5.5 ± 0.2) and RSCR-1 (5.2 ± 1.0) \. All three control cell lines, wild-type INS1, RVO-2, and RSCR-1, were not significantly different than each other. Significance was set at $p < 0.05$ and is denoted by asterisk for INS1 comparison and by circle for RVO-2 and RSCR-1 comparison. Statistical analysis was carried out by 1-way ANOVA followed by Dunnett's t-test with the reference set as INS1, RVO-2, or RSCR-1. Data represented as means + SEM.
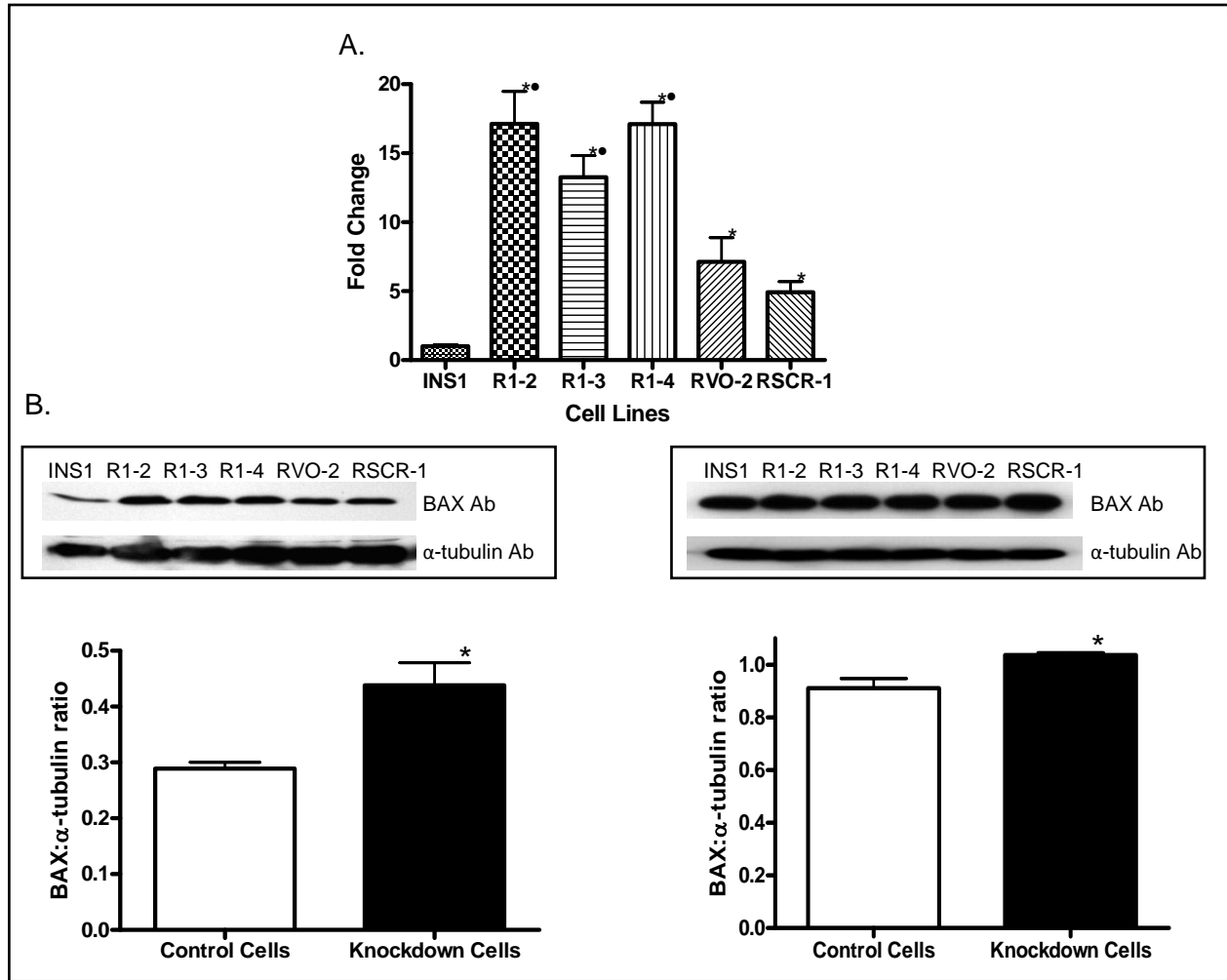
Figure 10. Transcriptional or translational expression of apoptotic markers *Chop* and BAX, respectively, increase in INS1 *Cisd2* knockdown cells compared with control lines. (A) *Chop* mRNA levels was measured in INS1 cells (n=3) using qRT-PCR revealing a significant 12- to 16-fold increase of *Chop* expression in Cisd2 knockdown cells R1-2, R1-3, and R1-4 compared with wild-type INS1 cells. The control cell lines RVO-2 and RSCR-1 show 6-fold and 4-fold increases in *Chop* expression respectively, which are still significantly lower than the *Cisd2* knockdown cells. GAPDH was used as an internal control. Significance was set at $p < 0.05$ and denoted by an asterisk for INS1 comparison and by a circle for RVO-2 and RSCR-1 comparisons. (B) Western blot analysis was used to detect levels of BAX, using α-tubulin as an internal control. Bands were measured using spot densitometry and the ratio of BAX to α-tubulin was determined. Since the ranges of the ratios between the two blots shown were highly variable, we did not combine the ratios of each cell type. However, for each blot the ratios of *Cisd2* knockdown cells were compared with the ratios of the control cells, and in both blots *Cisd2* knockdown cells show significantly higher level of BAX expression compared with control cells (left blot: 0.298 vs. 0.438; right blot: 0.911 vs. 1.04). Significance was set at $p < 0.05$ and is denoted by asterisk. For qRT-PCR, statistical analysis was carried out by 1-way ANOVA followed by Dunnett's t-test with the reference set as INS1, RVO-2, or RSCR-1. For Western

blot analysis, student t-test was used to compare control cell lines and knockdown cell lines. Data in graphs represented as means + SEM.

findings support the idea that *CISD2* deficiency causes increased apoptosis in cells, which contributes to the development of the disease.

4.2.3 CISD2 deficiency does not activate the UPR

Several lines of evidence implicate WFS1 in the regulation of the UPR. Specifically, inactivation of *WFS1* in INS 1 pancreatic β-cells causes upregulation of the UPR (Fonseca *et al*., 2005; Yamada *et al*., 2006). Since both ERIS and wolframin (WFS1 protein) are ER membrane proteins and mutations in both the *WFS1* and *WFS2* genes produce similar phenotypes, it was hypothesized that the pathogenesis of the disorder is similar and that the UPR is activated in

WFS2 affected and knockdown cells. To assess whether the UPR was activated in the *CISD2* deficient cells, we measured the changes of expression in several markers of an activated UPR, including spliced *XBP-1* using semi-quantitative RT-PCR, and phosporylated eIF2α (p-eIF2α) using Western blot analysis in *CISD2* deficient lymphoblastoid cells and INS1 *Cisd2* knockdown cells. N1E115 *Cisd2* knockdown cells were also used to measure changes in spliced *XBP-1*. In addition, expression of UPR markers BiP/GRP78 and GRP94 was measured by Western blot analysis in INS1 *Cisd2* knockdown cells. In all cell lines used, no increase in levels of spliced *XBP-1* was detected in any of the knockdown cells compared with wild-type and control cell lines (Lymphoblastoid cells: Figure 11A; INS1 cells: Figure 11C). UPR upregulation was confirmed by increased spliced *XBP-1* in INS1 and N1E115 cell treated with thapsigargin (Figure 12). Western blot analysis of p-eIF2α in lymphoblastoid cells (Figure 11B) and INS1 cells (Figure 11D) also revealed no changes of expression of this marker in any of the *CISD2* deficient cells compared with controls. Additionally, INS1 *Cisd2* knockdown cells did not reveal

any upregulation of the two UPR related proteins BiP/GRP78 and GRP94 (Figure 11D). Taken together, this data shows that the UPR is not activated under conditions of *CISD2* deficiency.

4.2.4 CISD2 is not upregulated under ER stress.

An increase in expression of *WFS1* and activation of the *WFS1* promoter is seen in several cell models under conditions of increased ER stress (Yamaguchi *et al*., 2004; Ueda *et al*., 2005). To assess whether *CISD2* expression increases under conditions of ER stress, INS1 and N1E115 cells were treated with thapsigargin, a known ER stressor that acts by inhibiting the SERCA ATPase pumps of the ER thereby stopping Ca^{2+} from entering the ER, severely affecting ER calcium homeostasis. Treatment of cells with thapsigargin led to an expected increase in spliced *XBP-1* in both cell types (Figure 12). *Cisd2* expression, however, remained unchanged in both cell types (Figure 12). These results indicate that under conditions of ER stress, such as thapsigargin treatment, the UPR is activated in both cell types, as indicated by the increase in spliced *XBP-1*, but *CISD2* expression is unaffected.
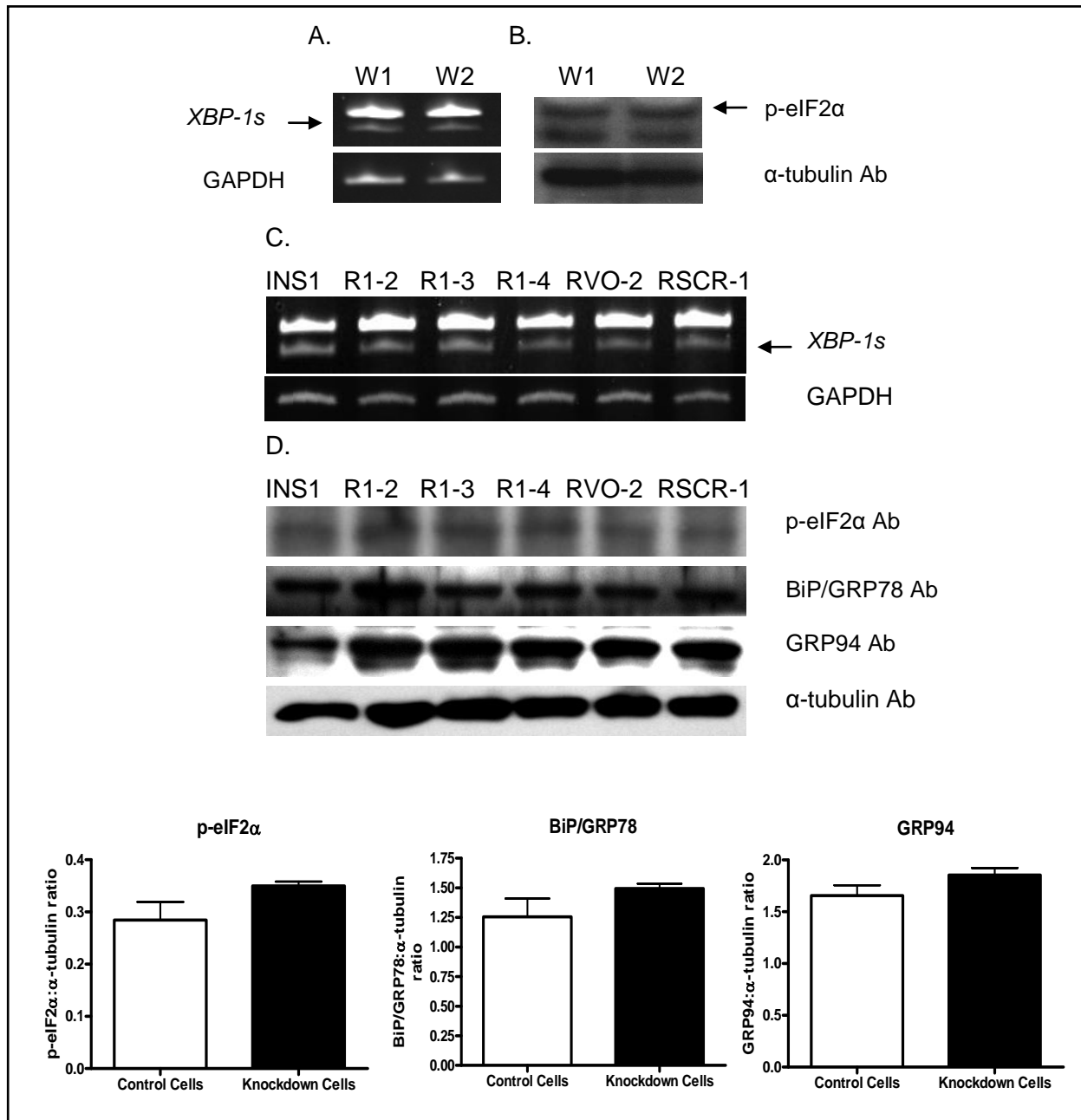
Figure 11. No change in UPR markers in *CISD2* deficient cells compared with control cells.
Spot densitometry was used to measure levels of expression of various UPR markers in *CISD2*
deficient cells, which were normalized to GAPDH for semi-quantitative RT-PCR and α-tubulin
for Western blot analysis. Ratios of marker to internal control were determined and used for
statistical analysis. (A) Levels of spliced *XBP-1* (*XBP-1s*) are measured in wild-type (W1) and
CISD2 mutant (W2) lymphoblastoid cells using semi-quantitative RT-PCR revealing no change
between them. The upper band seen is that of unspliced *XBP-1*. (B) Western blot analysis was
used to measure p-eIF2α protein levels in W1 and W2, which also showed no difference. (C) In
INS1 cells, no change in XBP-1s was detected between *Cisd2* knockdown cells and control cells.
(D) Western blot analysis showed no differences in INS1 *Cisd2* knockdown and INS1 control

cells for the UPR markers p-eIF2α, BiP/GRP78, and GRP94. Bands were measured using spot densitometry and the ratio of UPR marker to α-tubulin was determined. For each marker the ratios of *Cisd2* knockdown cells were compared with the ratios of the control cells, and in for all markers no significant difference was found between Cisd2 knockdown cells and control cells. N1E115 cells were also used for *XBP-1s* analysis also showing no change of spliced *XBP-1* levels in Cisd2 knockdown cells compared with wild-type control (data not shown). Significance was set at $p < 0.05$. For Western blot analysis, student t-test was used to compare control cell lines and knockdown cell lines. Data in graphs represented as means + SEM.

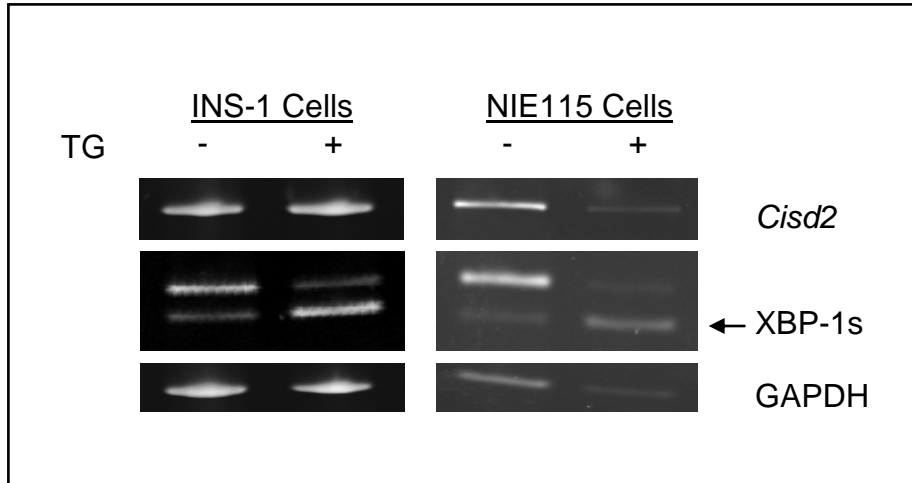**Figure 12. No change in *Cisd2* expression under ER Stress.** Wild-type INS1 and N1E115 cells were treated with the known ER stressor thapsigargin (TG; 1 µmol for 16 hrs) and expression of *Cisd2* and *XBP-1s* levels were measure in untreated (-) and treated (+) cells using semi-quantitative RT-PCR. In both cell types, an increase in *XBP-1s* is observed, while no increase in *Cisd2* is seen when cells are treated with TG.

4.2.5 Upregulation of oxidative stress markers in INS Cisd2 knockdown cells

Oxidative stress can contribute to the pathogenesis of several disease including diabetes and neurodegeneration. In addition, oxidative stress and with impaired Ca^{2+} homeostasis both contribute to mitochondrial PTP formation, mitochondrial failure, and eventually necrotic or apoptotic cell death (Ott *et al*., 2007; Jacobson & Duchen, 2002). Additionally, oxidative stress originating from mitochondrial ROS production promotes Ca^{2+} release from the ER, increasing mitochondrial Ca^{2+} (Jacobson & Duchen, 2002). We observed increased cytosolic Ca^{2+} in *CISD2* mutant lymphoblastoid cells compared with wild-type controls after treatment with thapsigargin, suggesting a Ca^{2+} homeostasis anomaly in *CISD2* deficient cells. To further investigate the role of oxidative stress in *CISD2* deficient cells, we measured expression of known oxidative stress markers including increased transcription of two antioxidant enzymes *SOD1* and *SOD2*, as well as the increases in global nitration of tyrosine residues- a downstream effect of the highly reactive molecule peroxynitrite.

Sod1 and *Sod2* in INS1 cell lines were measured by qRT-PCR (Figure 13). Both *Sod1* and *Sod2* expression was significantly increased in all INS1 *Cisd2* knockdowns cells compared with both wild-type INS1 cell lines and vector only and scrambled control cells. Specifically, *Sod1* showed a 91%, 61%, and 75% increase in R1-2 cells, R1-3 cells, and R1-4 cells respectively, compared with wild-type INS1 cells. *Sod2* had an even greater difference in expression with a 156%, 134%, and 240% increase in expression in R1-2 cells, R1-3 cells, and R1-4 cells respectively, compared with wild-type INS1 cells. In addition, Sod1 and Sod2 activity was measured using in-gel SOD activity assay. Although *Sod1* and *Sod2* expression was upregulated in INS1 *Cisd2* knockdown cells compared with controls, Sod1 activity was similar in all cell lines while Sod2 activity was undetectable in all cell lines (data not shown).
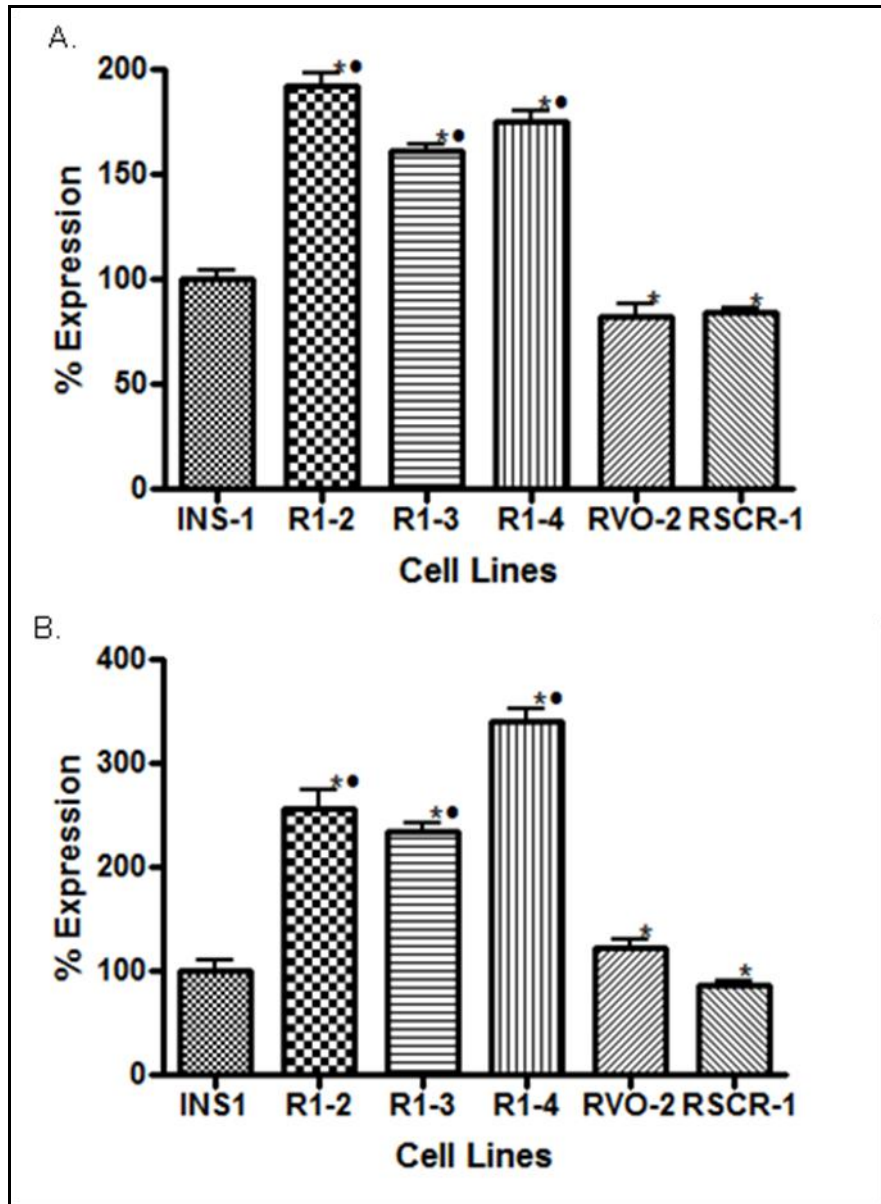
Figure 13. *Sod1* and *Sod2* expression increase in INS1 *Cisd2* knockdown cells compared with control cell lines. *Sod1* and *Sod2* mRNA expression was measured in INS1 cell lines (n=3) using qRT-PCR. (A) There was significantly greater *Sod1* expression in R1-2 (91.7% ± 4.1), R1-3 (61.4 ± 3.1), and R1-4 (75.3% ± 4.6) than in wild-type INS1 cells. *Cisd2* knockdown cell lines were also significantly greater than control cell lines RVO-2 and RSCR-1. (B) Additionally, *Sod2* expression was also significantly greater in the three knockdown cell lines compared with wild-type INS1 cells. The percent increases were 156% ± 18.0 for R1-2, 134% ± 6.6 for R1-3, and 240% ± 11.6 for R1-4. *Cisd2* knockdown cell lines were also significantly greater than control cell lines RVO-2 and RSCR-1. Significance was set at $p < 0.05$ and is denoted by an asterisk for INS1 comparisons and by circle for RVO-2 and RSCR-1 comparisons. For qRT-PCR, statistical analysis was carried out by 1-way ANOVA followed by Dunnett's t-test with the reference set as INS1, RVO-2, or RSCR-1. Data in graphs represented as means + SEM.

86

Upregulation of *Sod1* and *Sod2* mRNA in the knockdown cell lines suggests transcriptional activation due to increase in oxidative stress.

One of the effects of oxidative stress on macromolecules is the nitration of tyrosine residues on proteins. To measure levels of global tyrosine nitration in INS1 *Cisd2* knockdown cells we immunoprecipitated nitrated tyrosine containing proteins from whole cell lysates of the cells, ran the precipitate on an SDS-PAGE gel, transferred the proteins onto a PVDF membrane, and then blotted the membrane with an anti-nitrated tyrosine antibody - the same one used in the immunoprecipitation (Figure 14A, left). A negative control was used by running another SDS-PAGE gel using the same amount of immunoprecipitated proteins from the same samples which was run alongside the aforementioned gel. It was also transferred onto a PVDF membrane which was treated with a dithionite solution to reduce nitrotyrosines to aminotyrosines before blotting with the anti-nitrotrated tyrosine antibody (Figure 14A, right).

Using spot densitometry to measure regions on the membrane that were positive for nitrated tyrosines, integrated density values (IDV) for each cell line was determined. Then we compared the mean of the IDV of the INS1 *Cisd2* knockdown cell lines with the mean IDV of the INS1 wild-type, RVO-2, and RSCR-1 cells. Our results showed a significantly greater level of global nitrated tyrosine residues in *Cisd2* knockdown cells compared with control cells (Figure 14B), indicating that INS1 *Cisd2* knockdown cell lines are exposed to greater levels of oxidative stress or decreased capacity to neutralize reactive oxygen species
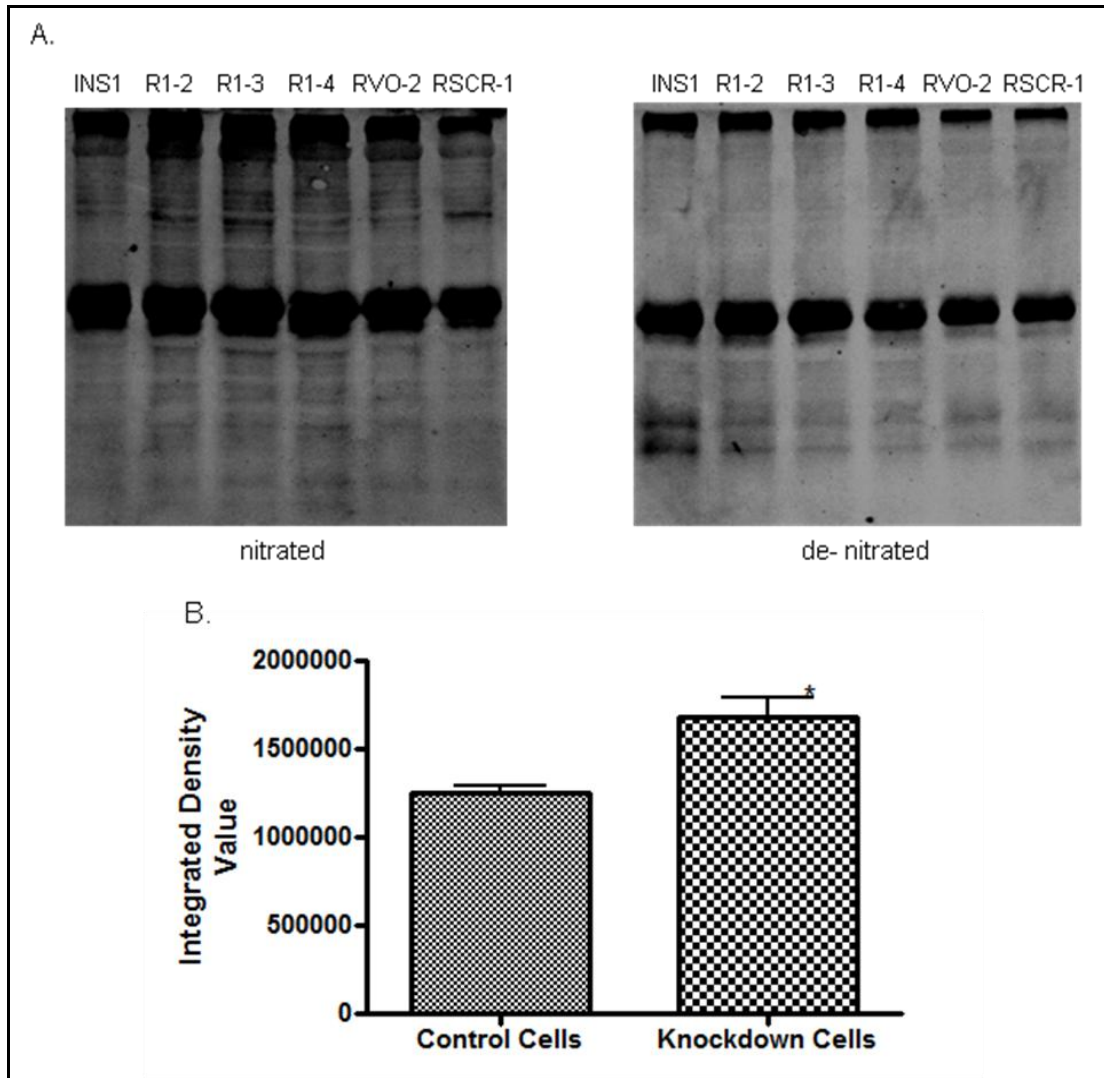
Figure 14. Increase in global protein nitration of tyrosine residues in *Cisd2* knockdown cells compared with control cell lines. (A) Whole cell lysates from INS1 cell lines were immunoprecipitated with anti-nitrotyrosine followed by Western blot analysis with anti-nitrotyrosine. The membrane on the left represents global nitrated tyrosines in whole cell lysates of INS1 cell lines. The membrane on the right contains the same immunoprecipitated product seen in the left, but the membrane was treated with dithionite solution (100 mM sodium hydrosulfite, 50 mM sodium bicarbonate, pH = 9.0) to reduce nitrotyrosine to aminotyrosine which can no longer bind to anti-nitrotyrosine antibodies. This membrane acted as a negative control. (B) Spot densitometry of nitration in the membrane on the left was used to measure levels of nitration of each cell line. The average IDV values for the knockdown cell lines were compared with the average IDV value of control cell lines The INS1 *Cisd2* knockdown cell lines R1-2, R1-3, R1-4 had a significantly higher level of nitration than that of the control cell lines (1,684,000 ± 109,400 IDV vs. 1,250,000 IDV ± 45,870) representing a 34.7% increase in nitration. Significance was set at $p < 0.05$ and is denoted by an asterisk. Student t-test was used to compare control cell lines and knockdown cell lines. Data in graphs represented as means + SEM. IDV, Integrated Density Value.

4.2.6 Cell death is exacerbated in INS1 Cisd2 knockdown cells under conditions of increased oxidative stress

Our previous results showed an increase in markers of oxidative stress in *Cisd2* knockdown cells. Next, we wanted to investigate whether *Cisd2* knockdown cells were more susceptible to oxidative stress. We accomplished this by treating cells with various known oxidative stressors, including thapsigargin, paraquat, H_2O_2, and high glucose, followed by detection of cell death via Annexin V/7AAD staining and subsequent analysis by flow cytometry. Due to the increased levels of oxidative stress at basal conditions, we expected to see a more profound effect of these oxidative stressors on *Cisd2* knockdown cells.

Thapsigargin, which is a known ER stressor, can also induce oxidative stress through ER stress signaling pathways (Hsieh *et al.*, 2007). INS1 cells were treated with either 25 nM or 100 nM thapsigargin for 24 hours and cell death was subsequently measured (Figure 15A). Two of the three INS1 *Cisd2* knockdown cells, R1-3 and R1-4, showed significantly greater increases in cell death after treatment with 25 nM or 100 nM thapsigargin. Increases in cell death in treated wild-type INS1 cells compared with untreated wild-type INS1 cells were much smaller and not significant. R1-2 showed a slightly higher, but not significant, increase in cell death with 100 nM thapsigargin treatment compared with the increase seen in wild-type cells, but the increases in cell death were comparable for the 25 nM treatment for the two cell lines.

Cell death with thapsigargin treatments, 25 nM and 100 nM, were pooled and subtracted from cell death in untreated cells to determine change in cell death with treatment for each cell line (Figure 15B). Change in cell death with thapsigargin treatment in R1-3 and R1-4 was significantly greater than change in cell death with thapsigargin treatment observed in the wild type INS1 cells. R1-2 cells treated with thapsigargin showed a change in cell death that was

greater than that seen in wild type INS1 cells but it was not found to be statistically significant. The other two control cell lines, RVO-2 and RSCR-1, had changes in cell death with thapsigargin treatment that were lower than the wild type INS1 cells and were not statistically significant.

A more direct inducer of oxidative stress, paraquat, was also used to treat cells. Paraquat is an herbicide that causes oxidative toxicity via ROS production (Bus & Gibson, 1984). Treatment of mice with paraquat caused selective loss of nigrostriatal dopaminergic neurons with increases in oxidative markers including 4-HNE and nitrotyrosines (McCormack *et al*., 2005). We treated INS1 cell lines with 250 nM paraquat for 24 hours followed by measurement of cell death for each sample (Figure 16). In all INS1 cell lines, treated cells showed a greater percentage of cell death compared with their respective untreated cells. The change in cell death was only statistically significant, however, in wild-type INS1 cells, R1-2 cells, and RSCR-1 cells. Interestingly, R1-3 and R1-4 showed the greatest amount of change in cell death with treatment, but that change was not found to be statistically significant, possibly in part due large standard deviation between samples within the treatment group for each cell line.

To compare change in cell death with paraquat treatment across different cell lines, cell death with paraquat treatment was subtracted from cell death in untreated cells for each cell line. Change in cell death in R1-3 was significantly greater than change in cell death in the wild type INS1 cell line. Change in cell death in R1-4 was greater than cell death in the wild type INS1 cell line, but was not found to be statistically significant possibly due to a large standard deviation and small number of samples tested. R1-2 and the two control cell lines, RVO-2 and RSCR-1, showed changes in cell death comparable to the wild type INS1 cell line.

Figure 15. Cell death exacerbated in INS1 *Cisd2* knockdown cells compared with control cells with thapsigargin treatment. (A) INS1 cell lines were treated with either 25 nM TG (n = 2) or 100 nM TG (n =3) for 24 hours and were assayed for cell death via Annexin V/7AAD staining. Two of the three INS1 *Cisd2* knockdown cell lines, namely R1-3 and R1-4, showed a significant increase in cell death under both concentrations of thapsigargin treatment compared with their respective untreated control. R1-3 cells showed a 19.89% ± 0.69 with 25 nM TG treatment and a 25.93% ± 6.0 with 100 nM TG treatment compared with untreated R1-3 cells. R1-4 cells showed a 22.13 ± 3.1 with 25 nM TG treatment and a 21.39% ± 5.6 with 100 nM TG treatment compared with untreated R1-4 cells The third knockdown cell line, R1-2, showed a

91

non-significant increase of cell death with 25 nM (4.92% ± 6.1 increase) and 100 nM (9.6% ± 3.9 increase). Wild-type INS1 cells also showed a non-significant increase (25 nM TG: 4.4% ± 2.7, and 100 nM TG: 6.9 ± 3.6). The vector only control cells, RVO-2, showed a small but significant increase in cell death with 25 nM thapsigargin treatment (2.4% ± 0.7), but the increase in cell death with 100 nM TG treatment (3.5% ± 2.2) was not significant. The significance in the increase in cell death with 25 nM TG treatment of RVO-2 may be attributed to small sample size and small standard deviation in both groups leading to greater sensitivity in detecting differences between the means. RSCR-1 cells showed a small and non significant increase in 100 nM TG cells (2.0% ± 1.7). Only one sample of 25 nM RSCR-1 cells was included in this experiment, due to the loss of another sample during the preparation. This sample, however, showed a 1.5% decrease in cell death compared with untreated RSCR-1 cells. (B) Cell death rates for both TG treatments were pooled and subtracted from the cell death rate of their respective untreated control for each cell line to determine the change in cell death for each line. R1-3 and R1-4 had the greatest change in cell death with TG treatment, having 23.5% ± 3.6 increase and 21.7% ± 2.4 increase in cell death respectively. R1-2 also showed a modest increase in cell death (8.7% ± 3.4) with TG treatment. The wild type INS1, RVO-2 and RSCR-1 cell lines showed 5.9% ± 1.8, 3.1% ± 1.0, and 0.8% ± 1.1 increases in cell death after TG treatment. Change in cell death for all lines were compared with change in cell death in the wild type INS1 cell line. Both R1-3 and R1-4 showed a significantly greater change in cell death after TG treatment compared with the change in cell death in the wild type INS1 cell line. Significance was set at $p < 0.05$ and is denoted by an asterisk. In (A) statistical analysis was carried out by unpaired student t-test comparing untreated and treated samples of each cell line individually. In (B) 1-way ANOVA followed by Dunnett's t-test with the reference set as wild-type INS1. Data represented as means + SEM.
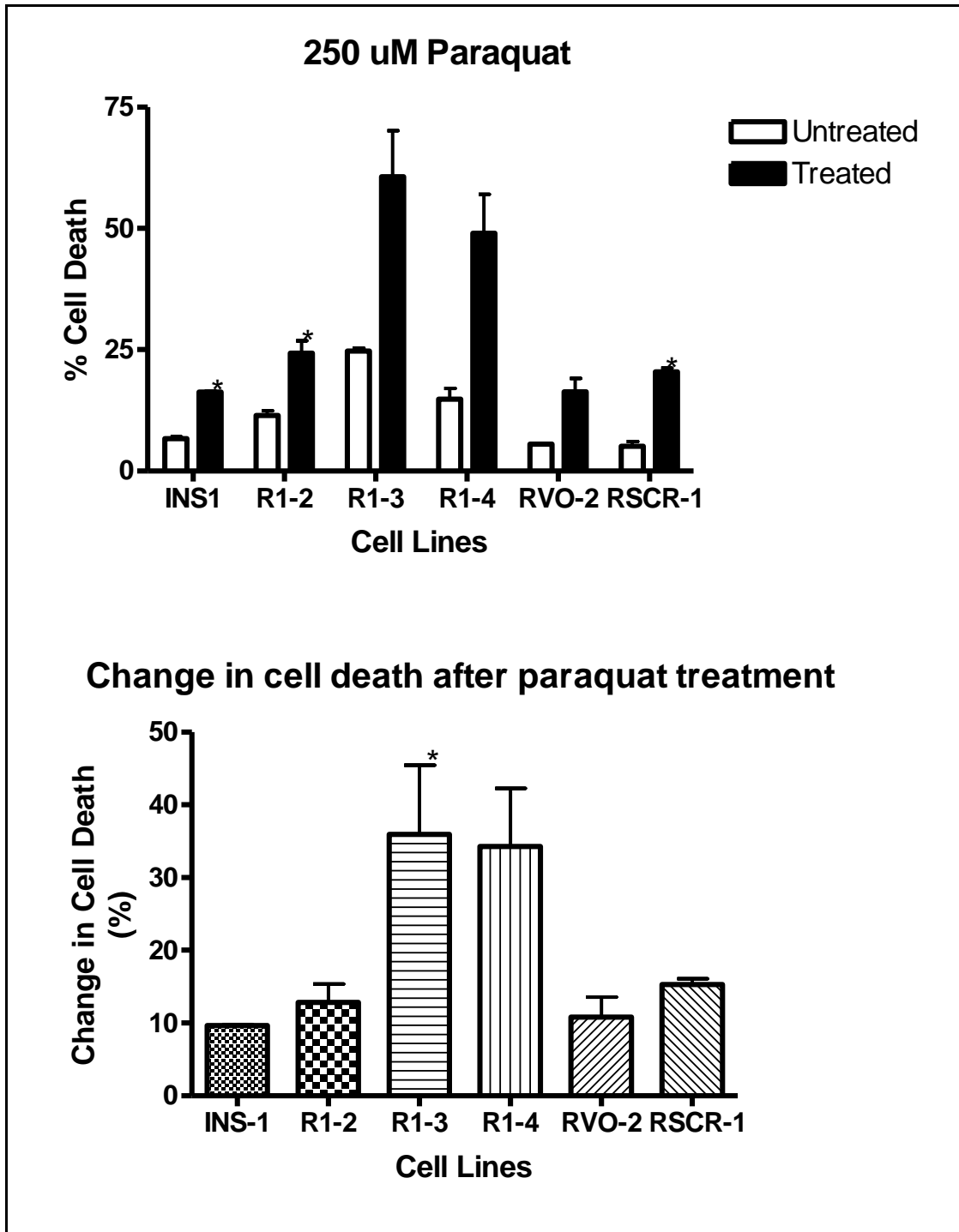
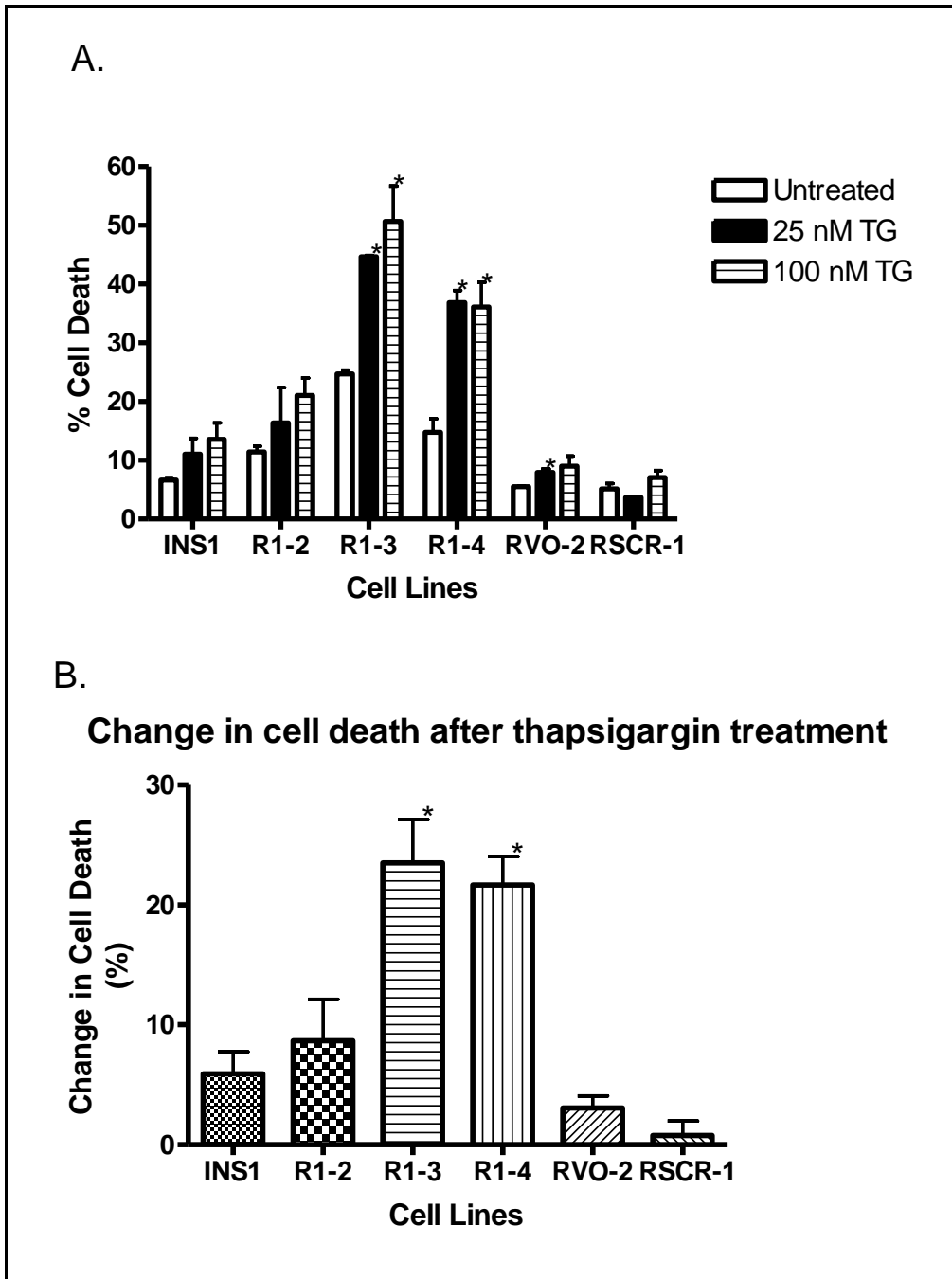**Figure 16. Cell death exacerbated in INS1 *Cisd2* knockdown cells compared with control cells with paraquat treatment.** (A) Paraquat treatment (250 nM for 24 hours) of INS1 cell lines (n = 2) led to an overall increase in cell death in each cell line compared with its respective untreated control. Treated wild-type INS1 cells resulted in a significant increase in cell death (9.6% ± 0.4) compared with untreated cells. The Cisd2 knockdown line, R1-2, also showed significant increase in cell death with treatment (12.0% ± 3.0). The two cell lines which showed

the greatest increase in cell death with paraquat treatment compared with their untreated controls were R1-3 (35.9% ± 9.5) and R1-4 (34.3.0% ± 8.4). These changes, however, were not deemed significant, possibly due to the small sample size and large standard deviation. The control line RVO-2 showed a nonsignificant increase (10% ± 2.8) in cell death with treatment. The RSCR-1 showed a significant increase in cell death with paraquat treatment (15.3% ± 1.2). (B) Cell death rates for paraquat treatment were subtracted from the cell death rate of their respective untreated control for each cell line to determine the change in cell death for each line. R1-3 and R1-4 had the greatest change in cell death with paraquat treatment, having 36.0% ± 9.5 increase and 34.5% ± 8.0 increase in cell death respectively. R1-2 also showed a modest increase in cell death (12.8% ± 2.5) with TG treatment. The wild type INS1, RVO-2 and RSCR-1 cell lines showed 9.6% ± 0.2, 10.8% ± 2.8, and 15.3% ± 0.8 increases in cell death after paraquat treatment. Change in cell death for all lines were compared with change in cell death in the wild type INS1 cell line. Although both R1-3 and R1-4 showed a greater increase in cell death with paraquat treatment compared with the increase seen in INS1 wild type cells, only R1-3 showed a statistically significantly greater change in cell death after paraquat treatment compared with the change in cell death in the INS1 cell line. Significance was set at $p < 0.05$ and is denoted by an asterisk. In (A) statistical analysis was carried out by unpaired student t-test comparing untreated and treated samples of each cell line individually. In (B) 1-way ANOVA followed by Dunnett's t-test with the reference set as wild-type INS1 was used. Data represented as means + SEM.

INS1 cell lines were also treated with the oxidative stressor hydrogen peroxide and with intermittent high glucose. Hydrogen peroxide, a molecule that is produced by superoxide anion and has the potential to form the highly reactive hydroxyl radical, was used to treat cells at a concentration of 10 µM for 24 hours. This concentration was chosen since, after treating INS1 wild-type cells with 10 µM, 25 µM, 50 µM, 75 µM, or 100 µM in 6 well plates for 24 hours, 10 µM was the only concentration that cells survived until the next day as determined visually under the light microscope. This treatment condition was used since it did not visibly kill wild-type INS1 cells and we wanted to use a treatment that may delineate a susceptibility to oxidative stress in different cell lines. After treatment of INS1 cell lines with 10 µM H_2O_2 for 24 hours, no significant increase in cell death was observed in any of the cell lines compared with their respective untreated controls (Figure 17A). Thus, *Cisd2* knockdown cells do not appear to be susceptible to cell death with this treatment.

Intermittent high glucose was reported by Hou *et al*. (2008) to cause glucotoxicity, via ER stress and oxidative stress pathways, in INS1 cells. According to their methods, INS1 cell lines were treated with intermittent high glucose for 72 hours followed by measurement of cell death. Intermittent high glucose treatment did not significantly increase cell death in any of the cell lines tested (Figure 17B). On the contrary, significant decrease of cell death was seen with glucose treatment in R1-3 cells (13.32 ± 0.5748) and in the wild-type INS1 cells (1.722 ± 0.389). To assess whether even higher glucose levels would cause cell death in the INS1 cells, wild-type INS1 cells were treated with 11.1 mM (no increase), 15 mM, 25 mM, 35 mM, 45 mM, or 55 mM for three days in six well plates and observed daily under light microscope. Cells at all concentrations appeared to grow normally and no increase in cell death was observed.
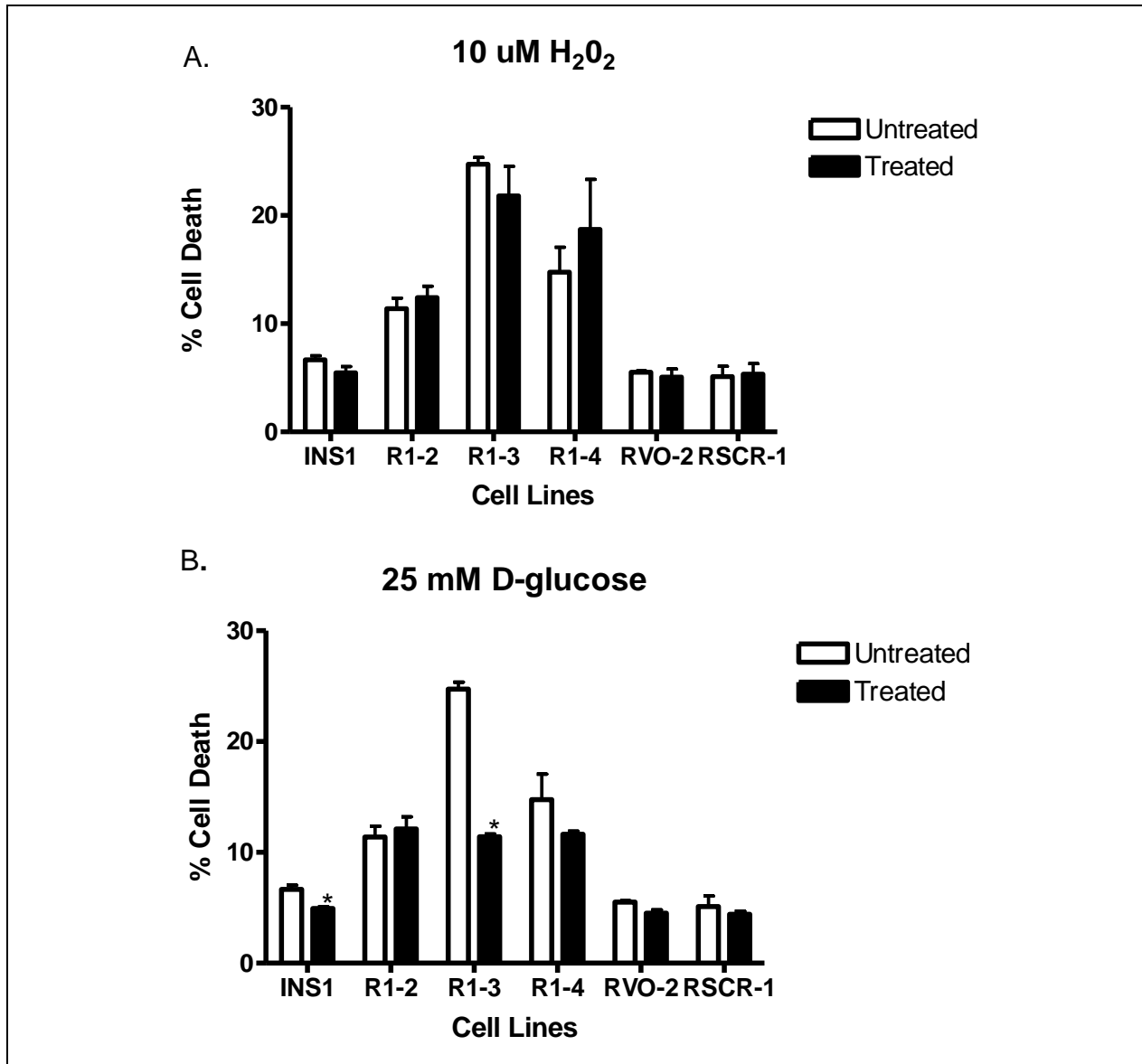
Figure 17. Treatment of INS1 cell lines with hydrogen peroxide (H_2O_2) and intermittent high glucose. INS1 cell lines were treated with 10 μM H_2O_2 for 24 hours (n = 3) or intermittent high glucose for 72 hours (n = 3). (A) Treatment with H_2O_2 yielded no significant change in cell death compared with untreated cells in all INS1 cell lines. (B) D-glucose was intermittently increased from 11.11 mM to 25 mM every 12 hours for 72 hours. Intermittent high glucose did not show a significant increase in cell death in any of INS1 cell lines compared with untreated cells. The *Cisd2* knockdown cell line, R1-3, showed a large significant decrease (13.32 ± 0.5748) with the D-glucose treatment. Wild-type INS1 cells also showed a significant, but small, decrease (1.722 ± 0.389) in cell death compared with untreated cells. Significance was set at $p < 0.05$ and is denoted by an asterisk. Statistical analysis was carried out by unpaired student t-test comparing untreated and treated samples of each cell line individually. Data represented as means + SEM.

4.2.7 The metabolic rate of INS1 cells is unaffected by Cisd2 knockdown.

ROS is generated in the mitochondria as a by-product of the electron transport change during cellular metabolism. We have shown that certain oxidative stress markers are increased in INS1 *Cisd2* knockdown cells. A study of mice with a targeted disruption of the MitoNEET gene, a protein with the conserved CDGSH domain also found in *CISD2* (referred to as Miner1 in this study), suggested that loss of MitoNEET resulted in a decreased capacity of mitochondria to carry out electron transport and oxidative phosphorylation (Wiley *et al.*, 2007). *CISD2*, which shares the same iron-binding CDGSH domain, may also play a role in regulating metabolic processes in the cell, as is common with iron-binding proteins. A decreased capacity of mitochondria to carry out the generation of ATP may lead to a need for those cells compensate for this deficiency by increasing their metabolic rate, and, in turn, increase ROS production. Thus, here we investigated whether INS1 *Cisd2* knockdown cells showed a higher metabolic rate than control INS1 cells.

The 3-[4,5-dimethylthiazol-2-yl]-2,5-diphenyltetrazolium bromide (MTT) assay is normally used to measure cellular viability and proliferation. This is a calorimetric assay that measures the reduction of yellow MTT by mitochondrial succinate dehydrogenase (Complex II of the mitochondrial electron transport chain) into a measurable colored formazan product. In one study, oxidative stress mediated tumor necrosis factor alpha dependent cell death, was accompanied in an increased reduction of MTT (Gomez *et al*., 1996). Another study, using INS1 cells, found a correlation between increased glucose metabolism and MTT reduction (Janjic & Wollheim, 1992). To investigate whether metabolic activity is increased in INS1 *Cisd2* knockdown cells, we used the MTT assay in conjunction with viable cell counts using trypan

blue exclusion assay. An increase in MTT reduction with decreasing number of viable cells would indicate an increase in metabolic activity.

Metabolic activity was determined in all INS1 cell lines by calculating the pooled ratio of MTT reduction to viable cells on cells grown for 6 days with MTT measurements and cell counts carried out on days 2, 4 and 6. We pooled the values for the different days because the metabolic activity of any given cell line should not change across time. Our data indicates there is no significant difference in our measurement of metabolic activity in any of the cell lines (Figure 18A).

The data from the MTT assay was analyzed to determine whether *Cisd2* knockdown had an effect on cellular viability over time (Figure 18B). At day 2, none of the cells showed any difference in viability. At days 4 and 6, wild-type INS1 cells had a significantly greater cellular viability than all other INS1 cell lines. R1-2 and R1-3 cells were significantly less viable than the control cell lines at day 4. At day 6, all *Cisd2* knockdown cell lines showed less viability than RVO-2 cells, but only R1-3 showed less viability than RSCR-1 cells.

4.2.8 Regulation of autophagy in INS1 Cisd2 knockdown cells is unaltered.

Autophagy is a cellular mechanism activated in conditions of starvation where cellular organelles and macromolecules are degraded, and is an integral part to cell survival and is thought to be anti-apoptotic. However, it can also lead to autophagic cell death, which could contribute to pathogenesis of diseases. Chen *et al*. (2009) reported that *Cisd2* knockout mice exhibit mitochondrial dysfunction accompanied by autophagic cell death in muscle, sciatic nerve, optic nerve, and brain tissue. Autophagic cell death was identified by the presence autophagic vacuoles and the upregulation of LC3 cleavage (Chen *et al*., 2009), both of which are
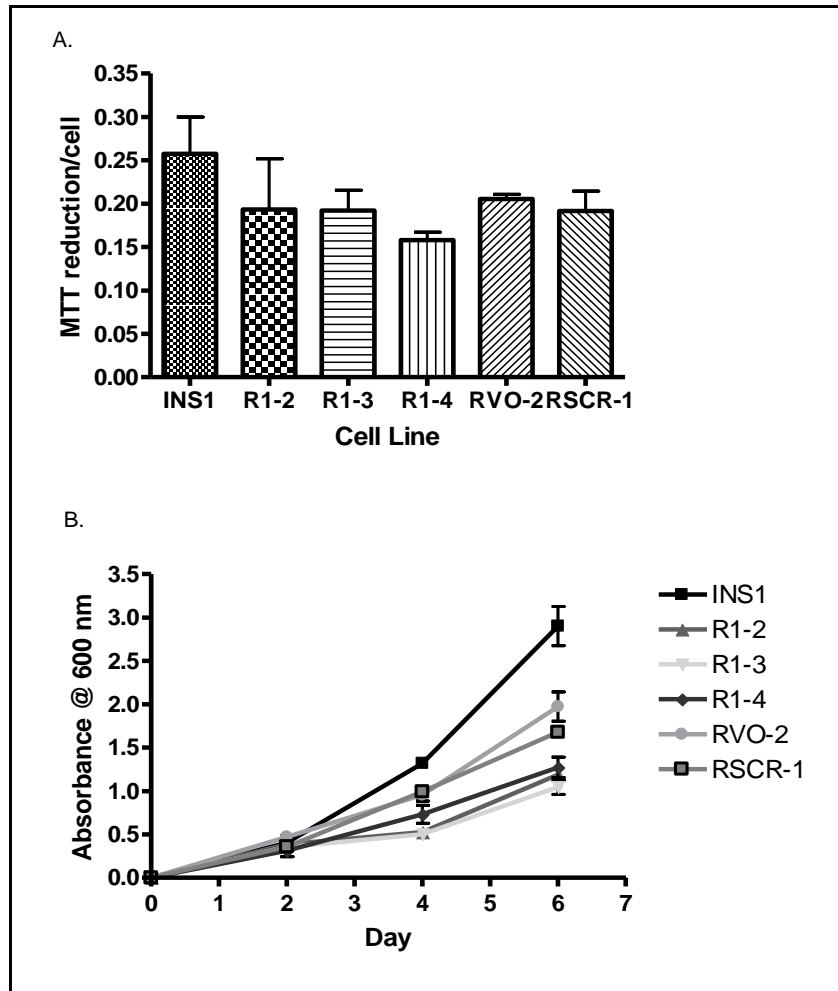
Figure 18. Measurement of metabolic rate of INS1 cells using MTT assay and cell counting.
INS1 cell lines (n=3) were grown for six days and MTT measurements and cell counts were
carried out on days 2, 4 and 6. MTT absorbance readings were divided by total cell number to
determine metabolic rate, identified here as MTT reduction per cell. (A) Metabolic rate of INS1
cell lines were not significantly different as determined by ANOVA. (B) MTT assay shows a
marked reduction in cellular viability over six days in INS1 *Cisd2* knockdown compared with
wild-type INS1 cells and the control cell lines, RVO-2 and RSCR-1. At day 2, all cell lines
showed no difference in cellular viability. At day 4, wild-type INS1 was significantly higher than
any of the cell lines, and, although RVO-2 and RSCR-2 were lower than wild type INS1 cells,
they were significantly higher than the INS1 Cisd2 knockdown cell lines R1-2 and R1-3, but not
R1-4. At day 6, wild-type INS1 continues to show significantly greater viability than all the cell
lines. All *Cisd2* knockdown cell lines showed significantly less viability than RVO-2 cells, but
R1-2 and R1-4 showed similar viability to the RSCR-1 cells. R1-3 cells were consistently less
viable than all control cell lines throughout the duration of the experiment. Significance was set
at $p < 0.05$. In (A) statistical analysis was carried out by 1-way ANOVA followed by Dunnett's
t-test with the reference set as wild-type INS1. In (B) 1-way ANOVA followed by Tukey's
multiple comparisons test was used to compare cell lines at each day. Data represented as means
± SEM.

well known autophagy markers. Interestingly, another study reported that interaction of ERIS to BCL-2 is required for BCL-2 inhibition of Beclin 1-mediated autophagy, by promoting Beclin 1 interaction with BCL-2 (Chang *et al.*, 2009). *CISD2* knockdown, mediated by lentiviral shRNA targeting, in H1299 epithelial carcinoma cells showed an increase in intensity of autophagy after starvation (Chang *et al.*, 2009). As none of these studies were carried out in a pancreatic β-cell line, we wanted to investigate whether the autophagic response was upregulated in INS1 *Cisd2* knockout cells under normal conditions and under starvation conditions.

To measure for autophagy, we used Western blot analysis to detect LC3-II levels, a cleaved form of LC3-I and a marker of autophagy. Under normal conditions, INS1 *Cisd2* knockdown cell lines did not exhibit any increase in LC3-II levels compared with INS1 control cell lines (Figure 19A). Ratios of LC3-II to α-tubulin of *Cisd2* knockdown cell lines also showed no significant difference to ratios of INS1 control cell lines (Figure 19B).

INS1 cell lines were serum starved and autophagic response was detected using the LC3-II marker. Since autophagy is a dynamic process in which LC3-II is degraded, cells were also treated with 100 nM bafilomycin A1 (BafA1), which inhibited the fusion of autophagosomes with lysomes, thus preventing the degradation of LC3-II. Under serum starvation, all cell lines showed an increase in LC3-II levels (Figure 19C). LC3-II to α-tubulin ratios comparison of *Cisd2* knockdown cells to control cells showed no difference between the LC3-II levels between the two groups of cells (Figure 19D). This finding is in contrast with findings by Chang *et al.*, (2009) who reported increases of the same autophagic marker, under starvation conditions, in *CISD2* knockdown cells compared with control cells.

This led us to examine whether, *Cisd2* was upregulated as a result of the starvation conditions in our INS1 *Cisd2* knockdown cells. Western blot analysis reveals that *Cisd2* levels in

100

the INS1 *Cisd2* knockdown cells were comparable to INS1 control cells after serum starvation (Figure 19C). Comparing the Cisd2:α-tubulin ratios of *Cisd2* knockdown cells with control cells showed no significant difference between the two groups (Figure 19E).
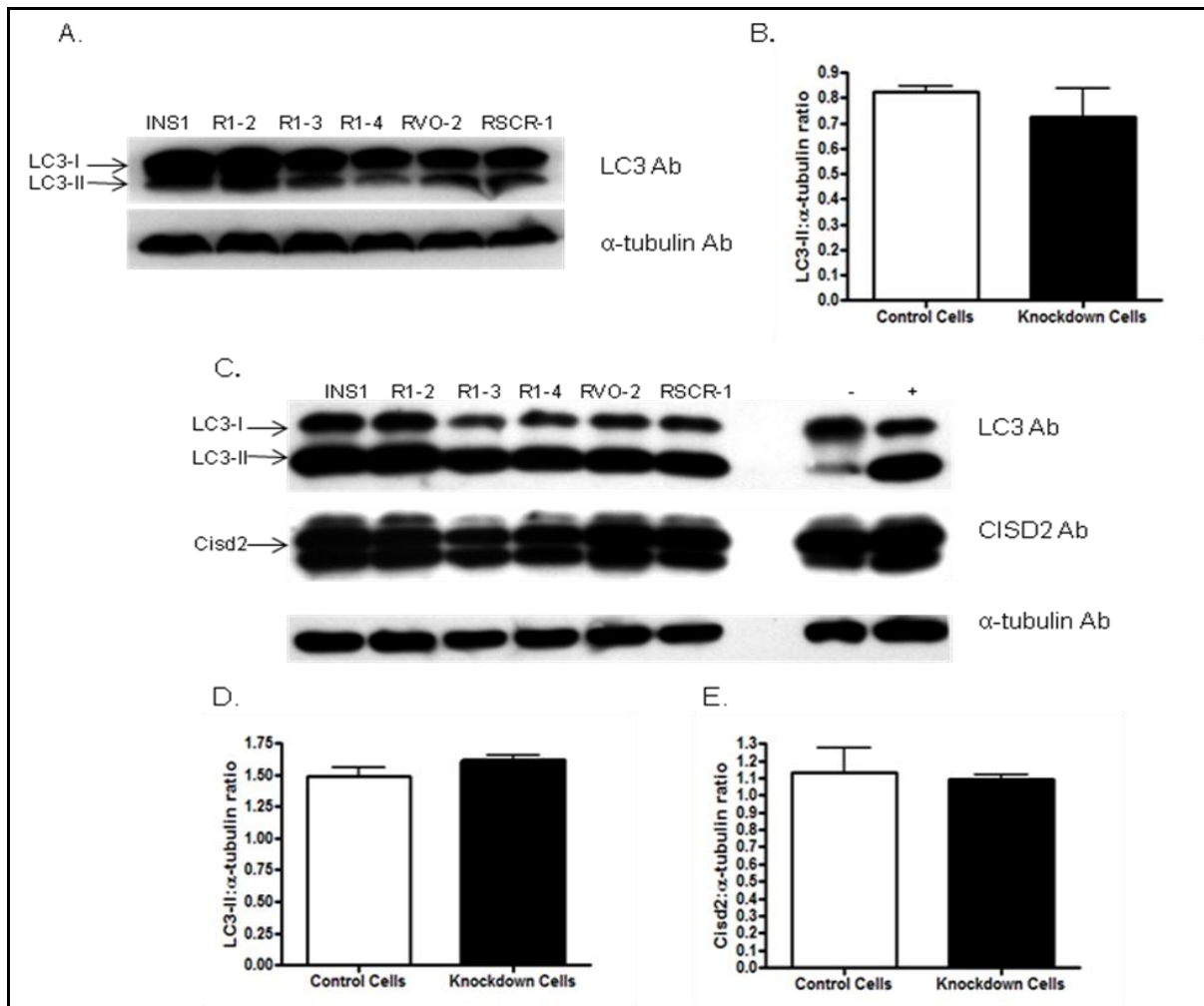
Figure 19. Detection of autophagic response in INS1 *Cisd2* knockdown cells under normal conditions and serum starvation conditions. INS1 cell lines were evaluated for autophagic response by detection of the autophagic marker LC3-II, the cleaved form of LC3-I using Western blot analysis. (A) Under normal conditions, levels of LC3-II in knockdown cell lines are similar to that of control cell lines. (B) Bands were measured using spot densitometry and the ratio of LC3-II to α-tubulin was determined. Ratios of INS1 *Cisd2* knockdown cell lines were compared with that of control cell lines, and no significant difference was found. (C) INS1 cell lines were serum starved (1% FBS for 24 hours) and LC3-II and *Cisd2* expression was detected using Western blot analysis. LC3-II levels in INS1 *Cisd2* knockdowns are observed to be similar to INS1 control cell lines. Additionally, *Cisd2* levels in Cisd2 knockdown cells appear to have returned to levels comparable to INS1 control cells levels. Bands were measured using spot densitometry and the ratio of LC3-II to α-tubulin (D) and Cisd2 to α-tubulin (E) was determined. For both proteins, ratios of INS1 *Cisd2* knockdown cells were not different than INS1 control cells. For all blots, α-tubulin was used as an internal control. In (C), (-) represents INS1 wild-type cells that were not serum starved, (+) represents INS1 wild-type cells that were starved. Significance was set at $p < 0.05$. In (B, D, &E) statistical analysis was carried out by unpaired student t-test comparing relative protein expression in control cell lines to knockdown cell lines. Data represented as means + SEM.

102

4.2.8 P19 neuronal differentiation is not inhibited by Cisd2 knockdown.

WFS patients exhibit diffuse neuronal loss in various parts of the brain. Furthermore, a study by Boucquey *et al*., (2006) identified *Cisd2* (referred to as *Noxp70*) as an early neuronal marker in the neuroectodermic precursor cell line 1C11. Additionally, high expression of *Cisd2* in the embryonic mouse brain led the authors to suggest a role for *Cisd2* in the early developing CNS (Boucquey *et al*., 2006). The question remained whether *CISD2* deficiency would have an effect on the development of neurons in the early brain.

The mouse embryonic carcinoma cell line P19, which is maintained in the undifferentiated state *in vitro*, can be induced to differentiate into a variety of cell types by aggregation and chemical treatment. By aggregation and retinoic acid, specifically, undifferentiated P19 cells can be differentiated in neuronal cells (Jones-Villenneuve *et al*., 1983). To assess whether the differentiation of neurons is inhibited or blunted in WFS2 as a result of *CISD2* deficiency, we induced neuronal differentiation in the P19 *Cisd2* knockdown cell line P19 1-5 and measured the expression of two known neuronal markers, the glutamate (NMDA) receptor zeta subunit gene *Grin1* and the neurogenic differentiation 1 gene *NeuroD1*.

P19 and knockdown P19 1-5 cells were grown in bacterialogical grade petridishes in normal media containing 500 nM retinoic acid (RA) for 4 days. Use of these specific plates prevents adherence of cells to plates and helps promote aggregation and neuronal differentiation. After day 4, cells were transferred to tissue culture plates for an additional 5 days in normal media also containing 500 nM RA. RA induced neuronal differentiation could be identified morphologically through visualization under a light microscope, specifically through the appearance of neuronal outgrowths. At day 9, differentiated P19 and P19 1-5 cells showed strong

expression of both neuronal markers, *Grin1* and *NueroD1*, as measured using qRT-PCR (Figure 20A and 20B).

Cisd2 knockdown in INS1 cells causes upregulation of expression of the antioxidant enzymes *Sod1* and *Sod2*. To determine if this relationship holds true in differentiated P19 cells expression of *Sod1* and *Sod2* were measured by qRT-PCR in differentiated P19 cell lines. *Sod1* expression in both differentiated cell types was significantly greater than undifferentiated P19 cells. *Sod1* expression, however, was not significantly different in the two differentiated cell lines (Figure 20C). Expression of *Sod2* was also significantly higher in the two differentiated cell lines compared with undifferentiated wild-type P19 cells. Similarly, there was no significant difference in Sod2 expression between differentiated P19 cells and differentiated P19 1-5 cells (Figure 20D).

As mentioned above, *Cisd2* expression increases during neuronal differentiation. To determine if *Cisd2* expression also increases after RA induction of neuronal differentiation in the knockdown cell line, its expression was measured by qRT-PCR. *Cisd2* expression increases in both differentiated wild-type and P19 1-5 cells (Figure 20E). Differentiated P19 1-5 cells showed significantly higher expression of *Cisd2* compared to the undifferentiated P19 1-5 cells and are found to have similar *Cisd2* levels to wild-type undifferentiated P19 cells. Differentiated wild-type P19 cells had significantly higher *Cisd2* expression than undifferentiated wild-type P19 cells as expected (Boucquey *et al*., 2006).
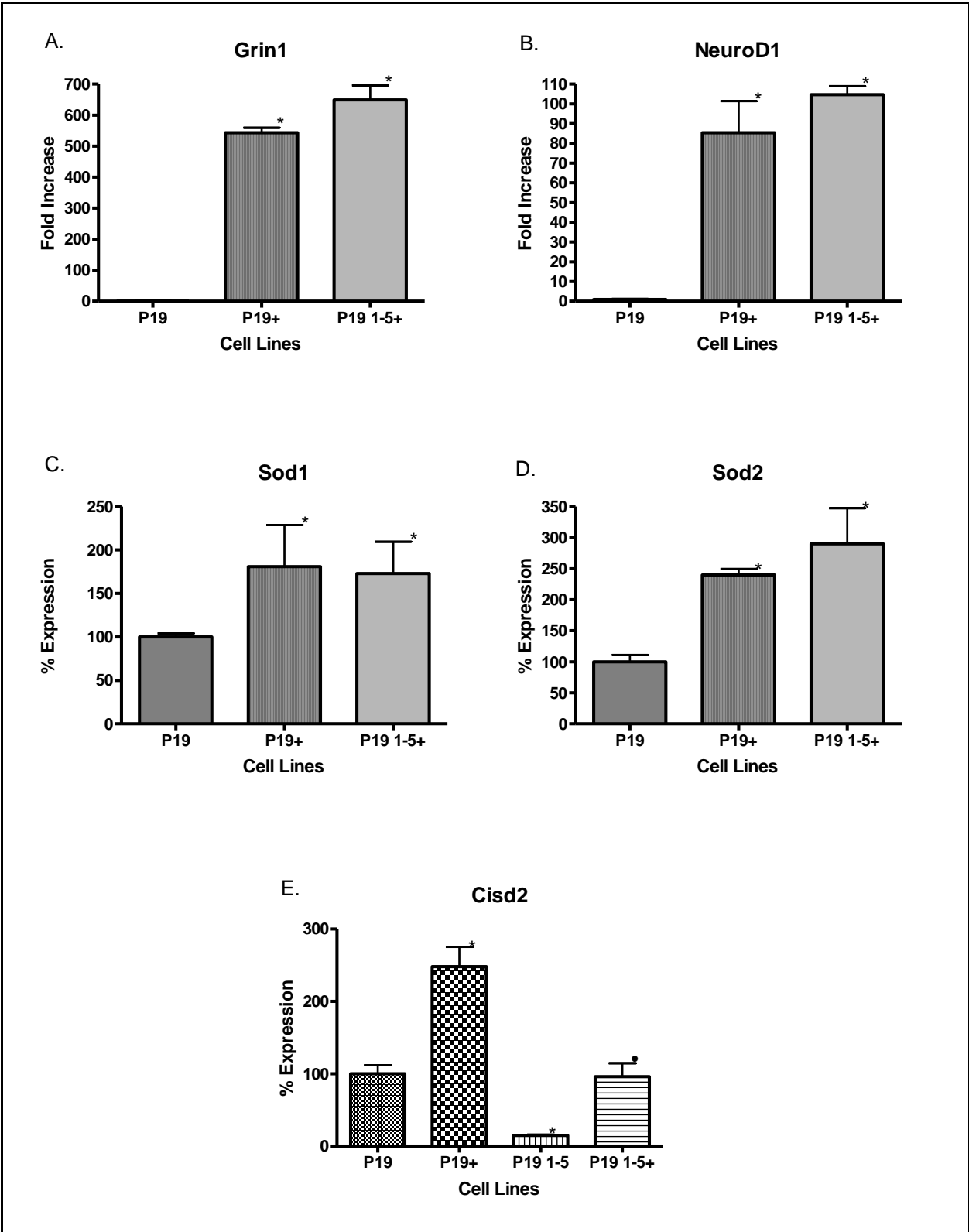
.

Figure 20. Neuronal differentiation of a P19 *Cisd2* knockdown cell line. Wild-type P19 (P19) and *Cisd2* knockdown P19 cells (P19 1-5) (n=3) were differentiated into neuronal cells by 500 nM retinoic acid treatment for 9 days (denoted with (+)). (A) Significant increase of expression of the neuronal marker *Grin1* was observed by qRT-PCR in both differentiated P19 and P19 1-5 cells compared with undifferentiated P19 cells, showing a 545 fold and a 605 fold increase respectively. (B) Similarly, differentiated P19 and P19 1-5 show significant increase in expression of a second neuronal marker, *NeuroD1*, compared with undifferentiated P19 cells. Increases were 85 fold in differentiated P19 and 105 fold in differentiated P19 1-5. (C) *Sod1* significantly increase in both differentiated cell lines compared to the undifferentiated P19 cell line. Differentiated P19 had an 81% ± 42.8 increase and differentiated P19 1-5 had a 73% ± 33.2 increase compared to undifferentiated P19 cells. No significant difference was found between the two differentiated cell lines. (D) *Sod2* also show a significant increase in expression in differentiated P19 (140% ± 9.3) and P19 1-5 (190% ± 52.3) cells compared with the undifferentiated control. However, there was no significant difference in Sod2 expression between the two differentiate cell lines. (E) *Cisd2* expression increases in both differentiated cell lines compared to undifferentiated levels. Differentiated P19 cells exhibit a 148% ± 27.1 increase in Cisd2 expression compared with undifferentiated P19. Differentiated P19 1-5 cells express *Cisd2* 81% ± 18.5 higher than undifferentiated P19 1-5 cells. Differentiated P19 1-5 cells show *Cisd2* levels similar to that of undifferentiated P19 cells. Significance was set at $p < 0.05$ and is denoted by an asterisk for comparisons with undifferentiated P19 cells and a circle for comparison with undifferentiated P19 1-5 cells in (E). Statistical analysis was carried out by unpaired student t-test comparing gene expression in wild type P19 cells and P19 1-5 cells. Data represented as means + SEM.

CHAPTER 5

DISCUSSION

5.1 Description of WFS2 and *CISD2*

Wolfram syndrome is a monogenic autosomal recessive disorder that is clinically diagnosed by the presence of juvenile-onset diabetes and optic atrophy. Early on in the study of genetic causes of Wolfram syndrome, it became apparent that this disease can be caused exclusively by a mutation in more than one gene, and shows, in effect, locus heterogeneity. When more closely examined, Wolfram syndrome patients can be categorized according to certain diagnostic criteria. While some clinical manifestations are variable across all Wolfram syndrome patients, some phenotypes, such as diabetes insipidus or bleeding tendency, are exclusive to one set of patients. This further supports the notion of locus heterogeneity, and hints at the idea that, although the diagnostic criterion for this disorder is met in most cases, the molecular pathogenesis of the disorder may be different. In short, different genes can lead to slight differences in a single clinical disease. Recently, this issue has been addressed by identifying the two different types of Wolfram syndrome as WFS1 for the wolframin associated syndrome and WFS2 for the ERIS associated syndrome (Kanki & Klionsky, 2009).

In the patient samples that were studied, WFS2 is caused by a G to C transversion in the 2nd exon of the *CISD2* gene (synonyms: *CISD2*, *Miner1*, *NAF-1*), that leads to a splicing error which is predicted to result in a severely truncated protein. The *CISD2* gene, located on the long arm of chromosome 4, has 3 exons that code for a 135 amino acid protein with a transmembrane domain and a highly conserved CDGSH domain near its C-terminus. This domain was found to be an iron/sulfur domain, also found in two mitochondrial proteins (Wiley *et al.,* 2007). The

CISD2 protein is localized in the ER (which led to it being named "ERIS") and *CISD2* mRNA is expressed in a wide variety of tissues. Additionally, lymphoblastoid cells from an affected individual show a significantly higher release of Ca^{2+} from the ER upon thapsigargin treatment compared with controls. These findings were some of the first clues on understanding the function of this novel protein and the pathogenesis of WFS2.

The *WFS1* and *WFS2* genes share some similarities. For instance, mutations in each cause similar clinical phenotypes in humans, the gene products are both localized in the ER, and although WFS1 deficient cells exhibit a lowered level of ER Ca^{2+}, which is opposite to our findings in the affected lymphoblastoid cells, both appear to affect cellular and ER Ca^{2+} homeostasis. Due to these similarities, we hypothesized that similar pathways of cell dysfunction and cell death led to the development of disease.

5.2 CISD2 deficient cells exhibit increased apoptosis

Beta cell and neuronal cell loss is seen in post-mortem tissue from WFS patients. Several lines of research showed increased apoptosis in *WFS1* knockdown cells. INS1 *Cisd2* knockdown cells also exhibit increased apoptosis. This has been shown by cellular changes, using Annexin V and 7AAD staining, and molecular changes, by measurement of expression of two pro-apoptotic molecules, *CHOP/GADD153* and BAX. These findings suggest that *CISD2* deficiency in cells are more susceptible to apoptosis. The pancreatic INS1 β-cells used in this study are derived from a rat insulinoma and are commonly used in studying diabetes for the ability to respond to glucose and secrete insulin. Pancreatic β-cells are particularly sensitive to rates of apoptosis and proliferation (Rhodes, 2005) and increased β-cell apoptosis has been reported in type 2 diabetic patients (Butler *et al.,* 2003). Additionally, the first clinical manifestation in WFS2 is diabetes,

presumably from the loss of β-cells, which may itself contribute to the development of other symptoms of the disease due to insulin deficiency.. To further complete our understanding of the contribution of apoptosis in WFS2, it would be important to study the expression of apoptotic markers in other cell types with *CISD2* knockdown, such as the neuronally derived cell line, N1E115.

We also investigated whether autophagy was responsible for cell death in INS1 Cisd2 knockdown cells. Our results showed no significant difference in the levels of the autophagic marker LC3-II in *Cisd2* knockdown cell lines compared with control cell lines, suggesting that autophagy is not upregulated due to *CISD2* deficiency under normal conditions. More recently, Chen *et al*. (2009) reported that *Cisd2* deficiency in mice resulted in mitochondrial dysfunction induced autophagic cell death in skeletal muscle and neuronal tissues. The discrepancy between this finding and our data may be attributed to the fact that this observation was not reported in the pancreatic β-cells of *Cisd2* deficient mice. Another point of uncertainty in these findings, as Maiuri *et al*. (2010) points out, it appears counterintuitive to attribute the pathological manifestation of WFS2 to enhanced autophagy, since autophagy is often responsible for increasing lifespan.

Cisd2 knockout mice, as described by Chen *et al*. (2009), exhibited a shortened life span and a premature aging phenotype such as prominent eyes and protruding ears. Additionally, mice developed opaque eyes and blindness, which was accompanied by corneal damage. These mice exhibited early depigmentation in the fur, hair follicle atrophy, decreased hair density, and a thickened dermis. Muscle degeneration was detected at 3 weeks age. The authors stated that *Cisd2* $^{-/-}$ do exhibit a neurodegenerative phenotype that includes optic nerve defects, but a milder glucose homeostasis phenotype (Chen *et al.,* 2009). The authors' assertion that the phenotype

features of *Cisd2* $^{-/-}$ mice reflect WFS2 phenotype in humans is highly debatable. WFS2 patients do not exhibit any premature aging phenotypes and their death is due to central respiratory failure (Hilson *et al.,* 2009). Skin or hair abnormalities and muscle degeneration have never been reported in WFS2 patients. Furthermore, one of the two diagnostic criteria of WFS2, diabetes mellitus, presents very mildly in the *Cisd2*$^{-/-}$ mice discussed above (Chen *et al.,* 2009). These observations challenge the ability to use the Cisd2$^{-/-}$ mice as a model of WFS2 and undermine the association of mitochondrial dysfunction and autophagic cell death seen in these mice with the pathogenesis in WFS2 patients.

5.3 Unlike *WFS1*, *CISD2* does not play a role in the UPR

The pathogenesis WFS1 has been intimately connected with dysfunction of the UPR. *WFS1* shows increased expression under conditions of ER stress, along with molecular members of the UPR. *WFS1* deficiency leads to the upregulation of markers of the UPR, while deficiency of UPR related proteins leads to attenuation of *WFS1* expression even under ER stress, suggesting that *WFS1* is regulated by molecular members of the UPR. The dysfunction of the UPR due to *WFS1* deficiency was implicated in the impaired function, proliferation, and increased apoptosis in β-cells. We investigated *CISD2* deficient cells for activation of the UPR and found no upregulation of this stress response. Additionally, increased ER stress in the form of thapsigargin treatment did not lead to an increase of *Cisd2* expression in two cell lines, INS1 and N1E115. Our findings lead us to believe that *CISD2* is not involved in the UPR and the pathogenesis of WFS2 occurs in a mechanism unrelated to the pathogenesis of WFS1. This is not surprising since we have also shown that WFS1 does not co-immunoprecipitate with ERIS, ER

Ca^{2+} homeostasis is affected differently in WFS1 and WFS2, and certain clinical manifestations of each subtype of WFS are exclusive.

The localization of ERIS in the ER and the increase in ER Ca^{2+} release in WFS2 lymphoblastoid cells, however, still hints at involvement of an ER related dysfunction in WFS2. Recently, Chang *et al*. (2009) reported a direct interaction of ERIS with the ER Ca^{2+} release channel, IP_3 receptor. Although they did not report an increase of ER Ca^{2+} release in *CISD2* knockdown cells upon treatment with thapsigargin, they did report that H1299 cells which had depressed ER Ca^{2+} release due to overexpression of ER-targeted BCL-2 showed a return to normal levels of ER Ca^{2+} release in cells with *CISD2* knockdown. The type of cells used in the study, a human epithelial carcinoma cell line, may not fully depict the Ca^{2+} dysregulation caused by *CISD2* deficiency in the highly active pancreatic β-cells. Highly active cells that depend on Ca^{2+} signaling and regulation for the function and viability, such as excitatory neuronal cells, skeletal muscle cells, and secretory pancreatic β-cells, are more vulnerable to a dysfunction of cellular Ca^{2+} regulation (Berridge *et al.,* 2000). Pancreatic β-cells, which their glucose stimulated insulin secretion mechanism is a Ca^{2+} dependent process, may be more susceptible to changes in Ca^{2+} homeostasis. Current projects in our laboratory seek to examine releasable levels of ER Ca^{2+} stores in INS1 *Cisd2* knockdown cells as well as steady-state cellular Ca^{2+} levels.

In Alzheimer's disease, a mutant form of the ER integral protein presinilin-1 (PS-1) shows increased stimulation of IP_3R Ca^{2+} release compared with wild-type PS1 (Leissring *et al.,* 1999). Wild-type and mutant forms of PS1 has been shown to physically interact with the IP3 receptor (Cheung *et al.,* 2008). In the Ca^{2+} studies of affected lymphoblastoid cells, the cells may express a mutant form of ERIS that can still interact with the IP_3 receptor causing our observed results. This gain of function of truncated ERIS interaction with the IP_3 receptor

represents one possible explanation to why increased cytosolic Ca^{2+} with thapsigargin treatment was not seen in the H1299 *Cisd2* knockdown cells in the Chang *et al*. (2009) study. Our laboratory has already determined that mutant *CISD2* mRNA is not degraded (Amr *et al.,* 2007) and is currently investigating whether a FLAG tagged version of the truncated protein could be expressed. It would of interest to express the mutant form of ERIS in wild-type INS1 cells and study its interaction with the IP_3 receptor and its effect on ER Ca^{2+} release.

5.4 *CISD2* deficiency increases susceptibility to oxidative stress

Oxidative stress is a major contributor to diabetes and neurodegeneration, and in both oxidative stress markers are observed preceding the disease and as an effect of the disease. Since we did not detect an activation of the UPR, we investigated the upregulation of oxidative stress markers in INS1 *Cisd2* knockdown cells. We found the transcriptional upregulation of two antioxidant enzymes, *SOD1* and *SOD2*, function in the inactivation of the superoxide anion molecule, in INS1 *Cisd2* knockdown cells. In addition, we showed a significant increase in global tyrosine nitration, an effect by the highly unstable peroxynitrite molecule, in INS1 *Cisd2* knockdown cells compared with control cell lines. These results suggest that oxidative stress is present due to *CISD2* deficiency, although it is unclear if it is a primary cause or a downstream consequence of WFS2 pathogenesis.

To answer this question, it is important to think about how oxidative stress may mediate cell death. Reactive oxygen species are a byproduct of mitochondrial oxidative phophorylation. Chen *et al*. (2009) reported a significant decrease in the oxygen consumption and decrease in electron transport activities of mitochondrial complexes isolated from skeletal muscle of *Cisd2* $^{-/-}$ mice, suggesting a mitochondrial dysfunction in WFS2. An increase in cytosolic Ca^{2+} from a

112

leaky ER can stimulate ROS production as a consequence of mitochondrial Ca^{2+} loading, stimulation of the TCA cycle, and through generation of nitric oxide (Malhotra & Kaufman, 2007). An increase in cytosolic Ca^{2+} and ROS production have a synergistic effect in mediating mitochondrial PTP formation, which if activated globally causes necrosis (Jacbson and Duchen, 2001), but if it occurs in a subpopulation of mitochondria in the cell can cause apoptosis (Ott *et al.,* 2007; Giacomello *et al.,* 2007). Additionally, the increase in metabolic demand in the cell due to the dysfunction of mitochondria may lead to an increase in ROS production further exacerbating their effects.

An increase in *CHOP* expression, as seen in INS1 *Cisd2* knockdown cells, has been reported to repress *BCL-2* expression and increase oxidative stress (McCullough *et al.,* 2001). This would indicate that the increase in oxidative stress markers seen in INS1 knockdown cells may be a downstream effect of *CHOP* upregulation. In a study utilizing type 2 diabetic mice, deletion of *Chop* reduced levels of oxidative stress, and decreased apoptosis in β-cells (Song *et al.,* 2008). In this scenario, *Chop* knockdown should alleviate the oxidative stress markers seen in INS1 *Cisd2* knockdown cells as well as decrease the cell death rates.

INS1 *Cisd2* knockdown cells treated with various oxidative stressors produced a large increase of cell death in two of the three INS1 *Cisd2* knockdown cells where there was a small to no increase of cell death in control lines with thapsigargin and paraquat treatment. Thapsigargin is an inhibitor of SERCA ATPase pumps, whose function is to transport Ca^{2+} into the ER. Thus, thapsigargin treatment leads to a greater concentration of cytosolic Ca^{2+} since there is Ca^{2+} efflux from the ER but no Ca^{2+} influx into the ER. This increase, in turn, will lead to an increase in ROS production and mitochondrial injury, leading to the dramatic increase in cell death seen in those cell lines.

Paraquat causes oxidative toxicity by undergoing reduction/oxidation cycling, being reduced by an electron donor such as NADPH, and then being oxidized by an electron acceptor such as O_2 to produce superoxide anion (Bus & Gibson, 1984). INS1 *Cisd2* knockdown cells R1-3 and R1-4 showed the largest increase in cell death compared to their respective untreated controls. The INS1 *Cisd2* knockdown line R1-2 showed an increase in cell death compared with controls, but this increase was not found to be statistically significant, possibly due to the fact that it showed the least amount of knockdown in qRT-PCR and Western blot analysis. This is direct evidence that *CISD2* deficiency increases susceptibility to oxidative stress. Although it does not answer the question whether ROS generation is a primary factor in the pathogenesis of WFS2, it does suggest that oxidative stress can exacerbate the development of the disease.

The two other stressors used in this experiment were H_2O_2 and intermittent high glucose. In both scenarios, no significant increase in cell death was seen in any of the cell lines. The inefficacy of H_2O_2 to produce a response may be due to the presence of the antioxidants glutathione, in the media formulation, and catalase, in the serum, which reduce H_2O_2 to produce H_2O. This led us to use the aforementioned treatments of oxidative stress, such as paraquat and thapsigargin. Other possible treatments to produce ROS include xanthine oxidase/hypoxanthine treatment for the production of superoxide anions (Moriscot *et al.,* 2007).

5.5 Metabolic activity of *Cisd2* deficient cells is unchanged

To measure metabolic activity in INS1 *Cisd2* deficient cells, MTT assays in conjunction with cell counting using trypan blue exclusion assay was performed. We expected to see an increase in metabolism in INS1 *Cisd2* knockdown cell lines to account for the suspected increase in ROS production. Our results showed no significant difference in metabolic activity between

INS1 *Cisd2* knockdown cells compared with control cells. Despite this, examination of Figure 18A reveals that the INS1 *Cisd2* knockdown cell lines are on the lower end of MTT reduction/cell values which may indicate a slightly lowered metabolism in INS1 *Cisd2* knockdown cell lines. Chen *et al*. (2009) reported lower mitochondrial activity and electron transport chain efficiency in mitochondria taken from *Cisd2*$^{-/-}$ mice. Dysfunction of the mitochondria is both a contributor of ROS and an effect of oxidative stress.

Our MTT results, however, show a decrease in viability and/or proliferation of INS1 *Cisd2* knockdown cells over a period of six days compared with INS1 wild-type cells. This is consistent with our previous findings of an increase in cell death in INS1 *Cisd2* knockdown cells. With regards to comparing the *Cisd2* knockdown cell lines with control cell lines RVO-2 and RSCR-1, knockdown cell lines had lower viability with some inconsistencies in significance (set at $p < 0.05$). This may have been due to the limited sensitivity of the assay. The R1-3 knockdown cell line, which showed the most percentage of cell death in Annexin V/7AAD staining, consistently show a decrease in viability compared with control cell lines.

5.6 Autophagic response is not upregulated in INS1 Cisd2 knockdown cells

A report by Chang *et al.,* (2009) showed an increase in autophagic markers in nutrient deprived *Cisd2* knockdown H1299 cells but not in unstressed cells. We tested this finding in our INS1 *Cisd2* knockdown cells and found increased levels of the autophagic marker LC3-II in INS1 *Cisd2* knockdown cells, but this increase was also seen in control cells, which is the expected result due to nutrient deprivation. Differences in levels of the increase in LC3-II between *Cisd2* knockdown and control cells were not detected. We did detect, however, an increase in the expression of *Cisd2* in knockdown cell lines to levels comparable to control cell

115

lines. This compensation of *Cisd2* protein levels may explain the lack of differences in autophagic response after nutrient deprivation as seen by Chang *et al*. (2009). In addition, it suggests that *CISD2* expression may be regulated by conditions that induce autophagy and suggest a role for it in the regulation of the autophagic response, perhaps inhibiting excess autophagy that could be detrimental to the cell.

Our collaborators have shown that *wfs2 (Drosophila CISD2)* knockdown in *Drosophila* modifies the effects of overexpressing two lysosomal storage disease genes, *PPT1* and *CLN3* (Jones *et al.,* in preparation). A degenerative eye phenotype caused by *PPT1* overexpression was suppressed by *wfs2* knockdown, while a different type of degenerative eye phenotype caused by *CLN3* overexpression was enhanced by *wfs2* knockdown. The notion that *CISD2* is an inhibitor of autophagy can help explain these findings. *PPT1* de-palmitates proteins for efficient lysosomal degradation, so if the eye phenotype due to overexpression of *PPT1* is overloading lysosomal machinery with de-palmitated proteins, activation of autophagy, via *CISD2* knockdown, will aid in the removal of these proteins. On the other hand, overexpression of *CLN3*, a lysosomal transmembrane protein, causes a degenerative eye phenotype possibly due to an increase in lysosomal activity, an effect that can be exacerbated by an increase in autophagy, since the autophagic process involves activation of lysosomes.

5.7 Neuronal differentiation of P19 cells is uninhibited by *Cisd2* knockdown

Boucquey *et al.,* (2006) identified *Cisd2* as an early neuronal marker in the neuroectoderm precursor cell line 1C11 and reported high expression of *Cisd2* in the mouse developing brain. We investigated whether *Cisd2* knockdown in the undifferentiated embryonic stem cell like cell line P19 affected its differentiation into neurons. Upon differentiation, the P19

116

Cisd2 knockdown cell line had increased expression of neuronal markers comparable to differentiated wild-type P19 cells. Additionally, no differences were found in *Sod1* and *Sod2* expression between the two differentiated cell lines. We did observe an increase of *Cisd2* expression in both differentiated wild-type P19 and *Cisd2* knockdown cells compared with their respective undifferentiated controls, which corroborates previous observation of the upregulation of *Cisd2* in neuronal differentiation and early brain development (Boucquey *et al.,* 2006). Differentiated *Cisd2* knockdown cells show similar mRNA levels of *Cisd2* compared with undifferentiated wild type P19 cells. This compensation in *Cisd2* levels may explain the lack of effect of *Cisd2* deficiency on neuronal differentiation. Alternative methods to effectively knockdown or knockout *Cisd2*, such as viral delivery systems or homologous recombination, can be utilized to ensure *Cisd2* knockdown throughout the differentiation process.

5.8 Possible mechanism of pathogenesis in WFS2

Autophagy is a conserved cellular stress adaptation that avoids apoptotic mediated cell death, known as type I cell death. Under certain stimuli, however, it can lead to an alternative pathway of cell death, known as autophagic or type II cell death. Circumstances under which cellular 'decisions' are made to activate cytoprotective autophagic mechanisms, autophagic cell death, or apoptotic cell death are still not fully understood. Although distinct events are characteristic of each type of cell death, both processes share several common stimuli and key regulatory pathways (Figure 21A) (Maiuri *et al.,* 2007; Scarlatti *et al.,* 2009). Furthermore, one process may precede or run congruently with the other (Gonzalez-Polo *et al.,* 2005; Maiuri *et al.,* 2007). Key molecular inhibitors of both autophagy and apoptosis are the BCL-2 family members BCL-2 and BCL-XL (Maiuri *et al.,* 2007), both of which have been shown to bind to

ERIS (Chang *et al.,* 2009). ERIS is said to exert an inhibitory effect on autophagy by contributing to the interaction between the autophagy inducer Beclin 1 (Bec1) and BCL-2 (Chang *et al.,* 2009), perhaps by inducing conformational changes in BCL-2 that enhances Bec1 binding (Maiuri *et al.,* 2010).

Chang *et al*. (2009) also showed that apoptosis induced by overexpression of the BCL-2 inhibitor BiK is unaffected by *Cisd2* knockdown. This, however, does not answer whether ERIS modulates BCL-2's anti-apoptotic function, since BiK overexpression may have overwhelmed any ERIS enhanced anti-apoptotic BCL-2 function. BCL-2 anti-apoptotic function is widely reported to require its mitochondrial localization (Maiuri *et al.,* 2007), but several studies have shown that apoptotic stimuli are inhibited with overexpression of ER targeted BCL-2 (Rudner *et al.,* 2001; Hacki *et al.,* 2000), highlighting it anti-apoptotic effect even when localized to the ER. ERIS may play a regulatory role with BCL-2 by either mediating its translocation to the mitochondria or enhancing its anti-apoptotic effect at the ER. Thus, the contribution of the ERIS/BCL-2 interaction to BCL-2 anti-apoptotic function still needs to be determined. We have shown that apoptotic cell death increases in INS1 *Cisd2* knockdown cells under normal conditions as well as in response to stressful stimuli such as thapsigargin and paraquat. Although these findings do not speak directly about the ERIS/BCL-2 interaction, it is possible that *CISD2* deficiency leads to a greater susceptibility of BCL-2 inhibition by its antagonists, leading to an exacerbated cell death response. The inhibition of BCL-2 antagonists, by siRNA targeting, may attenuate the apoptotic cell death response due to thapsigargin and paraquat treatment seen in INS1 *Cisd2* knockdown cells.

It is still not known how *CISD2* deficiency causes apoptotic cell death, as observed in INS1 *Cisd2* knockdown cells, under normal conditions. As mentioned above, cytosolic Ca^{2+}

elevation due to dysfunctional regulation of ER Ca^{2+} release from IP_3 receptors may cause a Ca^{2+} overload in the mitochondria favoring an apoptotic response. Distressed mitochondria may, in turn, increase production of ROS, further exacerbating the activation of apoptotic pathways. The weakened function of BCL-2 as an anti-apoptotic effector due to defective or absent ERIS may lower the threshold for the apoptotic stimuli. In addition, autophagic morphology can precede apoptosis, when the autophagy destroys large proportions of the cytosol and organelles beyond a certain threshold (Maiuri *et al.,* 2007). The de-inhibition of autophagy by *CISD2* deficiency may activate autophagy induced damage which in turn may lead to an apoptotic response. Any of these or all of these components may lead to the increased cell death seen in INS1 *Cisd2* knockdown cell lines under normal conditions. The decision for cells to undergo apoptosis or autophagy may depend on the kind of stimuli that are present. Under conditions of nutrient deprivation, autophagy prevails, but under conditions of Ca^{2+} elevation and increased ROS production, apoptosis is activated. Under normal conditions, *CISD2* deficiency may lead to an increase in the latter conditions resulting in stimulated apoptosis (Figure 21B). Apoptotic cell death of pancreatic β-cells and neurons contribute to the first clinical manifestations in WFS2.

In conclusion, Wolfram syndrome is an autosomal recessive neurodegerative disease caused by mutations in two genes: *WFS1* and *CISD2,* whose gene products are ER transmembrane proteins. The loss of expression or of a functional protein of either gene results in apoptosis in cells, but the pathways that are initially affected by disruption of each of these genes are different. Mutations in *WFS1* upregulates the UPR and lower calcium levels in the ER, while mutations in *CISD2* have no effect on the UPR and appear to increase calcium levels in the ER or causes increased release of ER calcium with thapsigargin stimulation. The function of ERIS has been associated with BCL-2 mediated inhibition of autophagy and is suggested to play a role

in neuronal differentiation and brain development. WFS2, caused by mutations in *Cisd2*, may develop as a result of a disruption of any of these proposed functions, or other consequences of *Cisd2* disruption such as abnormal ER calcium homeostasis and accelerated oxidative stress. Understanding the mechanism of pathogenesis in WFS2 will help to further uncover pathways to cell death commonly seen in disease and how ERIS, a dynamic protein, is involved in several cellular functions from autophagy to ER calcium homeostasis leading to apoptosis.
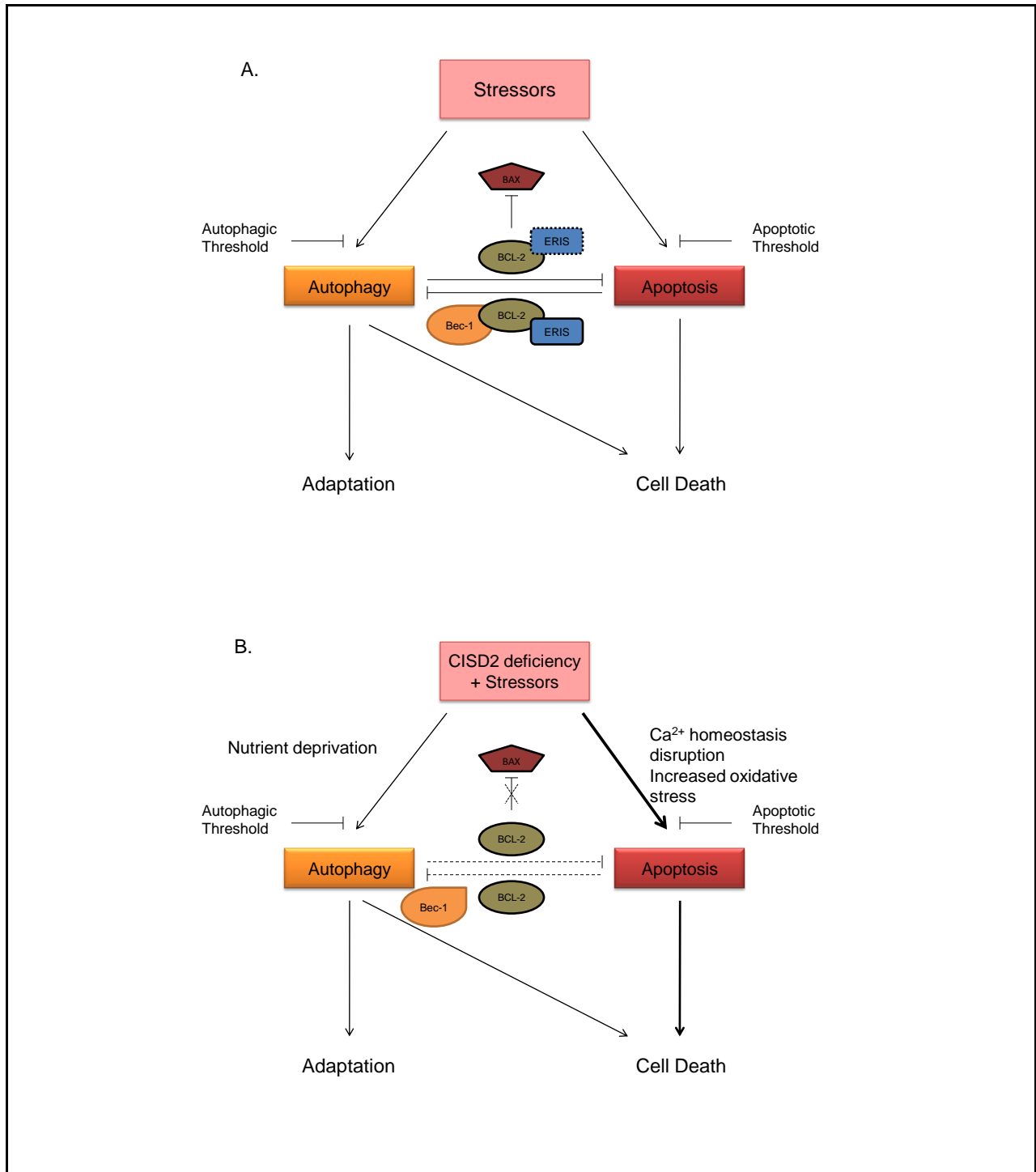
Figure 21. The relationship between apoptosis, autophagy, and *CISD2* deficiency. (A) Similar stressors can activate either apoptosis or autophagy, and the decision of the cell to undergo one process over the other is poorly understood, but different sensitivity thresholds to different stimuli may play a role in dictating cell fate. Autophagy is regarded as a cell survival mechanism and favors adaptation under stressful stimuli, however, under massive autophagy, autophagic cell death or apoptotic cell death may occur. The two processes exhibit some degree

of mutual inhibition that may be regulated by BCL-2. BCL-2 inhibits autophagy by binding to Beclin 1 (Bec 1) at the ER, while it blocks apoptosis by inhibiting BAX and other pro-apoptotic BCL-2 family members. While ERIS has been recently shown to play an important role in BCL-2 anti-autophagic function, it is still needs to be determined whether it also plays a role in BCL-2 anti-apoptotic function (ERIS is shown with a dotted line border to illustrate its unknown role in the BCL-2 apoptotic inhibition). (B) When cells are *CISD2* deficient, BCL-2 autophagy inhibition is disrupted under conditions of nutrient deprivation. *CISD2* deficiency also disrupts cellular Ca^{2+} homeostasis and increase oxidative stress, both of each contribute to overcoming the apoptotic threshold and stimulating apoptotic pathways (expressed in thicker line). Whether CISD2 deficiency directly disrupts BCL-2 inhibition of pro-apoptotic molecules such as BAX still needs to be determined (disruption of BCL-2 mediated BAX inhibition is shown with a dotted X to illustrate that that event is unknown if it occurs under CISD2 deficiency). (Modified from Maiuri *et al.*, 2007).

LIST OF REFERENCES

REFERENCES CITED

Ajlouni K, Jarrah N, El-Khateeb M, El-Zaheri M, El Shanti H, Lidral A. 2002. Wolfram syndrome: identification of a phenotypic and genotypic variant from Jordan. *Am J Med Genet.* 115(1):61-5.

Al-Sheyyab M, Jarrah N, Younis E, Shennak MM, Hadidi A, Awidi A, El-Shanti H, Ajlouni K. 2001. Bleeding tendency in Wolfram syndrome: a newly identified feature with phenotype genotype correlation. *Eur J Pediatr.* 160:243-246.

Altschul SF, Gish W, Miller W, Myers EW, Lipman DJ. 1990. Basic local alignment search tool. J Mol Biol 215:403-410.

Amr S, Heisy C, Zhang M, Xia X, Shows K, Ajlouni K, Pandya A, Satin L, El-Shanti H, Shiang R. 2007. A homozygous mutation in a novel zinc-finger protein, ERIS, is responsible for Wolfram syndrome 2. *Am J Hum Gen.* 81: 673-683.

Andersen JK. 2004. Iron dysregulation and Parkinson's disease. *J Alzheimers Dis.* 6(6 Suppl):S47-52.

Barnett AH, Eff C, Leslie RDG, Pyke DA. 1981. Diabetes in identical twins: a study of 200 pairs. *Diabetologia.* 20:87-93.

Barrett TG, Bundey SE, Fielder AR, Good PA. 1997. Optic atrophy in Wolfram (DIDMOAD) syndrome. *Eye* 11:882-888.

Barrett TG, Bundey SE, Macleod AF. 1995. Neurodegeneration and diabetes: UK nationwide study of Wolfram (DIDMOAD) syndrome. *Lancet.* 346:1458–1463.

Bassani JW, Yuan W, Bers DM . 1995. Fractional SR Ca release is regulated by trigger Ca and SR Ca content in cardiac myocytes. *Am J Physiol.* 268:C1313-C1319.

Bayir H, Kagan VE. 2008. Bench-to-bedside review: Mitochondrial injury, oxidative stress and apoptosis--there is nothing more practical than a good theory. *Crit Care.* 12(1):206.

Baz P, Azar ST, Medlej R, Bejjani R, *et al*. 1999. Role of early fundoscopy for diagnosis of Wolfram syndrome in type 1 diabetic patients. *Diabetes Care*. 22: 1376-8.

Berridge MJ, Lipp P, Bootman MD. 2000. The versatility and universality of calcium signalling. *Nat Rev Mol Cell Biol*. 1(1):11-21.

Bespalova IN, Van Camp G, Bom SJH, Brown DJ, Cryns K, DeWan AT, Erson AE, Flothmann K, Kunst HPM, Kurnool P, *et al*. 2001. Mutations in the Wolfram syndrome 1

gene (WFS1) are a common cause of low frequency sensorineural hearing loss. *Hum Mol Genet*. 10:2501-2508.

Blasi C, Pierelli F, Rispoli E, Saponara M, Vingolo E, Andreani D. 1986. Wolfram's syndrome: a clinical, diagnostic, and interpretative contribution. *Diabetes Care.* 9:521–528.

Bohr VA. 2002. Repair of oxidative DNA damage in nuclear and mitochondrial DNA, and some changes with aging in mammalian cells. *Free Radic Biol Med*. 32: 804-812.

Boucquey M, De Plaen E, Locker M, Poliard A, Mouillet-Richard S, Boon T, Kellermann O. 2006. Noxp20 and Noxp70, two new markers of early neuronal differentiation, detected in teratocarcinoma-derived neuroectodermic precursor cells. *J Neurochem*. 99(2):657-69.

Boyce M, and Yuan J. 2006. Cellular response to endoplasmic reticulum stress: a matter of life or death. *Cell Death and Differentiation.* 13: 363-373.

Bus JS, Gibson JE. 1984. Paraquat: model for oxidant-initiated toxicity. *Environ Health Perspect*. 55:37-46.

Butler AE, Janson J, Bonner-Weir S, Ritzel R, Rizza RA, Butler PC. 2003. Beta-cell deficit and increased beta-cell apoptosis in humans with type 2 diabetes. *Diabetes*. 52(1):102-10.

Butterfield D, Castegna A, Pocernich C, Drake J, Scapagnini G, Calabrese V. 2002. Nutritional approaches to combat oxidative stress in Alzheimer's disease. *J Nutr Biochem.* 13(8):444.

Cann HM, de Toma C, Cazes L, Legrand MF, Morel V, Piouffre L, Bodmer J, Bodmer WF, Bonne-Tamir B, Cambon-Thomsen A, *et al*. 2002. A human genome diversity cell line panel. *Science.* 296:5566:261–262.

Carlsson C, Borg LA, Welsh N. 1999. Sodium palmitate induces partial mitochondrial uncoupling and reactive oxygen species in rat pancreatic islets in vitro. *Endocrinology*. 140(8):3422-8.

Carson MJ, Slager UT, Steinberg RM. 1977. Simultaneous occurrence of diabetes mellitus, diabetes insipidus, and optic atrophy in a brother and sister. *Am J Dis Child*. 131:1382-1385.

Chang NC, Nguyen M, Germain M, Shore GC. 2010. Antagonism of Beclin 1-dependent autophagy by BCL-2 at the endoplasmic reticulum requires NAF-1. *EMBO J.* 29(3):606-18.

Chantrel-Groussard K, Geromel V, Puccio H, Koenig M, Munnich A, Rötig A, Rustin P. 2001. Disabled early recruitment of antioxidant defenses in Friedreich's ataxia. *Hum Mol Genet.* 10(19):2061-7.

Chen YF, Kao CH, Chen YT, Wang CH, Wu CY, Tsai CY, Liu FC, Yang CW, Wei YH, Hsu MT, Tsai SF, Tsai TF. 2009. Cisd2 deficiency drives premature aging and causes mitochondria-mediated defects in mice. *Genes Dev.* 23(10):1183-94.

Cheung KH, Shineman D, Müller M, Cárdenas C, Mei L, Yang J, Tomita T, Iwatsubo T, Lee VM, Foskett JK. 2008. Mechanism of Ca^{2+} disruption in Alzheimer's disease by presenilin regulation of InsP3 receptor channel gating. *Neuron.* 58(6):871-83.

Chipuk JE, Green DR. 2005. Do inducers of apoptosis trigger caspase-independent cell death? *Nat Rev Mol Cell Biol.* 6(3):268-75.

Clapham DE. 1995. Calcium signaling. *Cell.* 80(2):259-68.

Collier DA, Barrett TG, Curtis D, Macleod A, Arranz MJ, Maassen JA, Bundey S 1996. Linkage of Wolfram syndrome to chromosome 4p16.1 and evidence for heterogeneity. *Am J Hum Genet.* 59:855–863.

Collins TJ, Lipp P, Berridge MJ, Li W, Bootman MD. 2000. Inositol 1,4,5-triphosphate-induced Ca^{2+} release is inhibited by mitochondrial depolarization. *Biochem J.* 347:593-600.

Conlan AR, Axelrod HL, Cohen AE, Abresch EC, Zuris J, Yee D, Nechushtai R, Jennings PA, Paddock ML. 2009. Crystal structure of Miner1: The redox-active 2Fe-2S protein causative in Wolfram syndrome 2. *J. Mol. Biol.* 392: 143-153.

Cooper TA, Mattox, W. 1997. The regulation of splice-site selection and its role in human disease. *Am J Hum Genet.* 61:259-266.

Cremers CW, Wijdeveld, PG, Pinckers AJ. 1977. Juvenile diabetes mellitus, optic atrophy, hearing loss, diabetes insipidus, tonia of the urinary tract and bladder, and other abnormalities (Wolfram syndrome). A review of 88 cases from the literature with personal observations of 3 new patients. *Acta Paediatr Scand Suppl.* 264:1-16.

Davì G, Ciabattoni G, Consoli A, *et al.* 1999. In vivo formation of 8- iso prostaglandin F2 alpha and platelet activation in diabetes mellitus: effects of improved metabolic control and vitamin E supplementation. *Circulation.* 99: 224-229.

David V, Hochstenbach F, Rajagopalan S, Brenner MB. 1993. Interaction with newly synthesized and retained proteins in the endoplasmic reticulum suggests a chaperone function for human integral membrane protein IP90 (calnexin). *J Biol Chem.* 268:9585-9592.

Delépine M, Nicolino M, Barrett T, Golamaully M, Lathrop GM, Julier C. 2000. EIF2AK3, encoding translation initiation factor 2-alpha kinase 3, is mutated in patients with Wolcott-Rallison syndrome. *Nat Genet.* 25(4):406-9.

Dexter DT, Wells FR, Lees AJ, Agid F, Agid Y, Jenner P, Marsden CD. 1989. Increased nigral iron content and alterations in other metal ions occurring in brain in Parkinson's disease. *J Neurochem*. 52(6):1830-6.

Domenech E, Gomez-Zaera M, Nunes. 2006. V. Wolfram/DIDMOAD syndrome, a heterogenicand molecularly complex neurodegenerative disease. *Pediatr Endocrinol Rev*. 3(3):249-57.

Donath MY, Halban PA. 2004. Decreased beta-cell mass in diabetes: significance, mechanisms and therapeutic implications. *Diabetologia*. 47(3):581-9.

Duchen MR, Verkhratsky A, Muallem S. 2008. Mitochondria and calcium in health and disease. *Cell Calcium.* 44(1):1-5.

Eiberg H, Hansen L, Kjer B, Hansen T, Pederson O, Bille M, Rosenberg T, Tranebjaerg L. 2006. Autosomal dominant optic atrophy associated with hearing impairment and impaired glucose regulation caused by a missense mutation in the WFS1 gene. *J Med Genet*. 43:435-440.

El-Shanti H, Lidral AC, Jarrah N, Druhan L, Ajlouni K. 2000. Homozygosity mapping identifies an additional locus for Wolfram syndrome on chromosome 4q. *Am J Hum Genet*. 66:1229–1236.

Evans JL, Goldfine ID, Maddux BA, Grodsky GM. 2002. Oxidative stress and stress-activated signaling pathways: a unifying hypothesis of type 2 diabetes. *Endocr Rev*. 23(5):599-622.

Figueroa-Romero C, Sadidi M, Feldman EL. 2008. Mechanisms of disease: the oxidative stress theory of diabetic neuropathy. *Rev Endocr Metab Disord*. 9(4):301-14.

Fonseca SG, Fukuma M, Lipson KL, Nguyen LX, Allen JR, Oka Y, Urano F. 2005. WFS1 is a novel component of the unfolded protein response and maintains homeostasis of the endoplasmic reticulum in pancreatic b-cells. *J Biol Chem*. 280: 39609–39615.

Fraser F, Gunn T. 1977. Diabetes mellitus, diabetes insipidus and optic atrophy. An autosomal recessive syndrome? *J Med Genet*. 14:190-193.

Genís D, Dávalos A, Molins A, Ferrer I. 1997. Wolfram syndrome: a neuropathological study. *Acta Neuropathol*. 93(4):426-9.

Giacomello M, Drago I, Pizzo P, Pozzan T. 2007. Mitochondrial Ca^{2+} as a key regulator of cell life and death. *Cell Death Differ*. 14(7):1267-74.

Gómez EO, Mendoza-Milla C, Ibarra-Sánchez MJ, Ventura-Gallegos JL, Zentella A. 1996. Ceramide reproduces late appearance of oxidative stress during TNF-mediated cell death in L929 cells. *Biochem Biophys Res Commun.* 228(2):505-9.

Gómez-Zaera M, Strom TM, Rodríguez B, *et al*. 2001. "Presence of a major WFS1 mutation in Spanish Wolfram syndrome pedigrees.". *Mol. Genet. Metab*. 72 (1): 72–81.

González-Polo RA, Boya P, Pauleau AL, Jalil A, Larochette N, Souquère S, Eskelinen EL, Pierron G, Saftig P, Kroemer G. 2005. The apoptosis/autophagy paradox: autophagic vacuolization before apoptotic death. *J Cell Sci.* 118(Pt 14):3091-102.

Grankvist K, Marklund SL, Täljedal IB. 1981. CuZn-superoxide dismutase, Mn-superoxide dismutase, catalase and glutathione peroxidase in pancreatic islets and other tissues in the mouse. *Biochem J.* 199(2):393-8.

Green K, Brand MD, Murphy MP. 2004. Prevention of mitochondrial oxidative damage as a therapeutic strategy in diabetes. *Diabetes*. 53 Suppl 1:S110-8.

Guo Q, Fu W, Sopher BL, Miller MW, Ware CB, Martin GM, Mattson, MP. 1999. Increased vulnerability of hippocampal neurons to excitotoxic necrosis in presenilin-1 mutant knock-in mice. Nat Med 5:101-106.

Gyorke I, Gyorke S. 1998. Regulation of the cardiac ryanodine receptor channel by luminal Ca^{2+} involves luminal Ca^{2+} sensing sites. *Biophys J*. 75:2801-2810.

Gyorke I, Hester N, Jones LR, Gyorke S. 2004. The role of calsequestrin, triadin, and junctin in conferring cardiac ryanodine receptor responsiveness to luminal calcium. *Biophys J* 86:2121-2128.

Haber CA, Lam TK, Yu Z, Gupta N, Goh T, Bogdanovic E, Giacca A, Fantus IG. 2003. N-acetylcysteine and taurine prevent hyperglycemia-induced insulin resistance in vivo: possible role of oxidative stress. *Am J Physiol Endocrinol Metab*. 285(4):E744-53.

Häcki J, Egger L, Monney L, Conus S, Rossé T, Fellay I, Borner C. 2000. Apoptotic crosstalk between the endoplasmic reticulum and mitochondria controlled by Bcl-2. *Oncogene*. 19(19):2286-95.

Halliwell B, Gutteridge JMC. 1999. Free radicals in biology and medicine (3rd ed.). Oxford University Press.

Halliwell B. 2006. Oxidative stress and neurodegeneration: where are we now? *J Neurochem.* 97(6):1634-58.

Han S, Schiefer A, Isenberg G. 1994. Ca^{2+} load of guinea-pig ventricular myocytes determines efficacy of brief Ca^{2+} currents as trigger for Ca^{2+} release. J Physiol 480:411-421.

Harding HP, Zeng H, Zhang Y, Jungries R, Chung P, Plesken H, Sabatini DD, Ron D. 2001. Diabetes mellitus and exocrine pancreatic dysfunction in perk-/- mice reveals a role for translational control in secretory cell survival. *Mol Cell.* 7(6):1153-63.

Hardy C, Khanim F, Torres R, *et al*. 1999. Clinical and molecular genetic analysis of 19 Wolfram syndrome kindreds demonstrating a wide spectrum of mutations in WSF1. *Am J Hum Genet.* 65: 1279-1290.

Hensley K, Maidt ML, Yu Z, Sang H, Markesbery WR, Floyd RA. 1998. Electrochemical analysis of protein nitrotyrosine and dityrosine in the Alzheimer brain indicates region-specific accumulation. *J Neurosci*. 18(20):8126-32.

Hilson JB, Merchant SN, Adams JC, Joseph JT. 2009. Wolfram syndrome: a clinicopathologic correlation. *Acta Neuropathol.* 118(3):415-28.

Hirashima N, Etcheberrigaray R, Bergamaschi S, Racchi M, Battaini F, Binetti G, Govoni S, Alkon DL. 1996. Calcium responses in human fibroblasts: a diagnostic molecular profile for Alzheimer's disease. *Neurobiol Aging*. 17(4):549-55.

Hofmann S, Philbrook C, Gerbitz KD, and Bauer MF. 2003. Wolfram syndrome: structural and functional analyses of mutant and wild-type wolframin, the WFS1 gene product. *Hum. Mol. Genet.* 12, 2003–2011.

Hoozemans JJ, Veerhuis R, Van Haastert ES, Rozemuller JM, Baas F, Eikelenboom P, Scheper W. 2005. The unfolded protein response is activated in Alzheimer's disease. *Acta Neuropathol*. 110(2):165-72.

Hou ZQ, Li HL, Gao L, Pan L, Zhao JJ, Li GW. 2008. Involvement of chronic stresses in rat islet and INS-1 cell glucotoxicity induced by intermittent high glucose. *Mol Cell Endocrinol.* 291(1-2):71-8.

Hulo N, Bairoch A, Bulliard V, Cerutti L, De Castro E, Langendijk-Genevaux PS, Pagni M, Sigrist CJA. 2006. The PROSITE database. Nucleic Acids Res 34:D227-D230.

Inoue H, Tanizawa Y, Wasson J, Behn P, Kalidas K, Bernal- Mizrachi B, Mueckler M, Marshall H, Donis-Keller H, Crock P, *et al*. 1998. A gene encoding a transmembrane protein is mutated in patients with diabetes mellitus and optic atrophy (Wolfram syndrome). *Nat Genet.* 20:143–148.

Ishihara H, Takeda S, Tamura A, Takahashi R, Yamaguchi S, Takei D, Yamada T, Inoue H, Soga H, Katagiri H, Tanizawa Y & Oka Y. 2004. Disruption of the WFS1 gene in mice causes progressive b-cell loss and impaired stimulus-secretion coupling in insulin secretion. *Human Molecular Genetics*. 13: 1159–1170.

Jacobson J, Duchen MR. 2002. Mitochondrial oxidative stress and cell death in astrocytes--requirement for stored Ca^{2+} and sustained opening of the permeability transition pore. *J Cell Sci.* 115(Pt 6):1175-88.

Janjic D, Wollheim CB. 1992. Islet cell metabolism is reflected by the MTT (tetrazolium) colorimetric assay. *Diabetologia*. 35(5):482-5.

Jones-Villeneuve EM, Rudnicki MA, Harris JF, McBurney MW. 1983. Retinoic acid-induced neural differentiation of embryonal carcinoma cells. *Mol Cell Biol.* 3(12):2271-9.

Jouaville LS, Ichas F, Holmuhamedor EL, Camacho P, Lechieiter JD. 1995. Synchronization of calcium waves by mitochondrial substrates in Xenopus laevis oocytes. *Nature* 377:438-441.

Kanki T, Klionsky DJ. 2009. Mitochondrial abnormalities drive cell death in Wolfram syndrome 2. *Cell Res.* 19(8):922-3.

Kanner EM, Klein IK, Friedlander M, Simon SM. 2002. The amino terminus of opsin translocates "posttranslationally" as efficiently as cotranslationally. *Biochem* 41:7707-7715.

Khanim F, Kirk J, Latif F, Barret T. 2001. WFS1/wolframin mutations, Wolfram syndrome, and associated diseases. *Hum Mutat.* 17: 357-367.

Kim RH, Smith PD, Aleyasin H, Hayley S, Mount MP, Pownall S, Wakeham A, You-Ten AJ, Kalia SK, Horne P, Westaway D, Lozano AM, Anisman H, Park DS, Mak TW. 2005. Hypersensitivity of DJ-1-deficient mice to 1-methyl-4-phenyl-1,2,3,6-tetrahydropyrindine (MPTP) and oxidative stress. *Proc Natl Acad Sci U S A*. 102(14):5215-20.

Kuenzel EA, Mulligan JA, Sommercorn J, Krebs EG. 1987. Substrate specificity determinants for casein kinase II as deduced from studies with synthetic peptides. *J Biol Chem* 262:9136-9140.

Kuznetsov G, Brostrom MA, Brostrom, CO. 1992. Demonstration of a calcium requirement for secretory protein processing and export. Differential effects of calcium and dithiothreitol. *J Biol Chem* 267:3932-3939.

Lee AH, Iwakoshi NN, and Glimcher LH. 2003. *XBP-1* regulates a subset of endoplasmic reticulum resident chaperone genes in the unfolded protein response. *Mol. Cell. Biol.* 23:7448–7459.

Lein ES, Hawrylycz MJ, Ao N, Ayres M, Bensinger A, Bernard A, Boe AF, Boguski MS, Brockway KS, Byrnes EJ, *et al*. 2007. Genome-wide atlas of gene expression in the adult mouse brain. *Nature* 445:168-176.

Leissring MA, Akbari Y, Fanger CM, Cahalan MD, Mattson MP, LaFerla FM. 2000. Capacitative calcium entry deficits and elevated luminal calcium content in mutant presenilin-1 knockin mice. *J Cell Biol* 149:793-797.

Leissring MA, Paul BA, Parker I, Cotman CW, LaFerla FM. 1999. Alzheimer's presenilin-1 mutation potentiates inositol 1,4,5-trisphosphate-mediated calcium signaling in Xenopus oocytes. *J Neurochem.* 72(3):1061-8.

Li F, Calingasan NY, Yu F, Mauck WM, Toidze M, Almeida CG, Takahashi RH, Carlson GA, Flint Beal M, Lin MT, Gouras GK. 2004. Increased plaque burden in brains of APP mutant MnSOD heterozygous knockout mice. *J Neurochem.* 89(5):1308-12.

Li Y, Huang TT, Carlson EJ, Melov S, Ursell PC, Olson JL, Noble LJ, Yoshimura MP, Berger C, Chan PH, Wallace DC, Epstein CJ. 1995. Dilated cardiomyopathy and neonatal lethality in mutant mice lacking manganese superoxide dismutase. *Nat Genet.* 11(4):376-81.

Lin MT, Beal MF. 2006. Mitochondrial dysfunction and oxidative stress in neurodegenerative diseases. *Nature.* 443(7113):787-95.

Lindholm D, Wootz H, and Korhonen L. 2006. ER stress and neurodegenerative diseases. *Cell Death and Differentiation.* 13: 385-392.

Lodish HF, Kong N, Wikstrom L. 1992. Calcium is required for folding of newly made subunits of the asialoglycoprotein receptor within the endoplasmic reticulum. *J Biol Chem.* 267:12753-12760.

Lu T, Pan Y, Kao SY, Li C, Kohane I, Chan J, Yankner BA. 2004. Gene regulation and DNA damage in the ageing human brain. *Nature.* 429(6994):883-91.

Lytton J, Westlin M, Hanley MR. 1991. Thapsigargin inhibits the sarcoplasmic or endoplasmic reticulum Ca-ATPase family of calcium pumps. *J Biol Chem.* 266:17067-17071.

Mackay JP, Crossley M. 1998. Zinc fingers are sticking together. *Trends Biochem Sci.* 23:1-4.

Maiuri MC, Criollo A, Kroemer G. 2010. Crosstalk between apoptosis and autophagy within the Beclin 1 interactome. *EMBO J.* 29(3):515-6.

Maiuri MC, Zalckvar E, Kimchi A, Kroemer G. 2007. Self-eating and self-killing: crosstalk between autophagy and apoptosis. *Nat Rev Mol Cell Biol.* 8(9):741-52.

Malhotra JD, Kaufman RJ. 2007. Endoplasmic reticulum stress and oxidative stress: a vicious cycle or a double-edged sword? *Antioxid Redox Signal.* 9(12):2277-93.

Maritim AC, Sanders RA, Watkins JB 3rd. 2003. Diabetes, oxidative stress, and antioxidants: a review. *J Biochem Mol Toxicol.* 17(1):24-38.

Martin I, Jones MA, Rhodenizer D, Zheng J, Warrick JM, Seroude L, Grotewiel M. 2009. Sod2 knockdown in the musculature has whole-organism consequences in Drosophila. *Free Radic Biol Med*. 47(6):803-13.

Matés JM. 2000. Effects of antioxidant enzymes in the molecular control of reactive oxygen species toxicology. *Toxicology*. 153(1-3):83-104.

Mattiazzi M, D'Aurelio M, Gajewski CD, Martushova K, Kiaei M, Beal MF, Manfredi G. 2002. Mutated human SOD1 causes dysfunction of oxidative phosphorylation in mitochondria of transgenic mice. *J Biol Chem*. 277(33):29626-33.
Mayeux R. 2003. Epidemiology of neurodegeneration. *Annu Rev Neurosci*. 26:81-104.

McCormack A, Atienza J, Johnston L, Andersen J, Vu S, and Di Monte. 2005. Role of oxidative stress in paraquat-induced dopaminergic cell degeneration. *J Neurochem* 93(4): 1030-1037.

McCullough KD, Martindale JL, Klotz LO, Aw TY, Holbrook NJ. 2001. Gadd153 sensitizes cells to endoplasmic reticulum stress by down-regulating Bcl2 and perturbing the cellular redox state. *Mol Cell Biol.* 21(4):1249-59.

Meulener M, Whitworth AJ, Armstrong-Gold CE, Rizzu P, Heutink P, Wes PD,
Meulener MC, Xu K, Thomson L, Ischiropoulos H, Bonini NM. 2006. Mutational analysis of DJ-1 in Drosophila implicates functional inactivation by oxidative damage and aging. *Proc Natl Acad Sci U S A*. 103(33):12517-22.

Minton JA, Rainbow LA, Ricketts C, Barrett TG. 2003. Wolfram syndrome. *Rev Endocr Metab Disord.* 4(1):53-9.

Missiaen L, DeSmedt H, Bultynck G, Vanlingen S, Desmet P, Callewaert G, Parys JB. 2000. Calmodulin increases the sensitivity of type 3 inositol-1,4, 5 trisphosphate receptors to Ca^{2+} inhibition in human bronchial mucosal cells. *Mol Pharmacol.* 57(3):564-7.

Mogami H, Tepikin AV, Petersen OH. 1998. Terminatin of cytosolic Ca^{2+} signals: Ca^{2+} reuptake into intracellular stores is regulated by the free Ca^{2+} concentration in the store lumen. *EMBO J*. 17:425-442.

Moriscot C, Candel S, Sauret V, Kerr-Conte J, Richard MJ, Favrot MC, Benhamou PY. 2007. MnTMPyP, a metalloporphyrin-based superoxide dismutase/catalase mimetic, protects INS-1 cells and human pancreatic islets from an in vitro oxidative challenge. *Diabetes Metab*. 33(1):44-53.

Newman B, Selby JV, King ML, Slemenda C, Fabsitz R, Friedman GD. 1987. Concordance for type 2 (non-insulin dependent) diabetes mellitus in male twins. *Diabetologia*. 30:763-769.

Newsholme P, Haber EP, Hirabara SM, Rebelato EL, Procopio J, Morgan D, Oliveira-Emilio HC, Carpinelli AR, Curi R. 2007. Diabetes associated cell stress and dysfunction: role of

mitochondrial and non-mitochondrial ROS production and activity. *J Physiol.* 583(Pt 1):9-24.

Nishikawa T, Edelstein D, Du XL, Yamagishi S, Matsumura T, Kaneda Y, Yorek MA, Beebe D, Oates PJ, Hammes HP, Giardino I, Brownlee M. 2000. Normalizing mitochondrial superoxide production blocks three pathways of hyperglycaemic damage. *Nature.* 404(6779):787-90.

Nourooz-Zadeh J, Tajaddini-Sarmadi J, McCarthy S, Betteridge DJ, Wolff SP. 1995. Elevated levels of authentic plasma hydroperoxides in NIDDM. *Diabetes.* 44(9):1054-8.

Nunomura A, Perry G, Pappolla MA, Friedland RP, Hirai K, Chiba S, Smith MA. 2000. Neuronal oxidative stress precedes amyloid-beta deposition in Down syndrome. *J Neuropathol Exp Neurol.* 59(11):1011-7.

Ohyagi Y, Yamada T, Nishioka K, Clarke NJ, Tomlinson AJ, Naylor S, Nakabeppu Y, Kira J, and Younkin SG. 2000. Selective increase in cellular A beta 42 is related to apoptosis but not necrosis. *Neuroreport* 11:167–171.

Onorato JJ, Palczewski K, Regan JW, Caron MG, Lefkowitz RJ, Benovic JL. 1991. Role of acidic amino acids in peptide substrates of the beta-adrenergic receptor kinase and rhodopsin kinase. *Biochem* 30:118-125.

Orrenius S, Gogvadze V, Zhivotovsky B. 2007. Mitochondrial oxidative stress: implications for cell death. *Annu Rev Pharmacol Toxicol.* 47:143-83.

Osman AA, Saito M, Makepeace C, Permutt MA, Schlesinger P, Mueckler M. 2003. Wolframin expression induces novel ion channel activity in endoplasmic reticulum membranes and increases intracellular calcium. *J Biol Chem.* 278:52755– 52762.

Ott M, Gogvadze V, Orrenius S, Zhivotovsky B. 2007. Mitochondria, oxidative stress and cell death. *Apoptosis.* 12(5):913-22.

Oyadomari S, Mori M. 2004. Roles of CHOP/GADD153 in endoplasmic reticulum stress. *Cell Death Differ.* 11(4):381-9.

Pallanck LJ, Bonini NM. 2005. Drosophila DJ-1 mutants are selectively sensitive to environmental toxins associated with Parkinson's disease. *Curr Biol.* 15(17):1572-7.

Paschen W, Doutheil J.1999. Disturbances of the functioning of endoplasmic reticulum: a key mechanism underlying neuronal cell injury? *J Cereb Blood Flow Metab.* 19(1):1-18.

Pearson RB, Kemp BE. 1991. Protein kinase phosphorylation site sequences and consensus specificity motifs: tabulations. *Methods Enzymol.* 200:62-81.

Pedersen WA, Fu W, Keller JN, Markesbery WR, Appel S, Smith RG, Kasarskis E, Mattson MP. 1998. Protein modification by the lipid peroxidation product 4-hydroxynonenal in the spinal cords of amyotrophic lateral sclerosis patients. *Ann Neurol*. 44(5):819-24.

Peri S, Navarro JD, Amanchy R, Kristiansen TZ, Jonnalagadda CK, Surendranath V, Niranjan V, Muthusamy B, Gandhi TK, Gronborg M, *et al*. 2003. Development of human protein reference database as an initial platform for approaching systems biology in humans. *Genome Res* 13:2363-2371.

Pinton P, Giorgi C, Siviero R, Zecchini E, and Rizzuto R. 2008. Calcium and apoptosis: ER-mitochondria Ca2+ transfer in the control of apoptosis. *Oncogene* 27:6407-6418.

Pinton P, Ferrari D, Papizzi E, Di Virgilio F, Pozzan T, Rizzuto R. 2001. The Ca^{2+} concentration of the endoplasmic reticulum is a key determinant of ceramide-induced apoptosis: significance for the molecular mechanism of Bcl-2 action. *EMBO J*. 20:2690-2701.

Piro S, Anello M, Di Pietro C, Lizzio MN, Patanè G, Rabuazzo AM, Vigneri R, Purrello M, Purrello F. 2002. Chronic exposure to free fatty acids or high glucose induces apoptosis in rat pancreatic islets: possible role of oxidative stress. *Metabolism*. 51(10):1340-7.

Polymeropoulos MH, Swift RG, Swift M. 1994. Linkage of the genes for Wolfram syndrome to markers on the short arm of chromosome 4. *Nat Genet.* 8:95-97.
Praticò D, Uryu K, Leight S, Trojanoswki JQ, Lee VM. 2001. Increased lipid peroxidation precedes amyloid plaque formation in an animal model of Alzheimer amyloidosis. *J Neurosci*. 21(12):4183-7.

Rando TA, Horton JC, Layzer RB. 1992. Wolfram syndrome: evidence of a diffuse neurodegenerative disease by magnetic resonance imaging. *Neurology*. 42(6):1220-4.
Report on the Expert Committee on the Diagnosis and Classification of Diabetes Mellitus. *Diabetes Care*. 20:1183-1197, 1997.

Reynolds A, Laurie C, Mosley RL, Gendelman HE. 2007. Oxidative stress and the pathogenesis of neurodegenerative disorders. *Int Rev Neurobiol.* 82:297-325.

Rhodes CJ. 2005. Type 2 diabetes-a matter of beta-cell life and death? Science. 307(5708):380-4.

Robertson RP. 2004. Chronic oxidative stress as a central mechanism for glucose toxicity in pancreatic islet beta cells in diabetes. *J Biol Chem*. 279(41):42351-4.

Ron D, Walter P. 2007. Signal integration in the endoplasmic reticulum unfolded protein response. *Nat Rev Mol Cell Biol*. 8(7):519-29.

Rösen P, Nawroth PP, King G, Möller W, Tritschler HJ, Packer L. 2001. The role of oxidative stress in the onset and progression of diabetes and its complications: a summary of

a Congress Series sponsored by UNESCO-MCBN, the American Diabetes Association and the German Diabetes Society. *Diabetes Metab Res Rev.* 17(3):189-212.

Rudner J, Lepple-Wienhues A, Budach W, Berschauer J, Friedrich B, Wesselborg S, Schulze-Osthoff K, Belka C. 2001. Wild-type, mitochondrial and ER-restricted Bcl-2 inhibit DNA damage-induced apoptosis but do not affect death receptor-induced apoptosis. *J Cell Sci.* 114(Pt 23):4161-72.

Scarlatti F, Granata R, Meijer AJ, Codogno P. 2009. Does autophagy have a license to kill mammalian cells? *Cell Death Differ.* 16(1):12-20.

Schapira AH, Cooper JM, Dexter D, Jenner P, Clark JB, Marsden CD. 1989. Mitochondrial complex I deficiency in Parkinson's disease. *Lancet.* 1(8649):1269.

Scheuner D, Song B, McEwen E, Liu C, Laybutt R, Gillespie P, Saunders T, Bonner-Weir S, Kaufman RJ. 2001. Translational control is required for the unfolded protein response and in vivo glucose homeostasis. *Mol Cell.* 7(6):1165-76.

Scheuner D, Vander Mierde D, Song B, Flamez D, Creemers JW, Tsukamoto K, Ribick M, Schuit FC, Kaufman RJ. 2005. Control of mRNA translation preserves endoplasmic reticulum function in beta cells and maintains glucose homeostasis. Nat *Med.* 11(7):757-64.

Schröder M, Kaufman RJ. 2005. The mammalian unfolded protein response. *Annu Rev Biochem.* 74:739-89.

Senée V, Vattem KM, Delépine M, Rainbow LA, Haton C, Lecoq A, Shaw NJ, Robert JJ, Rooman R, Diatloff-Zito C, Michaud JL, Bin-Abbas B, Taha D, Zabel B,Franceschini P, Topaloglu AK, Lathrop GM, Barrett TG, Nicolino M, Wek RC, Julier C. 2004. Wolcott-Rallison Syndrome: clinical, genetic, and functional study of EIF2AK3 mutations and suggestion of genetic heterogeneity. *Diabetes.* 53(7):1876-83.

Shannon P, Becker L, Deck J. 1999. Evidence of widespread axonal pathology in Wolfram syndrome. *Acta Neuropathol.* 98(3):304-8.

Shimizu S, Manita M, Tsujimoto Y. 1999. Bcl-2 family proteins regulate the release of apoptogenic cytochrome c by the mitochondrial channel VDAC. *Nature* 399:483-487.

Skovronsky DM, Lee VM, Trojanowski JQ. 2006. Neurodegenerative diseases: new concepts of pathogenesis and their therapeutic implications. *Annu Rev Pathol.* 1:151-70.

Solovyova N, Veselovsky N, Toescu EC, Verkhratsky A. 2002. Ca^{2+} dynamics in the lumen of the endoplasmic reticulum in sensory neurons: direct visualization of Ca^{2+}-induced Ca^{2+} release triggered by physiological Ca^{2+} entry. *EMBO J* 21:622-630.

Song B, Scheuner D, Ron D, Pennathur S, Kaufman RJ. 2008. Chop deletion reduces oxidative stress, improves beta cell function, and promotes cell survival in multiple mouse models of diabetes. *J Clin Invest.* 118(10):3378-89.

Stadtman ER. 2004. Role of oxidant species in aging. *Curr Med Chem.* 11(9):1105-12.

Strom TM, Ho¨rtnagel K, Hofmann S, Gekeler F, Scharfe C, Rabl W, Gerbitz KD, Meitinger T. 1998. Diabetes insipidus, diabetes mellitus, optic atrophy and deafness (DIDMOAD) caused by mutations in a novel gene (wolframin) coding for a predicted transmembrane protein. *Hum Mol Genet.* 7:2021– 2028.

Stutzmann GE. 2005. Calcium dysregulation, IP3 signaling, and Alzheimer's disease. *Neuroscientist*. 11(2):110-5.

Swift RG, Sadler DB, Swift M. 1990. Psychiatric findings in Wolfram syndrome homozygotes. *Lancet.* 336: 667-669.

Szabadkai G, Duchen MR. 2008. Mitochondria: the hub of cellular Ca^{2+} signaling. *Physiology (Bethesda).* 23:84-94.

Takeda K, Hiroshi I, Tanizawa Y, Matsuzaki Y, Oba J,Watanabe Y, Shinoda K, Oka Y. 2001. WFS1 (Wolfram syndrome 1) gene product: predominant subcellular localization to endoplasmic reticulum in cultured cells and neuronal expression in rat brain. *Hum Mol Genet.* (10) 5:477-484.

Takei D, Ishihara H, Yamaguchi S, Yamada T, Tamura A, Katagiri H, Maruyama Y, Oka Y. 2006. WFS1 protein modulates the free Ca^{2+} concentration in the endoplasmic reticulum. *FEBS Lett*. 580:5635–5640, 477–484.

Talior I, Yarkoni M, Bashan N, Eldar-Finkelman H. 2003. Increased glucose uptake promotes oxidative stress and PKC-delta activation in adipocytes of obese, insulin-resistant mice. *Am J Physiol Endocrinol Metab.* 285(2):E295-302.

Ueda K, Kawona J, Takeda K, Yujiri T, Tanabe K, Anno T, Akiyama M, Nozaki J, Yoshinaga T, Koizumi A, Shinoda K, Oka Y, and Tanzawa Y. 2005. Endoplasmic reticulum stress induces Wfs1 gene expression in pancreatic Beta cells via transcriptional activation. *Eur J End.* 153: 167-176.

Valko M, Leibfritz D, Moncol J, Cronin MT, Mazur M, Telser J. 2007. Free radicals and antioxidants in normal physiological functions and human disease. *Int J Biochem Cell Biol.* 39(1):44-84.

Verkhratsky A and Toescu EC. 2003. Endoplasmic reticulum Ca^{2+} homeostasis and neuronal death. *J. Cell. Mol. Med.* 7(4): 351-361.

Verkhratsky A. 2005. Physiology and pathophysiology of the calcium store in the endoplasmic reticulum of neurons. *Physiol Rev.* 85(1):201-79.

Wiley S., Murphy A., Ross S., van der Geer P., Dixon J. 2007. MitoNEET is an iron-containing outer mitochondrial membrane protein that regulates oxidative capacity. *PNAS.* 104(13):5318-5323.

Wolfram DJ, Wagener HP. 1938. Diabetes mellitus and simple optic atrophy among siblings: report of four cases. *Mayo Clin Proc.* 13:715–718.

Yamada T, Ishihara H, Tamura A, Takahashi R, Yamaguchi S, Takei D, Tokita A, Satake C, Tashiro F, Katagiri H, *et al.* 2006. WFS1-deficiency increases endoplasmic reticulum stress, impairs cell cycle progression and triggers the apoptotic pathway specifically in pancreatic b-cells. *Hum Mol Genet.* 15: 1600–1609.

Yamaguchi S, Ishihara H, Tamura A, Yamada T, Takahashi R,Takei D, Katagiri H & Oka Y. 2004. Endoplasmic reticulum stress and ER stress induces Wfs1 gene expression 175N-glycosylation modulate expression of WFS1 protein. *Biochem and Biophys Res Comm.* 3: 250–256.

Yokoyama K, Su IH, Tezuka T, Yasuda T, Mikoshiba K, Tarakhovsky A, Yamamoto T. 2002. BANK regulates BCR-induced calcium mobilization by promoting tyrosine phosphorylation of IP(3) receptor. *EMBO J.* 21:83-92.

Young T-L, Ives E, Lynch E, Person R, Snook S, MacLaren L, Cator T, Griffin A, Fernanadez B, Lee MK, *et al.* 2001. Non-syndromic progressive hearing loss DFNA38 is caused by heterozygous missense mutation in the Wolfram syndrome gene WFS1. *Hum Mol Genet.* 10:2509-2514.

Zhang M, Goforth P, Bertram R, Sherman A, Satin L. 2003. The Ca^{2+} dynamics of isolated mouse b-cells and islets: implications for mathematical models. *Biophys J.* 84:2852-2870.

Zhao L, Ackerman SL. 2006. ER stress in disease. *Curr Opin Cel Biol* 18:1-9.

Vita

Sami Samir Amr was born in Amman, Jordan on April 25, 1979. He attended elementary and middle school in Dhahran, Saudi Arabia where his father worked, and then moved back to Amman, Jordan to attend the American Community School for high school. Sami graduated high school in 1997 and began his undergraduate studies at the College of William and Mary, Williamsburg, Virginia, in Biological Psychology, which were completed in 2002. Then, Sami attended the Jordan University of Science and Technology in Irbid, Jordan, where he completed a second undergraduate degree in Genetic Engineering and Biotechnology in 2005. Since 2005, Sami has been at Virginia Commonwealth University, Richmond, Virginia, pursuing his graduate degree in Human Genetics. His future plans include pursuing a clinical molecular genetics fellowship at Harvard Medical School Genetics Training Program in Boston, Massachussetts.